Rational Metalloprotein Design for Energy Conversion Applications

by

Rafael de Jesus Alcala-Torano

A Dissertation Presented in Partial Fulfillment
of the Requirements for the Degree
Doctor of Philosophy

Approved July 2019 by the
Graduate Supervisory Committee:

Giovanna Ghirlanda, Chair
Ana L. Moore
Jeremy H. Mills

ARIZONA STATE UNIVERSITY

August 2019

ABSTRACT

Continuing and increasing reliance on fossil fuels to satisfy our population's energy demands has encouraged the search for renewable carbon-free and carbon-neutral sources, such as hydrogen gas or CO_2 reduction products. Inspired by nature, one of the objectives of this dissertation was to develop protein-based strategies that can be applied in the production of green fuels. The first project of this dissertation aimed at developing a controllable strategy to incorporate domains with different functions (e. g. catalytic sites, electron transfer modules, light absorbing subunits) into a single multicomponent system. This was accomplished through the rational design of 2,2'-bipyridine modified dimeric peptides that allowed their metal-directed oligomerization by forming tris(bipyridine) complexes, thus resulting in the formation of a hexameric assembly.

Additionally, two different approaches to incorporate non-natural organometallic catalysts into protein matrix are discussed. First, cobalt protoporphyrin IX was incorporated into cytochrome b_{562} to produce a water-soluble proton and CO_2 reduction catalyst that is active upon irradiation in the presence of a photosensitizer. The effect of the porphyrin axial ligands provided by the protein environment has been investigated by introducing mutations into the native scaffold, indicating that catalytic activity of proton reduction is dependent on axial coordination to the porphyrin. It is also shown that effects of the protein environment are not directly transferred when applied to other reactions, such as CO_2 reduction.

Inspired by the active site of [FeFe]-hydrogenases, the second approach is based on the stereoselective preparation of a novel amino acid bearing a 1,2-benzenedithiol side chain. This moiety can serve as an anchoring point for the introduction of metal complexes into protein matrices. By doing so, this strategy enables

the study of protein interactions with non-natural cofactors and the effects that it may have on catalysis. The work developed herein lays a foundation for furthering the study of the use of proteins as suitable environments for tuning the activity of organometallic catalysts in aqueous conditions, and interfacing these systems with other supporting units into supramolecular assemblies.

A mi mamá, cuyo amor y apoyo incondicionales hicieron esto posible.

ACKNOWLEDGMENTS

To my advisor, Dr. Giovanna Ghirlanda, I would like to express my most sincere gratitude for her mentorship and encouragement, for trusting me with challenging projects, and giving me the freedom to navigate the ups and downs of scientific work. I would also like to thank my committee members, Dr. Ana Moore and Dr. Jeremy Mills for their professional guidance, support, and advice. Additionally, to Dr. Sidney Hecht for allowing me to do a research rotation and in his group. To my collaborators, Dr. Maoquing Dong and Dr. Lawrence Miller at the Mayo Clinic, thank you for letting me be the liaison between our groups, the patience throughout our projects, and allowing me to observe your side of the experimental work. Further, I would like to acknowledge the agencies responsible for the funding of my projects, namely the U. S. Department of Energy, the National Institutes of Health, and the Mayo Clinic-ASU Grant Seed Program.

To all my lab mates: thank you for your all the hours together in the lab. Dr. Dayn Sommer, thank you for the scientific discussions, assistance with molecular biology, the guidance, support, encouragement, and for helping me see I was good enough to be here. Nicholas Halloran, thank you for all the suggestions, the crazy (and not so crazy) ideas, all the discussions that often lead nowhere, and all the help in and out the lab. To my undergrads, in particular Garrett Booher, Carolyn Clark, and Noah Gwerder, for their hard work that was fundamental to my projects. To all my co-authors, thank you for your invaluable work. Dr. Kirtland Robinson, thank you for your help with analytical work on formate quantification, but mostly for your friendship and constant optimism. To Tara MacCulloch, thank you for your help with peptide synthesis, the conversations, and for being a great source of support and a true friend.

I am grateful to all the friends I have made during my time at ASU and who have been essential for keeping me sane, I truly value all of you. Timothy Baxter and Dr. Jesse Coe, thank you for the laughs and jokes, the bar times, and the good talks. Zachary Dobson, thank you for the countless nights in and out, the heart-to-heart conversations, and all the dumb but fun times. Dr. Lina Franco, I greatly appreciate you being there whenever I needed you, your unconditional love and support. Thank you, Dr. David Jennings, for all the silly jokes and all the deep talks—even we may not have remembered them the next day. Dr. Jimena Mora and Dr. Emmanuel Odella, thank you for always being there to give me a hand, for all the lunch hours, and all your support. Edgar Reyes, thank you for the laughs, memes, and for reminding me that life shouldn't always be taken so seriously. Dr. Marely Tejeda, thank you for being there right from the beginning, all the years of friendship, laughs, tears, trips, and all the other moments we shared together. Dr. Amanda Young-Gonzales, thank you for always listening, and for all the judging (but not really—maybe a little).

To Eric Dunn, thank you for the unconditional support, for believing in me and making me believe in myself. Thank you for all the times we've had together, for caring for me and doing everything you can to make my life better.

Agradezco a mi familia que ha sido una parte fundamental en estos años. Gracias, papá, por tu apoyo y estar ahí cuando lo necesité. Gracias, hermano, por tus consejos, enseñarme a ver por mi mismo, y hacerme ver que todo se puede, sólo falta tener fe. Por último, agradezco a mi mamá: haría falta cien de estas tesis para empezar a describir todo lo que has hecho por mí; gracias por creer en mí, estar conmigo en todo momento, apoyar mis decisiones, echarme porras, cuidarme, pero, sobre todo, por tu amor incondicional. ¡Los amo mucho!

TABLE OF CONTENTS

CHAPTER Page

LIST OF FIGURES

Figure Page

Figure Page

LIST OF TABLES

LIST OF SCHEMES

LIST OF ABBREVIATIONS

Abbreviation	Description
Acm	acetamidomethyl
AIBN	(*E*)-2,2′-(diazene-1,2-diyl)bis(2-methylpropanenitrile)
AscOH	ascorbic acid
AUC	Analytical Ultracentrifugation
bpy	2,2′-bipyridine
n-BuLi	*n*-butyl lithium
CD	Circular Dichroism spectroscopy
CMBP	2-(tributyl-λ^5-phosphaneylidene)acetonitrile
CoPPIX	cobalt protoporphyrin IX
COSY	Correlation Spectroscopy
cyt b_{562}	cytochrome b_{562}
DABCO	1,4-diazabicyclo[2.2.2]octane
dba	dibenzylideneacetone
DCE	1,2-dichloroethane
DCM	dichloromethane
DIAD	diisopropyl azodicarboxylate
DIBAL	diisobutylaluminum hydride
DIEA	*N*-ethyl-*N*-(propan-2-yl)propan-2-amine
DMEDA	*N*,*N*′-dimethylethane-1,2-diamine
DMF	*N*,*N*-dimethylformamide
DMSO	dimethyl sulfoxide
DPPA	diphenyl phosphorazidate
DSD	Domain Swapped Dimeric Three Helix Bundle

Abbreviation	Description
DSS	sodium 4,4-dimethyl-1-silapentane-1-sulfonate
DTT	dithiotreitol
EDT	1,2-ethanedithiol
EDTA	ethylenediaminotetraacetic acid
Et_2O	ethoxyethane
EtOAc	ethyl acetate
FID	Flame Ionization Detector
Fmoc	fluorenylmethyloxycarbonyl
FPLC	Fast Protein Liquid Chromatography
Gdn · HCl	guanidinium hydrochloride
H2BC	Heteronuclear Two-Bond Correlation
HBTU	*N*,*N*,*N*′,*N*′-tetramethyl-*O*-(1*H*-benzotriazol-1-yl)uronium hexafluorophosphate
HMBC	Heteronuclear Multiple Bond Correlation
HOBt	1-hydroxybenzotriazole
HSQC	Heteronuclear Single Quantum Coherence
ICP-OES	Inductively Coupled Plasma-Optical Emission Spectroscopy
Im_2CO	di(1*H*-imidazol-1-yl)methanone
Im_2CS	di(1*H*-imidazol-1-yl)methanethione
IPTG	β-D-thiogalactopyranoside
K_d	dissociation constant
KP_i	potassium phosphate
m. p.	melting point
MALDI	Matrix-Assisted Laser Desorption/Ionization

Abbreviation	Description
MS	Mass Spectrometry
NBS	*N*-bromosuccinimide
NHE	Normal Hydrogen Electrode
NiCA	[(*N*-benzyl-L-prolyl-κN)(2-{(*E*)-[(carboxylato-κO-methyl)imino-κN](phenyl)methyl}phenyl)azanido-κN]nickel
NMP	*N*-methyl-2-pyrrolidinone
NMR	Nuclear Magnetic Resonance
OD_{600}	Optical Density measured at 600 nm
PMB	(4-methoxyphenyl)methyl
r. t.	room temperature
R_f	retention factor
RP-HPLC	Reverse Phase High-Performance Liquid Chromatography
SPPS	Solid Phase Peptide Synthesis
TBAF	tetrabutylammonium fluoride
TCD	Thermal Conductivity Detector
TCEP · HCl	tris(2-carboxyethyl)phosphine hydrochloride
TFA	trifluoroacetic acid
THF	tetrahydrofuran
TIS	triisopropylsilane
TLC	Thin Layer Chromatography
T_m	melting temperature
TMSCl	trimethylsilyl chloride
TMSE	2-(trimethylsilyl)ethyl
TOF	Time of Flight

Abbreviation	Description
TON	turnover number
t_{R}	retention time
Tris	2-amino-2-(hydroxymethyl)propane-1,3-diol
Tris · HCl	2-amino-2-(hydroxymethyl)propane-1,3-diol hydrochloride
TsOH	4-methylbenzenesulfonic acid
UV	ultraviolet
UV-Vis	Ultraviolet-Visible spectroscopy
WT	wild type

CHAPTER 1

PREFACE

As the world population continues to exponentially grow, global energy demand increases apace. In the World Energy Outlook, the International Energy Agency projects that the world's yearly energy demand will rise by 27 %, from nearly 163 PW h in 2017 to 206 PW h by 2040. Almost 75 % of that energy demand will be met by carbon-based fuels. The use of these fuels has led to currently unprecedented atmospheric levels of CO_2,[1,2] a greenhouse gas that has detrimental effects in the environment, including an increase of Earth's surface and ocean's temperature, melting of ice sheets, and rise of sea levels.[2,3] Forecasts indicate that energy-related CO_2 production from human activities will increase to 36 Gt y^{-1} by 2040,[1] thus aggravating these environmental effects. As a response to this problem, several lines of research aim to discover or improve alternative renewable fuel production processes.

One of such ideas is to use molecular hydrogen as a fuel source, as this gas has more chemical energy per mass than liquid fuels (142 MJ kg^{-1} vs 47 MJ kg^{-1}), and its sole combustion product is water vapor (Reaction R-1.1).[4] However, despite hydrogen being the most abundant element on Earth, only about 1 % of it can be found in its molecular form.[4] As such, the use of hydrogen gas as combustible is limited by the methods that are used to produce it.

$$2\,H_2\,(g) + O_2\,(g) \longrightarrow 2\,H_2O\,(g) \qquad \text{(R-1.1)}$$

The majority of hydrogen gas is currently produced by methane steam reforming.[5] The process consists of a reaction between steam and methane to yield a mixture of carbon monoxide and hydrogen gas known as syngas. Carbon monoxide

and steam can later react to form carbon dioxide and hydrogen gas.[6] This practice is energy intensive and relies on the use of fossil fuels, diminishing the environmental benefits of the use of hydrogen as fuel. Other methods of production involve the electrolytic splitting of water into its elemental components; however, this feat requires catalysts such as platinum in order to be carried out efficiently.[4,6]

Another approach to the production of renewable fuels is to close the carbon cycle by taking the CO_2 that human activity produces and to reduce it back into usable fuels, such as methanol, methane, or other higher hydrocarbons. Unfortunately, this process currently requires hydrogen gas or high temperatures.[7] Additionally, carbon dioxide has a number of reduction products depending on the number electrons involved in the reaction, availability of protons, reduction potential, and other reaction conditions (Table 1.1).[8]

Table 1.1. Standard Reduction Potentials of CO_2.[8]

Reaction	$E^{\circ\prime}/\mathrm{V}$[a]
$CO_2 + e^- \longrightarrow CO_2^{\bullet -}$	-1.9
$CO_2 + 2\,H^+ + 2\,e^- \longrightarrow CO$	-0.53
$CO_2 + 2\,H^+ + 2\,e^- \longrightarrow HCO_2H$	-0.61
$CO_2 + 4\,H^+ + 4\,e^- \longrightarrow C + 2\,H_2O$	-0.20
$CO_2 + 4\,H^+ + 4\,e^- \longrightarrow HCHO + H_2O$	-0.48
$CO_2 + 6\,H^+ + 6\,e^- \longrightarrow CH_3OH + H_2O$	-0.38
$CO_2 + 8\,H^+ + 8\,e^- \longrightarrow CH_4 + 2\,H_2O$	-0.24

[a] In aqueous solution, pH 7, vs NHE.

To circumvent these limitations, it is necessary to come up with cost-effective methods that allow the production of hydrogen gas or the selective

reduction of CO_2 into usable fuels. Furthermore, these new methods should not rely on the use of fossil fuels for them to be environmentally beneficial.

At an average rate of 120 EW at the Earth's surface, solar power represents an abundant, accessible, and sustainable source of energy. Nature makes use of sunlight through photosynthesis, in which energy from light is stored in chemical bonds at an estimated global rate of 120 TW. However, solar energy is diffuse (about 100 mW cm^{-2}) and is limited to daylight hours.[9] Thus, if solar power is to be utilized to reduce protons into hydrogen gas, or CO_2 into other fuels, it is crucial to develop a system that can not only capture the sunlight, but also efficiently transform it into the desired products.

Ideally, an optimized catalyst would minimize the energy requirements to carry out the reactions by providing a suitable environment that stabilizes the transition state. A large number of organometallic small molecule catalysts have been prepared and studied over the last decades that can perform proton reduction and CO_2 reduction. Nonetheless, most of these catalysts must operate in organic solvents, need external acids as proton sources, and often function only at highly negative electrochemical potentials.

Millions of years of natural evolution have produced an arsenal of catalysts in the form of enzymes that incorporate organometallic active sites embedded in a protein matrix. Some of these enzymes, namely hydrogenases, can catalyze the reduction of protons into molecular hydrogen, whereas other enzymes of interest are involved in the reduction of CO_2, such as carbon monoxide dehydrogenase, which catalyzes the interconversion between CO_2 and CO, or formylmethanofuran dehydrogenase, which reduces CO_2 to formylate methanofuran during an early stage of methanogenesis. These catalysts operate in aqueous conditions, are finely

tuned to operate at physiological pH, and have higher turnover numbers than their small molecule counterparts.

Unfortunately, the direct use of these biological catalysts is not always straightforward. For instance, the expression of some of these enzymes often requires a complex biosynthetic machinery for their assembly, hampering the ability to express them recombinantly and resulting in low yields. Additionally, their large sizes result in low current density, as less molecules can be adsorbed into a surface at the same time. The presence of labile metal complexes typically requires the experiments to be carried out under anoxygenic conditions, which demands a physical separation of the reductive reaction center from their oxidative counterpart. Finally, the naturally occurring enzymes are only amenable to certain reactions and to include certain cofactors, limiting their use to such native active sites.

To circumvent these problems, our research group focuses on designing and evaluating protein-based architectures that are capable of catalyzing these chemical transformations in mild aqueous conditions while using light as a primary energy source. This type of reactions can be broken down into three main components: 1) the catalytic site, 2) an electron transfer relay, and 3) the photosensitizer. By following a modular approach, it is possible to evaluate and optimize each of them independently, thus the need for a strategy to integrate them together into a single architecture in order to increase the overall efficiency of the whole system.

This dissertation explores the latter by offering a strategy that can be utilized to control the assembly of the described components into an oligomeric entity in Chapter 2. The strategy presented herein is based on the rational modification of a robust dimeric peptide with a 2,2′-bipyridine moiety. By doing so, it is possible drive their assembly into a hexameric structure (i.e. a trimer of dimers) through the formation of divalent metal tris(bipyridine) complexes.[10]

Further, Chapters 3 and 4 describe the use and development of two different strategies for the incorporation of catalysts into protein scaffolds. Particularly, Chapter 3 details the design of cytochrome b_{562} mutants that incorporate cobalt protoporphyrin IX with aims at catalyzing the reduction of protons and CO_2 upon irradiation in the presence of a photosensitizer. More specifically, this work evaluated the effects of axial coordinating residues on the activity of the embedded catalyst in an aqueous environment.

Finally, Chapter 4 focuses on an alternative tool that allows the incorporation of a variety of organometallic mimics that cannot be found in nature. The proposed synthetic approach is inspired by the active site of natural enzymes capable of catalyzing the reversible reduction of protons into hydrogen gas, specifically [FeFe]-hydrogenases (Reaction R-1.2). This work details the synthesis of an unnatural amino acid, (*S*)-2-amino-3-(3,4-disulfanylphenyl)propanoic acid, which can act as a bridging ligand in diiron complexes that are catalytically active toward proton reduction.

$$2\,H^+ + 2\,e^- \rightleftharpoons H_2 \tag{R-1.2}$$

1.1 References

1. International Energy Agency. World Energy Outlook 2018. https://www.iea.org/weo/ (accessed 02/12/2019) (cit. on p. 1).

2. Allen, M.; Dube, O.; Solecki, W.; Aragón-Durand, F.; Cramer, W.; Humphreys, S.; Kainuma, M.; Kala, J.; Mahowald, N.; Mulugetta, Y.; Perez, R.; M.Wairiu; Zickfeld, K. Framing and Context. In *Global Warming of 1.5°C. An IPCC Special Report on the impacts of global warming of 1.5°C above pre-industrial levels and related global greenhouse gas emission pathways, in the context of strengthening the global response to the threat of climate change, sustainable development, and efforts to eradicate poverty*, Masson-Delmotte, V., Zhai, P., Pörtner, H.-O., Roberts, D., Skea, J., Shukla, P., Pirani, A., Moufouma-Okia, W., Péan, C., Pidcock, R., Connors, S., Matthews, J., Chen, Y., Zhou, X., Gomis, M., Lonnoy, E., Maycock, T., Tignor, M., Waterfield, T., Eds.; In Press: 2018 (cit. on p. 1).

3. Stips, A.; Macias, D.; Coughlan, C.; Garcia-Gorriz, E.; Liang, X. S. On the causal structure between CO_2 and global temperature. *Scientific Reports* **2016**, *6*, 21691 (cit. on p. 1).

4. Schlapbach, L.; Züttel, A. Hydrogen-storage materials for mobile applications. *Nature* **2001**, *414*, 353 (cit. on pp. 1, 2).

5. Turner, J. A. Sustainable Hydrogen Production. *Science* **2004**, *305*, 972 (cit. on p. 1).

6. Barelli, L.; Bidini, G.; Gallorini, F.; Servili, S. Hydrogen production through sorption-enhanced steam methane reforming and membrane technology: A review. *Energy* **2008**, *33*, 554–570 (cit. on p. 2).

7. Mikkelsen, M.; Jørgensen, M.; Krebs, F. C. The teraton challenge. A review of fixation and transformation of carbon dioxide. *Energy & Environmental Science* **2010**, *3*, 43–81 (cit. on p. 2).

8. Fujita, E. Photochemical carbon dioxide reduction with metal complexes. *Coordination Chemistry Reviews* **1999**, *185-186*, 373–384 (cit. on p. 2).

9. Moore, G. F.; Brudvig, G. W. Energy Conversion in Photosynthesis: A Paradigm for Solar Fuel Production. *Annual Review of Condensed Matter Physics* **2011**, *2*, 303–327 (cit. on p. 3).

10. Alcala-Torano, R.; Walther, M.; Sommer, D. J.; Park, C. K.; Ghirlanda, G. Rational design of a hexameric protein assembly stabilized by metal chelation. *Biopolymers* **2018**, *109*, e23233 (cit. on p. 4).

CHAPTER 2

RATIONAL DESIGN OF A HEXAMERIC PROTEIN ASSEMBLY STABILIZED BY METAL CHELATION

2.1 Abstract

Protein-based self-assembled nanostructures hold tremendous promise as smart materials. One strategy to control the assembly of individual protein modules takes advantage of the directionality and high affinity bonding afforded by metal chelation. Here, we describe the use of 2,2′-bipyridine units (bpy) as side chains to template the assembly of large structures (MW approx. 35 000 Da) in a metal-dependent manner. The structures are trimers of independently folded 3-helix bundles, and are held together by 2 $Me(bpy)_3$ complexes. The assemblies are stable to thermal denaturation, and are more than 90 % helical at 90 °C. Circular dichroism spectroscopy shows that one of the 2 possible $[M(bpy)_3]^{2+}$ enantiomers is favored over the other. Because of the sequence pliability of the starting peptides, these constructs could find use to organize functional groups at controlled positions within a supramolecular assembly.

2.2 Introduction

The formation of protein-based supramolecular assemblies plays a fundamental role in biological processes, such as in the structure of the cytoskeleton and intracellular compartments, or support for the life cycle of viruses.[1,2] Inspired by this complex set of functions, protein engineers have sought to generate supramolecular structures with novel functionalities by learning to control self-assembly and by exploiting symmetry.[3–17]

The use of metal binding motifs offers an attractive methodology to direct the assembly of smaller subunits into well-ordered systems, with the advantage of such association being dependent on presence of the metal and independent of intricate sequence-coded protein-protein interactions.[18–26] Further, this strategy allows the incorporation of metal-mediated functionality such as catalysis, redox activity, and electron transfer.[11,12,27–30] Beyond the metal-ligation properties of natural amino acids, chelating ligands such as 2,2′-bipyridine (bpy) are very attractive as means to mediate metal coordination and guide protein assemblies because they form high-affinity metal complexes with well-defined geometry and symmetry. Since the first reports using tris(2,2′-bipyridine) metal complexes to template the formation of three-helix bundles, this functionality has been used extensively as a structural element to stabilize trimeric entities upon addition of metal cations such as Fe^{2+}, Co^{2+}, and Ni^{2+}.[23,31–36] In a remarkable use of this ligand, by controlling the identity of the metal ion—thus the kinetics of ligand exchange—it was possible to select the most stable sequences for three helix bundles via formation of dynamic libraries.[18,37] Incorporating tris(bipyridine)ruthenium(II) directly in homotrimers has also allowed for simple systems to study electron transfer.[38,39] In these systems, the use of a single solvent-exposed metal binding site at the termini of a peptide led to multiple backbone conformations, in some cases allowing for the presence of multiple folds.[32]

This work makes use of metal chelation by bpy units to template the formation of a "trimer of dimers" assembly formed by nine helices, six of which are located in the central cavity—henceforth referred to as the "super-core", and three of which dock against this central ring (Figure 2.1). The hexamer is highly symmetric, with the central six helices arranged in an antiparallel fashion and displaying D_3 symmetry and containing an additional pseudo 2-fold symmetry axis. At the

structural level, the assembly is obtained by oligomerization of three-helix bundles, each formed by a dimer of a helix-loop-helix motif, in which one of the helices is about half the length of the other. The design is derived from the sequence of Hex-Phe,[40] which was in turn based on the sequence of a Domain Swapped Dimeric Three Helix Bundle (DSD) that formed hexamers in the crystal structure but not in solution.[41] DSD comprises a leucine-rich hydrophobic core and salt bridges positioned at the helix-helix interfaces to impart specificity, resulting in remarkable stability to chemical and thermal denaturation. Exploiting its unusual pseudo 2-fold symmetry, our group has used DSD as scaffold to generate mimics of ferredoxin by incorporating pairs of iron-sulfur clusters at controlled distances.[27,28,42]

Introducing hydrophobic residues in the solvent-exposed side of the long helices modulates the formation of DSD trimers in a sequence-dependent manner. Briefly, Hex-Phe utilized aromatic interactions to stabilize the super-core of the

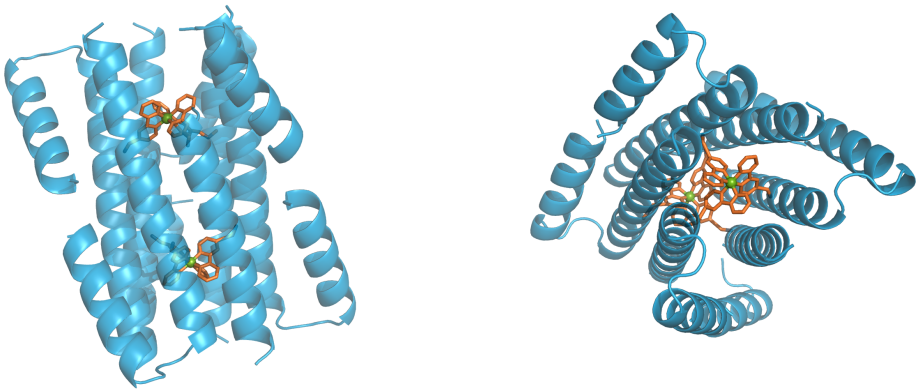

DSD	S LAALKSE LQALKKE GFSPEE LAALESE LQALEKK LAALKSK LQALKG
Hex-Phe	S LAALKSE LQALKKE GFSPEE LAALESF LQALEKW LAALKSF LQALKG
HB1	S LAALKSE LQALKKE GFSPEE LAALESC LQALEKA LAALKSF LQALKG
HB2	S LAALKSE LQALKKE GFSPEE LAALESC LQALEKA LAALKSA LQALKG

Figure 2.1. Model of the hexameric assembly stabilized by bpy-mediated metal chelation (top) and sequences of the prepared peptides (bottom).

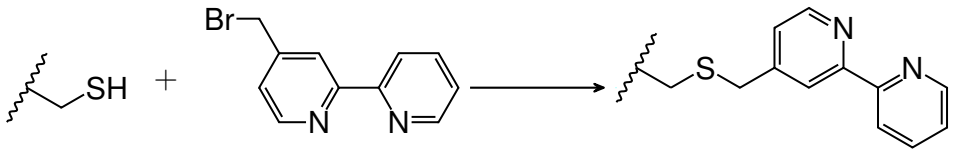

Cys side chain **2-1** bpy modified residue

Figure 2.2. Reaction between the cysteine side chain and **2-1** to form the bpy tagged peptides.

α-helical assembly observed in the crystal structure of DSD, resulting in spontaneous formation of the hexamer in solution. We speculated that replacement of one of the aromatic residues per monomer with a bpy unit results in positioning two sets of trimers at the super-core, at distances compatible with formation of $M(bpy)_3$ complexes. We designed two sequences, HB1 and HB2, differing by the number of aromatic residues predicted to be in the super-core of the hexamer, each containing a cysteine residue through which a bpy unit can be linked by nucleophilic substitution of 4-bromo-2,2′-bipyridine (**2-1**, Figure 2.2). We found that both sequences formed preferentially stable hexamers over dimers in the presence of divalent transition metals, and that the magnitude of the effect is dependent on the sequence of the peptide.

2.3 Materials and Methods

2.3.1 Synthesis of 4-bromomethyl-2,2′-bipyridine

Solvents and reagents were purchased from Sigma-Aldrich. Dry solvents were purchased from Sigma-Aldrich in Sure Seal® bottles. Standard Schlenk techniques were used for air and moisture sensitive reactions. Diisopropylamine was distilled over CaH_2, and used within 24 h. Pyridine was distilled at atmospheric pressure over KOH. Nuclear Magnetic Resonance (NMR) data were obtained on a Varian MR400 400 MHz instrument at 25 °C and are referenced to the solvent peak

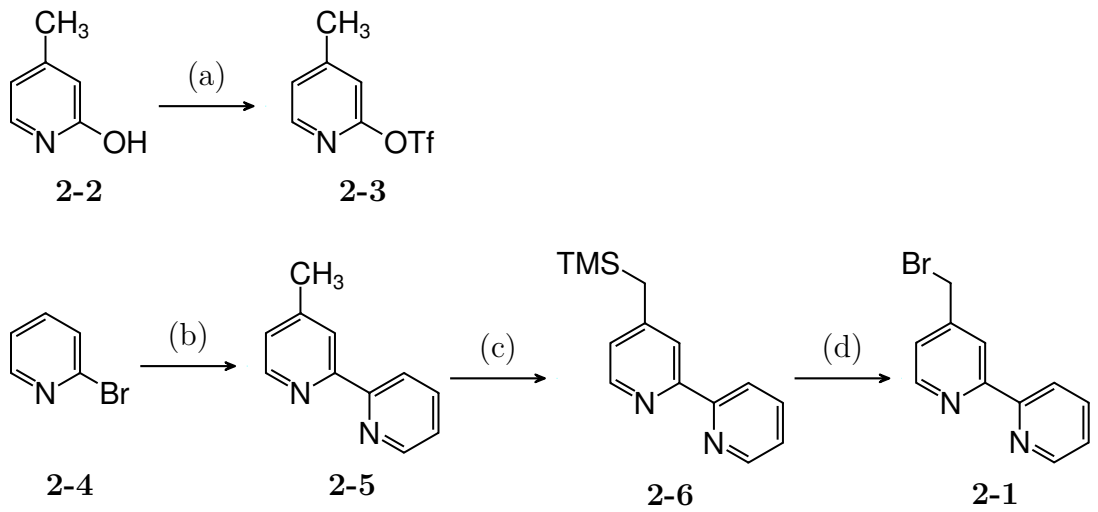

Scheme 2.1. Synthetic route for **2-1**. (a) Tf_2O, pyridine, 0 °C; (b) *i*) *n*-BuLi, THF, −78 °C, *ii*) $ZnCl_2$, *iii*) LiCl, **2-3**, $[Pd(PPh_3)_4]$, r. t. to reflux; (c) $^iPr_2NLi$, TMSCl, THF, −78 °C; (d) $C_2Br_2F_4$, CsF, DMF, r. t.

($CDCl_3$ at 7.26 ppm); all chemical shifts are given in ppm. 4-Bromomethyl-2,2′-bipyridine (**2-1**) was prepared in several steps by Negishi coupling as described before (Scheme 2.1).[43]

4-Methylpyridin-2-yl trifluoromethanesulfonate (2-3). Under nitrogen atmosphere, 2-hydroxy-4-methylpyridine (**2-2**, 5.0 g, 45.8 mmol) was dissolved in pyridine (135 mL). The brown solution was cooled to 0 °C and trifluoromethanesulfonic anhydride (18.6 mL, 110.6 mmol) was added dropwise. After 1.5 hours, water (50 mL) was added to quench the reaction and dissolve the formed white precipitate. The solution was extracted with dichloromethane (DCM, 5 × 200 mL). The organic layers were combined, dried over $MgSO_4$, and the solvent evaporated at reduced pressure to give a dark brown oil. The pure product was obtained by silica gel column chromatography using hexane/ethyl acetate/triethylamine 89:10:1 as solvent system to yield a colorless oil (10.5 g, 95 %). ^{1}H NMR (400 MHz, $CDCl_3$): δ 8.24 (d, 1 H, $J = 5.1$ Hz), 7.20 (d, 1 H, $J = 5.1$ Hz), 7.00 (s, 1 H), 2.45 (s, 3 H).

4-Methyl-2,2'-bipyridine (2-5). In a three-neck round bottom flask with a nitrogen inlet and a reflux condenser, 2-bromopyridine (**2-4**, 1.0 mL, 10.3 mmol) was dissolved in anhydrous THF (20 mL) under nitrogen. The solution was cooled down to −78 °C and *n*-butyl lithium (*n*-BuLi, 1.6 M in hexanes, 11.9 mL, 19.0 mmol) was added dropwise to give a dark red solution. The mixture was stirred for 30 minutes and was let to warm up to room temperature, at which point $ZnCl_2$ (3.5 g, 25.8 mmol) was added. While the reaction was stirred for 2 hours at room temperature, a solution of $[Pd(PPh_3)_4]$ was prepared by mixing $[Pd_2(dba)_3]$ (dba = dibenzylideneacetone) (259 mg, 0.28 mmol) and triphenylphosphine (0.71 g, 2.71 mmol) in anhydrous THF (10 mL). After the first reaction was stirred for 2 h, lithium chloride (0.9 g, 21.0 mmol), **2-3** (2.0 g, 8.33 mmol), and the freshly prepared $[Pd(PPh_3)_4]$ solution were added, and the brown-red solution was refluxed overnight under nitrogen. A solution of ethylenediaminotetraacetic acid (EDTA, 10 % w/v, 200 mL) was then added, followed by a saturated solution of $NaHCO_3$ (600 mL). The aqueous layer was extracted with DCM (3 × 200 mL), the organic layers combined, dried over $MgSO_4$, and the solvent evaporated under reduced pressure. The obtained brown oil was purified by column chromatography on silica gel using hexane/ethyl acetate/triethylamine 79:20:1 as eluent, giving the pure product as a yellow oil that rapidly crystallized as a white solid upon standing (1.36 g, 96 %). ^{1}H NMR (400 MHz, $CDCl_3$): δ 8.68 (d, 1 H, J = 4.6 Hz), 8.54 (d, 1 H, J = 5.0 Hz), 8.39 (d, 1 H, J = 7.9 Hz), 8.23 (s, 1 H), 7.81 (d, 1 H, J = 7.6 Hz), 7.30 (m, 1 H), 7.14 (d, 1 H, J = 4.9 Hz), 2.44 (s, 3 H).

4-(Trimethylsilyl)methyl-2,2'-bipyridine (2-6). A nitrogen flushed 100 mL round flask was charged with diisopropylamine (2.4 mL, 17.0 mmol) in dry THF (10 mL). The solution was cooled to −78 °C and *n*-BuLi (1.6 M in hexanes, 10.2 mL, 16.3 mmol) is added dropwise. After 10 min, the mixture was slowly

warmed up to 0 °C, stirred for another 10 min, and cooled down again to −78 °C. A solution of **2-5** (2.59 g, 15.2 mmol) in 10 mL of anhydrous THF (10 mL) was then added dropwise to obtain a thick maroon solution. The resulting mixture was stirred for 80 min, after which trimethylsilyl chloride (TMSCl, 2.2 mL, 17.3 mmol) was added, turning the solution blue. The reaction was quenched by a slow addition of 5 mL of absolute ethanol. The cold reaction was then transferred to a separatory funnel, washed with a saturated solution of $NaHCO_3$ (40 mL), and the aqueous layer extracted with DCM (4 × 50 mL). The organic fractions were combined, dried over $MgSO_4$, and evaporated under reduced pressure to obtain an orange oil. The crude product was purified by column chromatography in silica gel using hexanes/ethyl acetate/triethylamine 89:10:1 as mobile phase to give a colorless oil (1.62 g, 44 %). ^{1}H NMR (400 MHz, $CDCl_3$): δ 8.68 (m, 1 H), 8.47 (d, 1 H, $J = 5.0$ Hz), 8.38 (d, 1 H, $J = 8.0$ Hz), 8.06 (s, 1 H), 7.80 (td, 1 H, $J = 1.8, 7.8$ Hz), 7.29 (m, 1 H), 6.95 (dd, 1 H, $J = 1.6, 5.0$ Hz), 2.22 (s, 2 H), 0.04 (s, 9 H).

4-Bromomethyl-2,2'-bipyridine (2-1). In a 100 mL round bottom flask under nitrogen atmosphere in the dark, cesium fluoride (0.91 g, 5.99 mmol) and 1,2-dibromotetrafluoroethane (1.54 g, 5.93 mmol) were added to a solution of **2-6** (0.70 g, 2.89 mmol) in anhydrous *N*,*N*-dimethylformamide (DMF, 25 mL). The reaction was stirred at room temperature overnight to obtain an orange solution. The reaction was washed with water (150 mL) and extracted with ethyl acetate (3 × 100 mL). The organic layers were combined, washed with brine (100 mL), dried over $MgSO_4$, and the solvent is removed under reduced pressure. The crude brown oil is purified by silica gel column chromatography using hexane/ethyl acetate/triethylamine 79:20:1 to give a colorless oil (0.65 g, 90 %). ^{1}H NMR (400 MHz, $CDCl_3$): δ 8.71 (m, 1 H), 8.67 (d, 1 H, $J = 5.0$ Hz), 8.42 (m, 2 H), 7.84 (m, 1 H), 7.34 (m, 2 H), 4.49 (s, 2 H).

2.3.2 Peptide Synthesis and Purification

All peptides were synthesized by automated microwave-assisted Solid Phase Peptide Synthesis (SPPS) on a Liberty instrument (CEM Corporation). The synthesis was carried out using standard Fmoc protection procedures. Briefly, Rink Amide resin was deprotected using 0.1 M 1-hydroxybenzotriazole (HOBt) in a 20 % v/v piperidine in DMF solution. Amino acid couplings were achieved using 0.45 M *N*,*N*,*N*′,*N*′-tetramethyl-*O*-(1*H*-benzotriazol-1-yl)uronium hexafluorophosphate (HBTU) in DMF, 2 M *N*-ethyl-*N*-(propan-2-yl)propan-2-amine (DIEA) in *N*-methyl-2-pyrrolidinone (NMP), and 0.2 M fluorenylmethyloxycarbonyl (Fmoc) protected amino acid (Novabiochem), followed by microwave irradiation to pre-established temperatures according to CEM protocols. Peptides were acetylated at the *N*-terminus via addition of acetic anhydride under coupling conditions. The peptides were cleaved from the resin using 94 % trifluoroacetic acid (TFA), 2.5 % water, 2.5 % 1,2-ethanedithiol (EDT), and 1 % triisopropylsilane (TIS) for 3 h. The solution was then evaporated under a stream of N_2, and the peptide was precipitated with cold ether. Crude, lyophilized peptides were purified using preparatory-scale HPLC on a C18 reverse-phase column, with a linear gradient of Solvent A (99.9 % water with 0.1 % TFA) and Solvent B (95 % acetonitrile, 4.9 % water, and 0.1 % TFA) at a flow rate of 10 mL min^{-1}. Peptide identity was confirmed by MALDI-TOF-MS; peptides were >99 % pure as assessed by C18 analytical Reverse Phase High-Performance Liquid Chromatography (RP-HPLC).

2.3.3 Conjugation

The synthesized peptide (7.0 mg, 1.4 µmol) was dissolved in guanidinium hydrochloride (Gdn · HCl, 6 M)/2-amino-2-(hydroxymethyl)propane-1,3-diol (Tris, 100 mM)

buffer at pH 9.6. A solution of tris(2-carboxyethyl)phosphine hydrochloride (TCEP · HCl, 20.8 mg, 73 µmol) in this same buffer (2 mL) was added, and the mixture was heated to 70 °C for 30 min. A solution of **2-1** (23.6 mg, 95 µmol) in buffer/acetone (4:1 by volume) was added and the reaction was stirred at 70 °C overnight. The peptide was then purified by preparative RP-HPLC as described above.

2.3.4 Metal Incorporation and Quantification

Divalent metal ions were incorporated into peptide variants by adding an excess amount (20 eq) of the metal chloride salt ($CoCl_2 \cdot 6\,H_2O$ or $NiCl_2 \cdot 6\,H_2O$, respectively) in Gdn · HCl (6 M)/ Tris (100 mM) buffer at pH 7.5. The mixture was incubated overnight at 4 °C. The resulting dark brown solution was subjected to desalting with a PD10 G25 column (GE Healthcare) that was pre-equilibrated with 100 mM Tris at pH 7.5 to obtain the holo protein.

2.3.5 Gel Filtration

Size exclusion chromatography was performed on a G-25 gel filtration column fit to an Agilent Technologies 1260 Insight Fast Protein Liquid Chromatography (FPLC) system. The column was pre-equilibrated in 100 mM Tris pH 7.5, and 200 µL of 150 µM apo or holo peptide were used for each injection.

2.3.6 Analytical Ultracentrifugation

Sedimentation velocity experiments were carried out with a Beckman Coulter XL-I instrument equipped with a monochromator and interference scanning optics (632 nm) using a Ti-50 rotor as described before.[44] Briefly, analytical ultracentrifugation cells were loaded with 420 µL of the samples at starting concentration

of approximately ∼100 µM and allowed to equilibrate for 2 h at 4 °C. The buffers used in the measurements contained 10 mM 2-amino-2-(hydroxymethyl)propane-1,3-diol hydrochloride (Tris · HCl) pH 8.5 and 479 µM $CoCl_2$ or $NiCl_2$, where relevant. The samples were spun at 40 000 rpm (115 000*g*) and absorbance scans were taken continuously at 298 nm (Co-HB1 and Ni-HB1), 290 nm (Hex-Phe), or 286 nm (HB1 and HB2), respectively, with a 0.003 cm step size, until the last of the boundaries had moved to the bottom of the solution column (at least 12 h). Data was reduced using Sedfit[44] using calculated values for buffer viscosity and density from SEDNTERP. C(s) analysis was used to determine relative amounts and sizes of species observed.

Sedimentation equilibrium experiments were carried out with a Beckman XL-I and Ti-50 rotor at 4 °C. Briefly, samples (110 µL) containing varied concentrations of sample (0.1–0.8 mg mL^{-1}) were loaded into 3 chambers of a 6-chamber centerpiece, with buffer in each of the remaining 3. The samples were then subjected to centrifugal speeds of 14 000, 20 000, and 26 000 rpm for a period of 72–96 h. Equilibrium was established when a reasonable (<0.07) and constant rmsd was found between sequential scans 4 hours apart. High resolution scans were taken at various wavelengths (280, 282, and 298 nm), with a radial step size of 0.001 cm. The data were analyzed using global fitting in Sedfit with a single species. Buffer density was calculated from SEDNTERP and partial specific volumes were determined from the sequence.

2.3.7 Circular Dichroism Spectroscopy

Spectra were recorded on a JASCO J-815 spectropolarimeter in the range of 190–260 nm or 300–400 nm. Data were recorded every 1 nm and averaged over 3 scans. The concentration of apo and holo-peptides was kept at 50 µM in 100 mM Tris,

pH 7.5. Chemical denaturation titrations were carried out through addition of an 8 M stock solution of Gdn · HCl, followed by mixing and incubation for 5 min to allow for equilibration. Holo peptide was titrated under anaerobic conditions. Spectra were normalized to protein concentration in the sample and converted to fraction folded relative to the apo or holo protein signal, which lacked Gdn · HCl.

2.4 Results and Discussion

2.4.1 Protein design and synthesis

Starting with the crystal structure of DSD (PDB ID 1G6U), we chose position 28, which is found in the super-core, for attachment of a bpy moiety via conjugation to a cysteine residue. The octahedral metal-chelated $[M(bpy)_3]^{2+}$ complex can exist as two enantiomers, the Δ and Λ, with coordinates available from the Cambridge Structural Database (CSD ID Co^{2+}: BPCOFC10, Ni^{2+}: ADOCOM).[45] Each complex was modeled in Pymol and functionalized with a methyl group in position 4, which will provide the chemical moiety for conjugation to the thiol moiety of cysteine upon nucleophilic attack. We manually docked each pre-formed complex within the super-core within the chosen layer. We then explored the possible rotamers of Cys28 in helical conformation to identify the ones that placed the thiol at a distance compatible with ligation to the methyl group. We found that the Δ enantiomer was a better fit for the super-core. Because of the D_3 pseudosymmetry of the assembly, this operation results in the creation of two metal binding sites in the super-core (Figure 2.1). To explore the interplay between aromatic interactions and metal chelation in forming a stable assembly, two versions of the peptide were designed. Compared to Hex-Phe, HB1 conserves a phenylalanine residue at position

42 while HB2 contains an alanine at that position. The remaining position at the super-core, 35, was also mutated to alanine to relieve steric clashes.

Peptides corresponding to HB1 and HB2 were readily synthesized utilizing microwave-assisted solid phase peptide synthesis followed by purification via reverse-phase HPLC purification on a C18 analytical and semi-prep column. 4-Bromomethyl-2,2′-bipyridine (**2-1**)was synthesized via Negishi cross-coupling following published protocols.[43] Coupling of 4-bromomethyl-2,2′-bipyridine to cysteine 28 of each peptide was carried out overnight at 70 °C in highly denaturing conditions (6 M Gdn · HCl) to ensure peptide unfolding, under argon and in buffered reducing conditions. The products, HB1 and HB2, were purified by reverse-phase HPLC and verified by MALDI-TOF-MS (Figure A.1).

2.4.2 Protein characterization and metal binding

The incorporation of bipyridine moieties is also verified by the presence in the Ultraviolet-Visible spectroscopy (UV-Vis) spectra of apo HB1 and HB2 of absorption bands corresponding to the intraligand $\pi \rightarrow \pi^*$ transition at 244 and 286 nm characteristic of bipyridine, which overlaps with the aromatic residues (Figures 2.3 and A.2). When the peptides were reconstituted with Ni^{2+} and Co^{2+}, the $\pi \rightarrow \pi^*$ absorption bands underwent a characteristic red shift to 298 nm (Ni^{2+}) and 297 nm (Co^{2+}), respectively, with shoulders visible at 307 nm.[46] A binding stoichiometry of 2.8 and 3.4 peptides per metal respectively was obtained by titrating $CoCl_2$ and $NiCl_2$ into of HB2 (Figure 2.4), and of 3.4 and 3.5 into HB1 (Figure A.3). No changes were observed in titrating Hex-Phe, used as control, with Ni^{2+} and Co^{2+}, indicating that other amino acids on the peptide scaffold do not interact with divalent metals (Figures A.7 and A.8).

Both peptides fold into structures with high helical content in solution, as indicated by the two peaks at 208 and 222 nm in the far-UV Circular Dichroism spectroscopy (CD) data, typical of α-helical peptides (Figures 2.5 and A.4), suggesting that incorporation of the bipyridine ligand into the peptide structure did not affect the overall structure relative to the parent peptides DSD and Hex-Phe. Reconstitution of HB1 and HB2 with Ni^{2+} and Co^{2+} results in preservation of the α-helical content, indicating that the structure of the peptides was maintained. In the case of NiHB2, however, the CD spectrum shows a variation of the ratio of the CD signal at 208 and 222 nm, which is typically close to one in highly symmetric and well-ordered helical systems (Figure 2.5). To further investigate the stability of the metal-chelated assemblies, we monitored helical content as a function of temper-

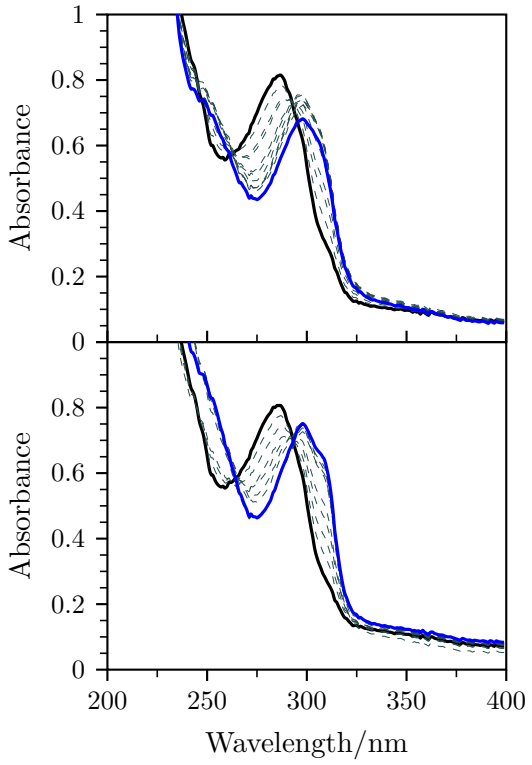

Figure 2.3. UV-Vis traces for the titration of HB2 (black trace) with $CoCl_2$ (top) or $NiCl_2$ (bottom; blue traces).

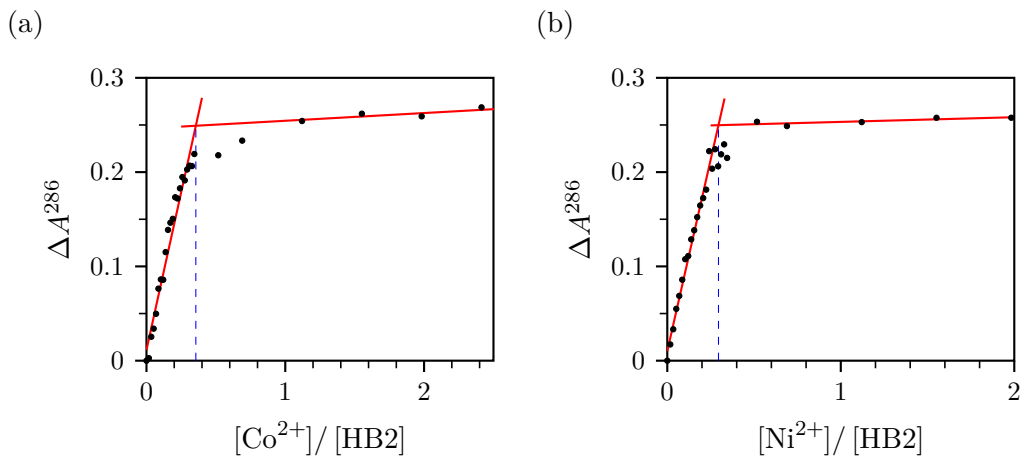

Figure 2.4. Binding curves of HB2 titrated with $CoCl_2$ (left) and $NiCl_2$ (right) as monitored by UV-Vis. The calculated binding stoichiometry was (a) 2.8 peptides per metal ion, (b) 3.4 peptides per metal ion.

ature. In keeping with the parent peptides, determination of melting temperature (T_m) is not possible because of the high stability of the assemblies to thermal denaturation (Figure A.5).[40,41] However, HB2 reconstituted in the presence of the metals is less stable than the apo peptides, despite a higher content in hexameric structures (see section 2.4.3). In particular, we observed higher loss of secondary structure for the Ni-bound HB1 and HB2, suggesting that these complexes are less compatible with the super-core than the cobalt ones. One possible reason is that nickel(II) forms much stronger complexes with bpy than cobalt(II), resulting in distortion to the helical structure in the hexameric assembly.[46,47] Bpy has the ability of forming chiral metal complexes, namely the Δ and the Λ enantiomers, which give rise to characteristic dichroic signals in the near-UV region, corresponding to the $\pi \rightarrow \pi^*$ transitions. In solution, neither of the two forms is favored, resulting in net dichroic signal of zero (Figure A.6). In contrast, both the Ni^{2+} and Co^{2+} complexes of HB2 display a CD signature in the 290–330 nm range, with peaks at 304 and 311 nm (Ni^{2+}), and 306 and 313 nm (Co^{2+}), consistent with the Δ isomer.[46] The presence of a net dichroic signal indicates that formation of one enantiomer

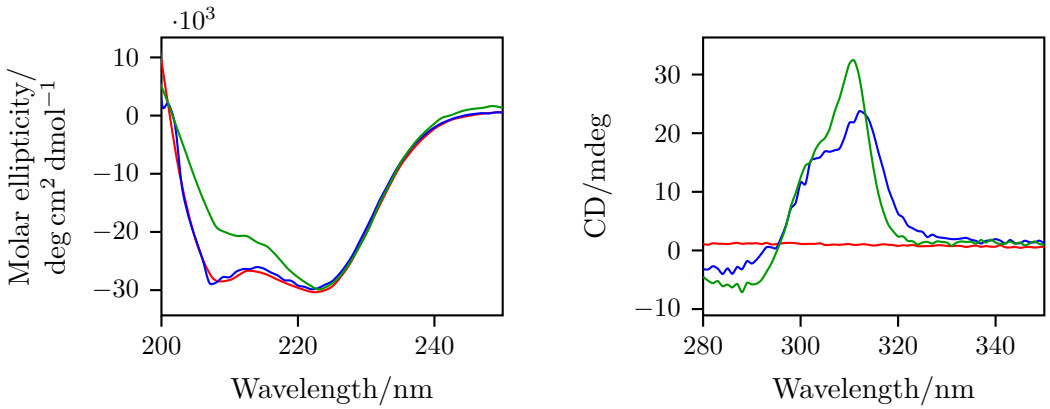

Figure 2.5. CD spectra (left) and CD signal (right) corresponding to the bpy absorption of HB2 (red), CoHB2 (blue), and NiHB2 (green).

is preferred over the other, possibly because it is energetically favored when incorporated within the super-core. The emergence of a dichroic signal was previously observed in constructs that utilized tris(bpy) complexes to template a three-helix bundle,[32] or a trimeric assembly.[23] Interestingly, the Λ enantiomer was favored in those designs.

2.4.3 Metal-mediated oligomerization

We utilized Analytical Ultracentrifugation (AUC) to assess the association state of the apo- and metal-reconstituted peptides in solution. The results of sedimentation velocity experiments are summarized in Figure 2.6. The bpy-modified peptides behave similarly to their non-modified counterparts:[40,41] the HB1 peptide formed hexamers when loaded at high peptide concentrations, while favoring dimers at lower peptide concentrations. Conversely, HB2 is predominantly dimeric in solution, with a small percent forming larger hexameric structures. In both cases, chemical modification with the bipyridyl moiety shifts the equilibrium towards the hexameric form compared to the parent peptides. As predicted, reconstitution with a divalent metal further shifts the equilibrium towards the hexamer, reflecting the formation

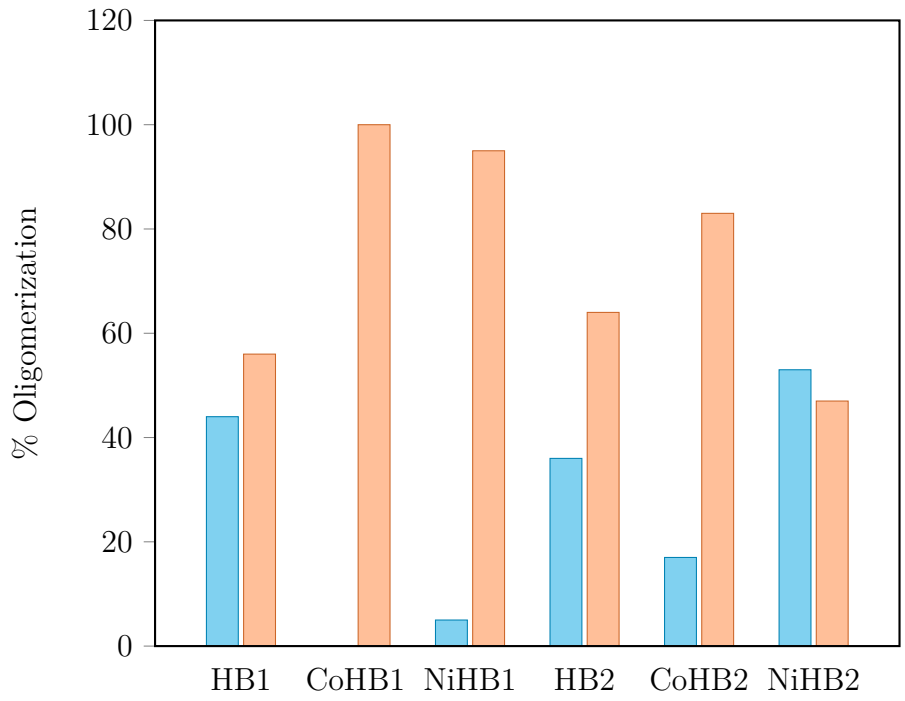

Figure 2.6. Oligomerization state of the peptides in presence and absence of divalent metals (blue, dimer; orange, hexamer).

of the complex. Addition of Co^{2+} results in formation of 83 % and 100 % hexamer for CoHB2 and CoHB1 respectively. Following suit, addition of Ni^{2+} to HB2 increases hexamer formation to 95 % total. In stark contrast, the addition of Ni^{2+} to HB1 decreases hexamer fraction to only 47 % of total, 17 % less than metal free peptide. Control experiments were carried out to assess the effect of divalent metals on the oligomerization state of Hex-Phe by sedimentation ultracentrifugation. No significant changes to the sedimentation profile were observed, indicating that the species are identical (Figure A.9).

2.5 Conclusion

We have shown that metal chelation, mediated by the incorporation of bipyridyl moieties into the solvent exposed surface of a three-helix bundle, stabilizes the for-

mation of trimers and results in the formation of stable supramolecular assemblies. Compared to natural amino acids, the bpy ligand contains two pyridyl nitrogen atoms in orientation compatible with metal chelation, thus forming complexes with higher energies of formation and, in the trimer form, octahedral geometry. Modeling suggested that this geometry is compatible with the hexameric assembly observed in the crystal structure of DSD (1G6U).[41] We found that addition of nickel or cobalt resulted in shifting the dimer-hexamer equilibrium to the hexamer in a sequence dependent manner, while preserving the helical structure of the peptides. Because of the unique symmetry of the assembly, this design is unique in allowing for further functionalization. For example, we have previously inserted two iron-sulfur clusters at controlled distances in the DSD scaffold, and demonstrated that the redox potentials can be modulated with single-point mutations.[27,28,42] Our current results suggest that metal chelation could be used to organize redox-active moieties in a spatially controlled manner, utilizing self-assembly of the DSD scaffold in closed hexamers. Further, this strategy may be used to stabilize fibrillar assemblies observed in DSD mutants.[41]

2.6 References

1. Jones, E. Y. Structure and function in complex macromolecular assemblies: Some evolutionary themes. *Current Opinion in Structural Biology* **2012**, *22*, 197–199 (cit. on p. 8).

2. Aussignargues, C.; Pandelia, M.-E.; Sutter, M.; Plegaria, J. S.; Zarzycki, J.; Turmo, A.; Huang, J.; Ducat, D. C.; Hegg, E. L.; Gibney, B. R.; Kerfeld, C. A. Structure and function of a bacterial microcompartment shell protein engineered to bind a [4Fe-4S] cluster. *Journal of the American Chemical Society* **2016**, *138*, 5262–5270 (cit. on p. 8).

3. King, N. P.; Bale, J. B.; Sheffler, W.; McNamara, D. E.; Gonen, S.; Gonen, T.; Yeates, T. O.; Baker, D. Accurate design of co-assembling multi-component protein nanomaterials. *Nature* **2014**, *510*, 103–108 (cit. on p. 8).

4. Bale, J. B.; Gonen, S.; Liu, Y.; Sheffler, W.; Ellis, D.; Thomas, C.; Cascio, D.; Yeates, T. O.; Gonen, T.; King, N. P.; Baker, D. Accurate design of megadalton-scale two-component icosahedral protein complexes. *Science* **2016**, *353*, 389–394 (cit. on p. 8).

5. King, N. P.; Sheffler, W.; Sawaya, M. R.; Vollmar, B. S.; Sumida, J. P.; Andre, I.; Gonen, T.; Yeates, T. O.; Baker, D. Computational design of self-assembling protein nanomaterials with atomic level accuracy. *Science* **2012**, *336*, 1171–1174 (cit. on p. 8).

6. Lai, Y.-T.; King, N. P.; Yeates, T. O. Principles for designing ordered protein assemblies. *Trends in Cell Biology* **2012**, *22*, 653–661 (cit. on p. 8).

7. Zhang, J.; Zheng, F.; Grigoryan, G. Design and designability of protein-based assemblies. *Current Opinion in Structural Biology* **2014**, *27*, 79–86 (cit. on p. 8).

8. Boyle, A. L.; Woolfson, D. N. De novo designed peptides for biological applications. *Chemical Society Reviews* **2011**, *40*, 4295–4306 (cit. on p. 8).

9. Woolfson, D. N.; Mahmoud, Z. N. More than just bare scaffolds: Towards multi-component and decorated fibrous biomaterials. *Chemical Society Reviews* **2010**, *39*, 3464–3479 (cit. on p. 8).

10. Dang, B.; Wu, H.; Mulligan, V. K.; Mravic, M.; Wu, Y.; Lemmin, T.; Ford, A.; Silva, D.-A.; Baker, D.; DeGrado, W. F. De novo design of covalently constrained mesosize protein scaffolds with unique tertiary structures. *Pro-*

ceedings of the National Academy of Sciences of the United States of America **2017**, *114*, 10852–10857 (cit. on p. 8).

11. Song, W. J.; Tezcan, F. A. A designed supramolecular protein assembly with in vivo enzymatic activity. *Science* **2014**, *346*, 1525–1528 (cit. on pp. 8, 9).

12. Brodin, J. D.; Carr, J. R.; Sontz, P. A.; Tezcan, F. A. Exceptionally stable, redox-active supramolecular protein assemblies with emergent properties. *Proceedings of the National Academy of Sciences of the United States of America* **2014**, *111*, 2897–2902 (cit. on pp. 8, 9).

13. Ljubetič, A.; Gradišar, H.; Jerala, R. Advances in design of protein folds and assemblies. *Current Opinion in Chemical Biology* **2017**, *40*, 65–71 (cit. on p. 8).

14. Ljubetič, A.; Lapenta, F.; Gradišar, H.; Drobnak, I.; Aupič, J.; Strmšek, Ž.; Lainšček, D.; Hafner-Bratkovič, I.; Majerle, A.; Krivec, N.; Benčina, M.; Pisanski, T.; Veličković, T. Ć.; Round, A.; Carazo, J. M.; Melero, R.; Jerala, R. Design of coiled-coil protein-origami cages that self-assemble in vitro and in vivo. *Nature Biotechnology* **2017**, *35*, 1094–1101 (cit. on p. 8).

15. Luo, Q.; Hou, C.; Bai, Y.; Wang, R.; Liu, J. Protein assembly: Versatile approaches to construct highly ordered nanostructures. *Chemical Reviews* **2016**, *116*, 13571–13632 (cit. on p. 8).

16. Howorka, S. Rationally engineering natural protein assemblies in nanobiotechnology. *Current Opinion in Biotechnology* **2011**, *22*, 485–491 (cit. on p. 8).

17. Kobayashi, N.; Yanase, K.; Sato, T.; Unzai, S.; Hecht, M. H.; Arai, R. Self-assembling nano-architectures created from a protein nano-building block using an intermolecularly folded dimeric de novo protein. *Journal of the American Chemical Society* **2015**, *137*, 11285–11293 (cit. on p. 8).

18. Case, M. A.; McLendon, G. L. Metal-assembled modular proteins: Toward functional protein design. *Accounts of Chemical Research* **2004**, *37*, 754–762 (cit. on p. 9).

19. Tezcan, F. A.; Crane, B. R.; Winkler, J. R.; Gray, H. B. Electron tunneling in protein crystals. *Proceedings of the National Academy of Sciences of the United States of America* **2001**, *98*, 5002–5006 (cit. on p. 9).

20. Salgado, E. N.; Lewis, R. A.; Mossin, S.; Rheingold, A. L.; Tezcan, F. A. Control of protein oligomerization symmetry by metal coordination: C_2 and

C_3 symmetrical assemblies through Cu^{II} and Ni^{II} coordination. *Inorganic Chemistry* **2009**, *48*, 2726–2728 (cit. on p. 9).

21. Sontz, P. A.; Song, W. J.; Tezcan, F. A. Interfacial metal coordination in engineered protein and peptide assemblies. *Current Opinion in Chemical Biology* **2014**, *19*, 42–49 (cit. on p. 9).

22. Salgado, E. N.; Radford, R. J.; Tezcan, F. A. Metal-directed protein self-assembly. *Accounts of Chemical Research* **2010**, *43*, 661–672 (cit. on p. 9).

23. Mills, J. H.; Sheffler, W.; Ener, M. E.; Almhjell, P. J.; Oberdorfer, G.; Pereira, J. H.; Parmeggiani, F.; Sankaran, B.; Zwart, P. H.; Baker, D. Computational design of a homotrimeric metalloprotein with a trisbipyridyl core. *Proceedings of the National Academy of Sciences of the United States of America* **2016**, *113*, 15012–15017 (cit. on pp. 9, 22).

24. Plegaria, J. S.; Pecoraro, V. L. De Novo Design of Metalloproteins and Metalloenzymes in a Three-Helix Bundle. In *Computational Design of Ligand Binding Proteins*, Stoddard, B. L., Ed.; Methods in Molecular Biology, Vol. 1414; Humana Press: New York, NY, 2016, pp 187–196 (cit. on p. 9).

25. Zastrow, M. L.; Pecoraro, V. L. Designing functional metalloproteins: From structural to catalytic metal sites. *Coordination Chemistry Reviews* **2013**, *257*, 2565–2588 (cit. on p. 9).

26. Mocny, C. S.; Pecoraro, V. L. De novo protein design as a methodology for synthetic bioinorganic chemistry. *Accounts of Chemical Research* **2015**, *48*, 2388–2396 (cit. on p. 9).

27. Roy, A.; Sommer, D. J.; Schmitz, R. A.; Brown, C. L.; Gust, D.; Astashkin, A.; Ghirlanda, G. A de novo designed 2 [4Fe-4S] ferredoxin mimic mediates electron transfer. *Journal of the American Chemical Society* **2014**, *136*, 17343–17349 (cit. on pp. 9, 10, 24).

28. Sommer, D. J.; Roy, A.; Astashkin, A.; Ghirlanda, G. Modulation of cluster incorporation specificity in a de novo iron-sulfur cluster binding peptide. *Biopolymers* **2015**, *104*, 412–418 (cit. on pp. 9, 10, 24).

29. Ni, T. W.; Tezcan, F. A. Structural characterization of a microperoxidase inside a metal-directed protein cage. *Angewandte Chemie-International Edition* **2010**, *49*, 7014–7018 (cit. on p. 9).

30. Zastrow, M. L.; Peacock, A. F. A.; Stuckey, J. A.; Pecoraro, V. L. Hydrolytic catalysis and structural stabilization in a designed metalloprotein. *Nature Chemistry* **2012**, *4*, 118–123 (cit. on p. 9).

31. Lieberman, M.; Sasaki, T. Iron(II) organizes a synthetic peptide into 3-helix bundles. *Journal of the American Chemical Society* **1991**, *113*, 1470–1471 (cit. on p. 9).

32. Ghadiri, M. R.; Soares, C.; Choi, C. A convergent approach to protein design. Metal ion-assisted spontaneous self-assembly of a polypeptide into a triple-helix bundle protein. *Journal of the American Chemical Society* **1992**, *114*, 825–831 (cit. on pp. 9, 22).

33. Koide, T.; Yuguchi, M.; Kawakita, M.; Konno, H. Metal-assisted stabilization and probing of collagenous triple helices. *Journal of the American Chemical Society* **2002**, *124*, 9388–9389 (cit. on p. 9).

34. Kang, M.; Light, K.; Ai, H.-w.; Shen, W.; Kim, C. H.; Chen, P. R.; Lee, H. S.; Solomon, E. I.; Schultz, P. G. Evolution of iron(II)-finger peptides by using a bipyridyl amino acid. *Chembiochem* **2014**, *15*, 822–825 (cit. on p. 9).

35. Luo, X.; Wang, T.-S. A.; Zhang, Y.; Wang, F.; Schultz, P. G. Stabilizing protein motifs with a genetically encoded metal-ion chelator. *Cell Chemical Biology* **2016**, *23*, 1098–1102 (cit. on p. 9).

36. Mills, J. H.; Khare, S. D.; Bolduc, J. M.; Forouhar, F.; Mulligan, V. K.; Lew, S.; Seetharaman, J.; Tong, L.; Stoddard, B. L.; Baker, D. Computational design of an unnatural amino acid dependent metalloprotein with atomic level accuracy. *Journal of the American Chemical Society* **2013**, *135*, 13393–13399 (cit. on p. 9).

37. Roy, L.; Case, M. A. Electrostatic determinants of stability in parallel 3-stranded coiled coils. *Chemical Communications* **2009**, 192–194 (cit. on p. 9).

38. Fedorova, A.; Ogawa, M. Y. Site-specific modification of de novo designed coiled-coil polypeptides with inorganic redox complexes. *Bioconjugate Chemistry* **2002**, *13*, 150–154 (cit. on p. 9).

39. Fedorova, A.; Chaudhari, A.; Ogawa, M. Y. Photoinduced electron-transfer along alpha-helical and coiled-coil metallopeptides. *Journal of the American Chemical Society* **2003**, *125*, 357–362 (cit. on p. 9).

40. Ghirlanda, G.; Lear, J. D.; Ogihara, N. L.; Eisenberg, D.; DeGrado, W. F. A hierarchic approach to the design of hexameric helical barrels. *Journal of Molecular Biology* **2002**, *319*, 243–253 (cit. on pp. 10, 21, 22).

41. Ogihara, N. L.; Ghirlanda, G.; Bryson, J. W.; Gingery, M.; DeGrado, W. F.; Eisenberg, D. Design of three-dimensional domain-swapped dimers and fibrous oligomers. *Proceedings of the National Academy of Sciences of the United States of America* **2001**, *98*, 1404–1409 (cit. on pp. 10, 21, 22, 24).

42. Roy, A.; Sarrou, I.; Vaughn, M. D.; Astashkin, A. V.; Ghirlanda, G. De novo design of an artificial bis [4Fe-4S] binding protein. *Biochemistry* **2013**, *52*, 7586–7594 (cit. on pp. 10, 24).

43. Savage, S. A.; Smith, A. P.; Fraser, C. L. Efficient synthesis of 4-, 5-, and 6-methyl-2,2'-bipyridine by a Negishi cross-coupling strategy followed by high-yield conversion to bromo- and chloromethyl-2,2'-bipyridines. *Journal of Organic Chemistry* **1998**, *63*, 10048–10051 (cit. on pp. 12, 19).

44. Park, C. K.; Stiteler, A. P.; Shah, S.; Ghare, M. I.; Bitinaite, J.; Horton, N. C. Activation of DNA cleavage by oligomerization of DNA-bound SgrAI. *Biochemistry* **2010**, *49*, 8818–8830 (cit. on pp. 16, 17).

45. Hauser, A.; Mader, M.; Robinson, W. T.; Murugesan, R.; Ferguson, J. Electronic and molecular-structure of Cr(2,2'-bipyridine)$_3^{3+}$. *Inorganic Chemistry* **1987**, *26*, 1331–1338 (cit. on p. 18).

46. Mason, S. F. The electronic spectra and optical activity of phenanthroline and dipyridyl metal complexes. *Inorganica Chimica Acta Reviews* **1968**, *2*, 89–109 (cit. on pp. 19, 21).

47. Irving, H.; Mellor, D. H. 1002. The stability of metal complexes of 1,10-phenanthroline and its analogues. Part I. 1,10-Phenanthroline and 2,2′-bipyridyl. *Journal of the Chemical Society* **1962**, 5222–5237 (cit. on p. 21).

CHAPTER 3

EVALUATION OF THE CATALYTIC ACTIVITY OF COBALT CYTOCHROME B_{562} TOWARD CO_2 REDUCTION IN WATER

3.1 Introduction

The ongoing use of fossil fuels has led to an increase in atmospheric CO_2 concentrations, causing severe consequences for the environment.[1] As a response to this, current research efforts are focused on developing energetic alternatives that can help curb CO_2 emissions. Although nature aids in the removal some of this greenhouse gas through photosynthesis,[2,3] negative emissions technologies are necessary to reduce the excess gas from the atmosphere.[4]

One path to do so is through artificial photosynthesis, where light is utilized as the energy source to drive the chemical transformation of CO_2 into usable chemicals such as fuels. Nonetheless, selectivity between the product of water reduction (namely H_2 gas) and the variety of products that can be obtained from CO_2 (Table 1.1) poses a problem when reducing CO_2 in aqueous conditions.[5]

Artificial metalloenzymes can potentially be used as selective catalysts for this reaction by offering an optimized environment not only to minimize the energy landscape of the rate limiting step, but also to provide channels for reactant binding and product release to and from the active site while protecting the organometallic center from degradation.[6,7]

Our group and others have demonstrated increased catalytic lifetime and overall turnover number of well-characterized H_2 production catalysts, both in water and in mild conditions. Recent work with nickel cyclam complexes has shown that catalytic CO_2 reduction can be enhanced by incorporation into the protein matrix, and that product selectivity can be controlled by the protein environment.[8,9]

Additionally, our group has shown that exchange of the metal ion to cobalt in heme-binding proteins or peptides results in an increase of H_2 production compared to the porphyrin in solution. Moreover, altering the protein sequence results in fine modulation of the total activity, further supporting the crucial role of the protein environment throughout the catalytic cycle.[10–12]

The use of metalloporphyrins as molecular CO_2 reduction electrocatalysts has been extensively explored in the recent years.[13–17] Remarkably, modifications of reaction conditions or the porphyrin framework, particularly those that are able to directly participate in the reaction (such as by stabilizing catalytic intermediates through hydrogen bonding) have shown increased activities of these catalysts toward CO_2 reduction.[18–23] Further, the higher turnover numbers and the product selectivity upon incorporation of cobalt porphyrins into supramolecular structures such as metal-organic frameworks[24–26] and polymers[27] suggest that catalysis by these metal complexes could be enhanced by binding to a protein environment.

This chapter describes the reengineering of cytochrome b_{562} (cyt b_{562}) into water-soluble catalysts capable of reducing CO_2 in aqueous conditions. Cyt b_{562} is a small, water-soluble, four-helix bundle that natively binds a heme cofactor via bis-axial ligation from the side chains of residues His102 and Met7 (Figure 3.1). In previous work, our group probed the effect of mutating the coordinating methionine to alanine, aspartate, or glutamate in hydrogen production, showing an increase in hydrogen production of the mutant M7A over wild type (WT).[12] This project expands this investigation by analyzing the effect of axial mutations on the efficiency of CO_2 reduction in water, which yields formate, carbon monoxide, and hydrogen upon light irradiation conditions by making use of a photosensitizer and a sacrificial electron donor. The generated mutants were designed to either remove axial ligation sites (M7A and H102A) or alter axial ligation (M7H) in order to probe the

(a) (b)

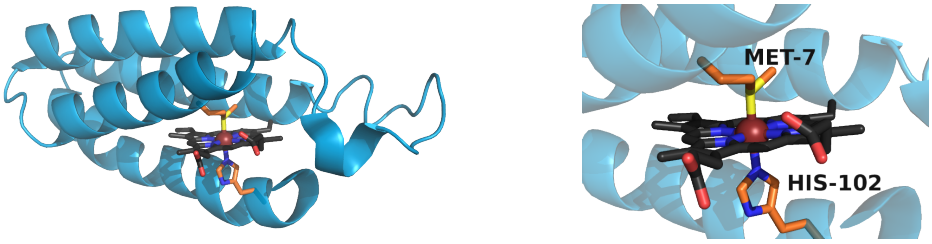

Figure 3.1. Structure of cyt b_{562} showing the coordinating axial ligands. PDB entry: 1QPU. Colors represent carbon (porphyrin: black, axial residues: orange), oxygen (red), nitrogen (blue), sulfur (yellow). The metal ion is shown as a sphere (brown).

electronic and steric effects that these ligands (or lack thereof) may have during catalysis.

3.2 Materials and Methods

All chemicals were purchased from Sigma-Aldrich and used without further purification unless otherwise noted. Calibration gases were obtained from Matheson in 14 L lecture bottles. All aqueous solutions were prepared using deionized water with a resistivity greater or equal to 18 MΩ. Cobalt(III) protoporphyrin IX chloride was purchased from Sigma-Aldrich and used without further purification.

3.2.1 Protein Expression

Mutants were generated using Gibson assembly and sequenced directly in the pET30c(+) vector utilizing the T7 promoter sequence. The verified mutants were transformed into a BL21(DE3) *E. coli* cell line and grown in 1 L of 2xTY media at 37 °C with shaking. Cells were induced with 1 mM β-D-thiogalactopyranoside (IPTG) at an OD_{600} of 0.6 and cells were harvested after 4 h of expression. The cell pellets were suspended in 20 mM Tris · HCl, 1 mM dithiotreitol (DTT), 0.5 mM

EDTA and lysed by multiple cycles of ultrasonication. The clarified lysate was brought to 75 % saturation with solid ammonium sulfate, and precipitated proteins were removed by centrifugation. The supernatant, containing the cytochrome mutants, was dialyzed against two changes of 10 mM Tris pH 7.5 and one of water at 4 °C.

Following dialysis, the protein solution was lyophilized and redissolved in 10 mM NaCl for further purification via RP-HPLC using a preparatory scale C18 column with a linear gradient from 100 % solvent A (0.1 % v/v TFA in water) to 100 % solvent B (4.9 % v/v water, 0.1 % v/v TFA in acetonitrile). The fractions containing the desired protein were then lyophilized to yield the pure apo-protein. The protein identities were confirmed via MALDI-TOF-MS and their purity determined by C18 analytical analysis.

Purified proteins were reconstituted with cobalt protoporphyrin IX (CoPPIX) similarly to previously reported procedures. Samples in 100 mM Tris pH 8.5 were subjected to 50 M excess of DTT for 30 min, followed by a 50 M excess of CoPPIX for 1 h. Excess porphyrin was removed by subjecting protein to a PD10 desalting column equilibrated in 50 mM Tris pH 7.5. Sample concentrations were determined via UV-Vis utilizing extinction coefficients determined by Inductively Coupled Plasma-Optical Emission Spectroscopy (ICP-OES), normalizing spectrum to the measured cobalt concentration. The protein was used immediately or frozen at −80 °C for future characterization.

3.2.2 Binding Assays

The dissociation constants (K_d) for each of the mutants was estimated by titrating a solution of CoPPIX in 1 M potassium phosphate (KP_i) pH 6.0 with a solution of the appropriate protein containing the same total concentration of CoPPIX and

monitoring the change in absorbance of the Soret band of the free or bound porphyrin (417 nm or *ca.* 425 nm, respectively).

Since both Soret peaks overlap with each other, we can write the absorbance at a particular wavelength λ as:

$$A^{\lambda} = \varepsilon^{\lambda}_{\mathrm{Co}}[\mathrm{Co}] + \varepsilon^{\lambda}_{\mathrm{CoP}}[\mathrm{CoP}] \tag{3.1}$$

Further, when no protein has been added, equation 3.1 becomes:

$$A^{\lambda}_{0} = \varepsilon^{\lambda}_{\mathrm{Co}}[\mathrm{Co}]_{\mathrm{T}} \tag{3.2}$$

where $[\mathrm{Co}]_{\mathrm{T}}$ corresponds to the total CoPPIX concentration. Subtracting equation 3.1 from equation 3.2 and simplifying we obtain:

$$\Delta A^{\lambda} = A^{\lambda}_{0} - A^{\lambda} = \varepsilon^{\lambda}_{\mathrm{Co}}\left([\mathrm{Co}]_{\mathrm{T}} - [\mathrm{Co}]\right) - \varepsilon^{\lambda}_{\mathrm{CoP}}[\mathrm{CoP}] \tag{3.3}$$

For the dissociation equilibrium of CoP shown in reaction R-3.1, we can write the mass balance equation for CoPPIX as equation 3.4.

$$\mathrm{CoP} \rightleftharpoons \mathrm{Co} + \mathrm{P} \tag{R-3.1}$$

$$[\mathrm{Co}]_{\mathrm{T}} = [\mathrm{Co}] + [\mathrm{CoP}] \tag{3.4}$$

By using equation 3.4, equation 3.3 becomes:

$$\Delta A^{\lambda} = \Delta\varepsilon^{\lambda}[\mathrm{CoP}] \tag{3.5}$$

where $\Delta\varepsilon^{\lambda} = \varepsilon^{\lambda}_{\mathrm{Co}} - \varepsilon^{\lambda}_{\mathrm{CoP}}$. The K_{d} expression for the dissociation of CoP is given by equation 3.6, and the mass balance equation for protein is shown in equation 3.7.

$$K_{\mathrm{d}} = \frac{[\mathrm{Co}][\mathrm{P}]}{[\mathrm{CoP}]} \tag{3.6}$$

$$[\mathrm{P}]_{\mathrm{T}} = [\mathrm{P}] + [\mathrm{CoP}] \tag{3.7}$$

Making use of mass balance equations 3.4 and 3.7, substituting equation 3.5 appropriately, and solving for $[\mathrm{P}]_{\mathrm{T}}$ we can modify equation 3.6 to obtain:

$$[\mathrm{P}]_{\mathrm{T}} = \frac{K_{\mathrm{d}} \cdot \Delta A^{\lambda}}{\Delta\varepsilon^{\lambda}[\mathrm{Co}]_{\mathrm{T}} - \Delta A^{\lambda}} + \frac{\Delta A^{\lambda}}{\Delta\varepsilon^{\lambda}} \tag{3.8}$$

which can be used to fit our data, albeit in the less conventional way of having ΔA^{λ} as the independent variable, rather than $[\mathrm{P}]_{\mathrm{T}}$.

3.2.3 Circular Dichroism Spectroscopy (CD)

CD spectra were recorded on a JASCO J-815 spectropolarimeter in the range of 190–260 nm. Data points were recorded every 1 nm and averaged over 3 scans. The concentrations of apo and holo-proteins were kept at 10 µM in 10 mM Tris pH 7.5. Thermal denaturation was performed by heating samples from 4 to 90 °C, monitoring loss of signal at 222 nm.

3.2.4 Photocatalysis Experiments

The stock buffer was prepared by making a solution containing 200 mM KP_{i} and 125 mM ascorbic acid (AscOH) and adjusting it to pH 6.0. The solution was then bubbled with CO_2 or Ar, and adjusted back to pH 6.0 with KOH if necessary. Finally, solid $[\mathrm{Ru(bpy)_3}]\mathrm{Cl_2} \cdot 6\,\mathrm{H_2O}$ was added to make a 1.25 mM solution, and the

buffer aliquoted out, the headspace evacuated with the appropriate gas, and the aliquots flash frozen and stored at −80 °C. Before each assay, CoPPIX was dissolved in 100 mM KOH to make a saturated solution, and the concentration is determined by UV-Vis using the Soret peak at 417 nm with an extinction coefficient of $\varepsilon = 143\,540\,\mathrm{M}^{-1}\,\mathrm{cm}^{-1}$ (as determined by ICP-OES measurements). The frozen buffer is thawed under an atmosphere of the corresponding gas, and an appropriate amount of CoPPIX and/or protein (in 200 mM KP_i) is added to obtain a working solution containing 20 µM CoPPIX, 30 µM protein, 100 mM AscOH, and 1 mM $[Ru(bpy)_3]^{2+}$ in 200 mM KP_i.

For each trial, 400 µL of the prepared sample was added to a 10 mm × 1 mm gas tight cuvette of known headspace volume, and the headspace sparged with the appropriate gas (Ar or CO_2) for 20 min. The cuvettes were then irradiated with a white light LED source for 8 h. The gaseous products, H_2 and CO, were analyzed at different time intervals using gas chromatography, while formate was quantified at the end of the experiment using ^{1}H NMR as detailed in the next section. All experiments were done in triplicate and the variation is reported as the standard deviation of the sample.

3.2.5 Product Quantification

At the appropriate time intervals, the headspace was sampled with a gas-tight syringe for H_2 and CO quantification by first injecting the same volume of Ar or CO_2 to be withdrawn, mixing thoroughly, and removing the corresponding sample.

The samples were analyzed in an SRI Instruments gas chromatograph equipped with a 3′ × 1/8″ molecular sieve 5 Å packed column with a Thermal Conductivity Detector (TCD) and a Flame Ionization Detector (FID) with a methanizer connected in series. The analytes are eluted using Ar as a carrier gas

with a temperature program starting at 60 °C for 1 min, ramping at 20 °C min^{-1} until 80 °C, holding for 2 min, ramping at 50 °C min^{-1} to 250 °C, and holding until the CO_2 exits the instrument, with a retention time (t_R) *ca.* 12 min. A peak corresponding to H_2 was seen on the TCD channel at $t_R = 0.400$ min, while the peak corresponding to CO appeared at $t_R = 3.42$ min on the FID channel. By comparing the peak areas to a calibration curve, we are able to quantify the number of moles of each gas in the injected sample.

After irradiation was stopped, the solution was frozen at −80 °C for future analysis. Formate was quantified by diluting the sample to make a solution containing 10 % v/v D_2O in water and 100 µM sodium 4,4-dimethyl-1-silapentane-1-sulfonate (DSS) as an internal standard. The samples were then analyzed by ^1H NMR using a water suppression method with 64 scans and a 30 s relaxation delay. The formate concentration was determined by comparing the integration area of the singlet at 8.45 ppm to the DSS peak at 0.0 ppm.

3.3 Results and Discussion

3.3.1 Protein Expression and Characterization

All apo proteins were obtained as described in section 3.2 with the analytical HPLC traces showing >95 % purity of the protein. The CD characterization of WT and M7A has been previously reported by our group.[12] The apo M7H and H102A mutants were also characterized by CD where they showed the typical signals of α-helical proteins, with local minima at 208 and 222 nm (Figures B.5 and B.6). Further, the signal intensity increases upon addition of CoPPIX indicating an increase in helical content upon binding of the cofactor. This gain in stability was corroborated by following the loss of intensity of the 222 nm peak with increasing temper-

ature to obtain the thermal denaturation curves (Figures B.5 and B.6). Table 3.1 shows that the T_m for all of the mutants increases with addition of CoPPIX, further indicating an increase in stability of the fold upon reconstitution with their cofactor.[12]

Table 3.1. CD characterization data of apo and holo cyt b_{562} mutants.

Mutant	T_m (apo) / °C	T_m (holo) / °C	ΔT_m / °C
WT[a]	58	85	+21
M7A[a]	52	64	+12
M7H	47	62	+15
H102A	56	61	+5

[a] From reference 12.

Binding of the cofactor was also analyzed through UV-Vis titration of apo protein to a solution of CoPPIX. In all cases the Soret peak showed a bathochromic shift, with a $\lambda_{max} = 230$ nm for WT and 425 nm for the mutants (Figures B.1 to B.4). The $\Delta\varepsilon$ (at 430 nm for WT to minimize signal overlap, 417 nm for the mutants) and K_d values for each titration were obtained by fitting the data to equation 3.8 (Figures B.1 to B.4) and are summarized in Table 3.2. The $\Delta\varepsilon$ values corresponded to the those calculated from the last points on each of the titrations (2–5 eq) within 5 % error. All the obtained K_d values were on the low nanomolar range, indicating that all mutants bind CoPPIX with similar affinity, thus suggesting that binding is driven mainly by the hydrophobic sequestration of the porphyrin rather than by binding of the axial ligands.

Table 3.2. Binding data of CoPPIX-cyt b_{562} mutants as monitored by UV-Vis.

Mutant	$\Delta\varepsilon^{417}$/ $mM^{-1}\,cm^{-1}$	K_d / nM	Adj. R^2
WT	78.47 [a]	217 ± 30	0.9743
M7A	98.21	170 ± 7	0.9814
M7H	101.64	126 ± 42	0.8825
H102A	116.30	28 ± 17	0.8678

[a] At 430 nm.

3.3.2 Photocatalytic Activity

The cyt b_{562} mutants were assayed to investigate their ability to reduce CO_2 under photoinduced conditions by using $[Ru(bpy)_3]^{2+}$ as photosensitizer and ascorbic acid as sacrificial electron donor in water. Upon irradiation $[Ru(bpy)_3]^{2+}$ achieves an excited state that can be reduced by ascorbic acid into $[Ru(bpy)_3]^{+}$, which can then transfer electrons to the catalyst for the reduction of substrate (Figure 3.2, steps 1–3).[28]

Under the studied experimental conditions, the catalysts were capable of reducing protons into H_2 both in the presence and absence of CO_2 as substrate. Further, carbon monoxide and formate were also observed as products when CO_2 was present. Controls lacking CoPPIX showed little H_2 was produced and no CO or HCO_2^- were detected, indicating that these species were indeed produced by the cobalt catalyst. The presence of each of these products can be explained on the basis of previous mechanistic studies of cobalt porphyrins used as catalysts for these reactions (Figure 3.2). Briefly, the metal site is reduced to Co(I) by the photosensitizer as described above (step 3), which is capable of binding H^+ to form

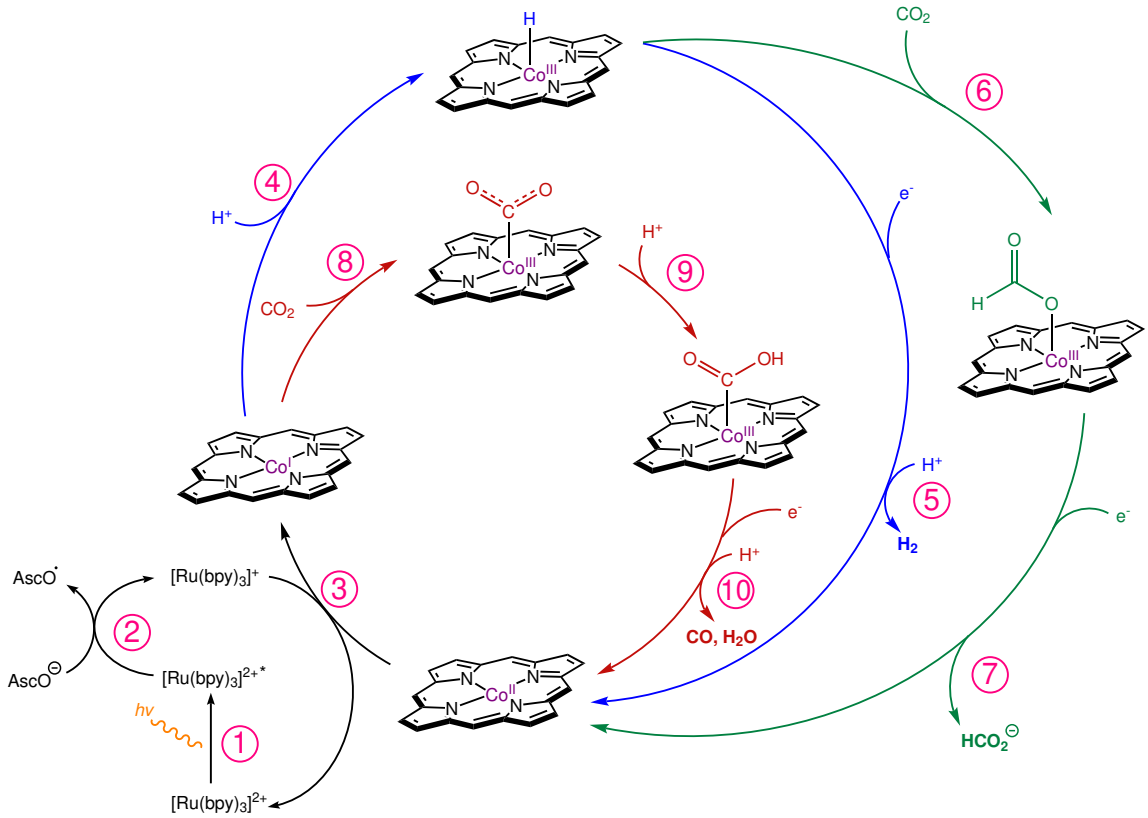

Figure 3.2. Catalytic cycles for the generation of H_2, CO, and HCO_2^- by cobalt porphyrins through photoirradiation in the presence of $[Ru(bpy)_3]^{2+}$ and ascorbic acid as sacrificial electron donor. Based on references 28 and 33.

a metal hydride complex (step 4), or CO_2 to form the corresponding adduct (step 8). The metal hydride complex can then be protonated to form H_2 gas (step 5), or it can undergo an insertion reaction with CO_2 to form formate (steps 6 and 7); while the CO_2 adduct can proceed through a series of proton transfer events that culminate in the loss of water and formation of CO (steps 9 and 10).[28–32]

Not surprisingly, experiments that lacked the protein scaffold in solution soon showed a precipitate in the cuvettes. This is consistent with the fact that CoPPIX forms insoluble aggregates in water. The trials that included any of the cyt b_{562} mutants did not show any discernable precipitate throughout the length of the experiment.

The activity of the catalyst was followed over time and is reported as the turnover number (TON) of each catalyst, defined as the total number of moles of product produced during the experiment divided by the initial number of moles of catalyst (8 nmol). The catalysts were initially evaluated under 1 atm CO_2 in a buffer saturated with this gas at pH 6.0 (Figures 3.3 and 3.4). Figure 3.5 summarizes the final TON for the catalysts in the assayed conditions (8 nmol). Interestingly, all mutants showed similar activity for CO production (TON ∼35), albeit still higher than that observed for the porphyrin alone (TON 19 ± 1), indicating that activity is increased by the interaction of the protein with the porphyrin. Surprisingly, formate concentrations where similar in the experiments with free porphyrin and for all of the mutants with the exception of M7A, which showed slightly lower formate concentrations (TON ∼35 vs. 20 ± 3). Nonetheless, the mutants did show variation in their H_2 production activity at pH 6.0 (Figure 3.3): M7A showed a (20 ± 5) % increase in H_2 compared to the porphyrin alone, followed by M7H ((45 ± 7) %), then WT ((72 ± 7) %), and finally H102A with the highest increase in activity ((113 ± 5) %).

To determine if there was any net effect of the presence of CO_2 on the reduction of protons, the catalysts' activity was assayed under the same conditions without CO_2 by sparging the solution and headspace with Ar instead (Figure B.9). As expected, no CO or HCO_2^- were detected, which is consistent with the fact that these compounds are indeed the product of CO_2 reduction in the previous experiments. As shown in Figure 3.5, the TON values for H_2 for CoPPIX and the cyt b_{562} mutants remained the same, indicating that overall H_2 production is not affected by the presence of CO_2.

These results indicate that the activity trends observed for H_2 production are independent of the presence of CO_2. This suggests that axial ligation at posi-

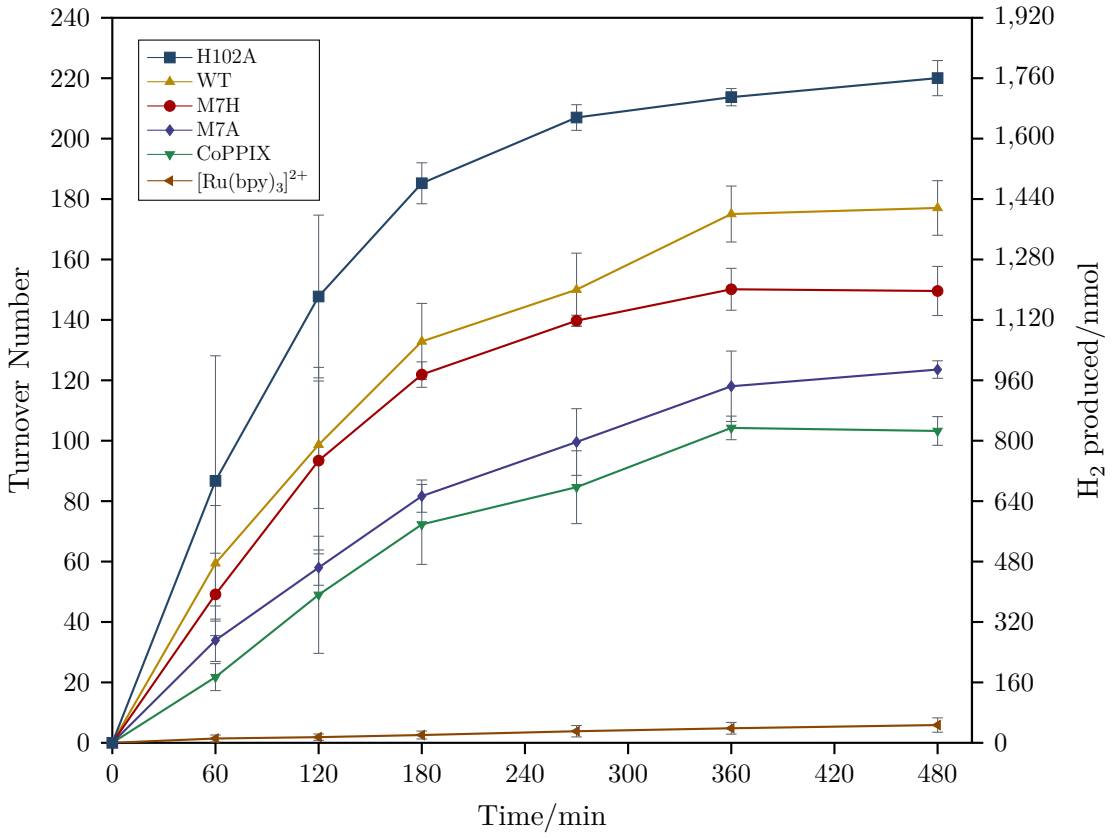

Figure 3.3. Produced H_2 over time from the photoinduced reduction of protons by $[Ru(bpy)_3]^{2+}$, CoPPIX, and cobalt cyt b_{562} mutants at pH 6.0 under 1 atm CO_2. The experiments were carried out in 100 mM AscOH, 1 mM $[Ru(bpy)_3]^{2+}$, 200 mM KP_i, and 20 µM catalyst (when appropriate). The error bars represent the standard deviation of the sample.

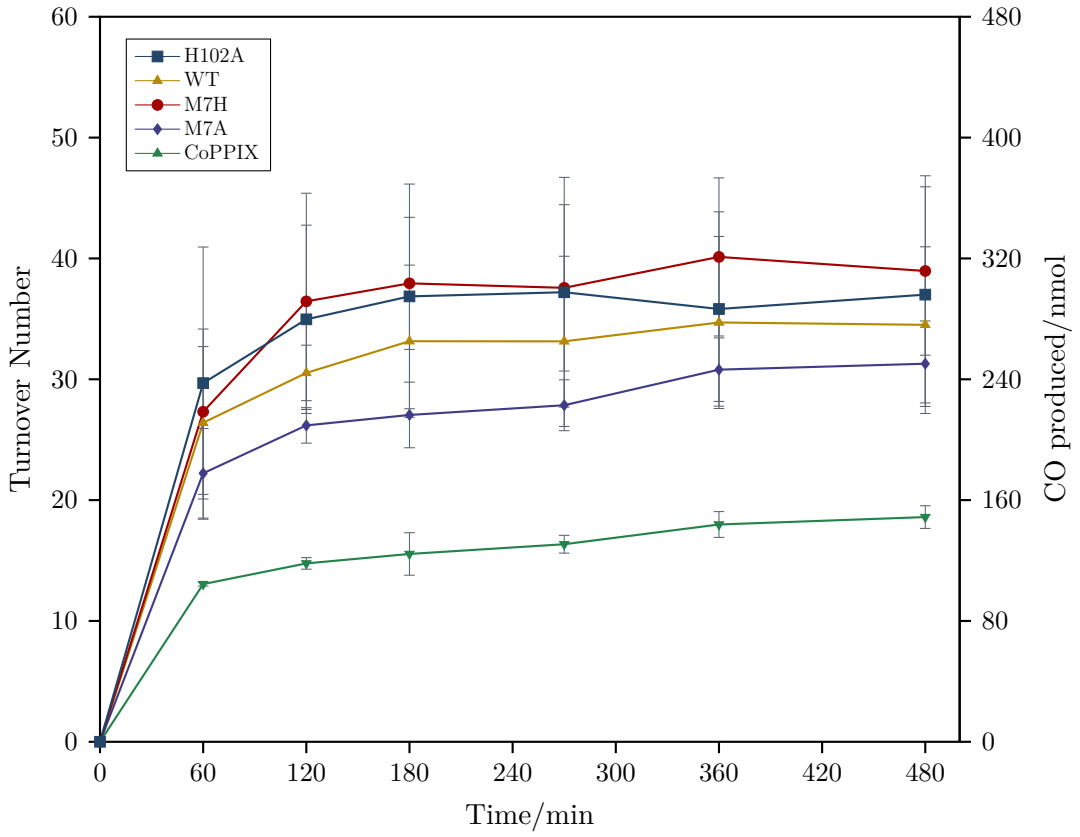

Figure 3.4. Produced CO over time from the photoinduced reduction of protons by CoPPIX and cobalt cyt b_{562} mutants at pH 6.0 under 1 atm CO_2. The experiments were carried out in 100 mM AscOH, 1 mM $[Ru(bpy)_3]^{2+}$, 200 mM KP_i, and 20 µM catalyst. The error bars represent the standard deviation of the sample.

tion 7 results in the highest activity, thus explaining why M7A, which lacks coordination at this position, exhibits the lowest increase in H_2 production among the studied Co-cyt b_{562} mutants. Further, the data supports the fact that the methionine coordination at this position results in a higher overall activity, as mutants bearing this residue (WT, H102A) resulted in the highest TON values. A possible explanation of these observations is that as the metal center becomes more electron rich, a softer ligand—such as methionine's thioether side chain—is capable of better

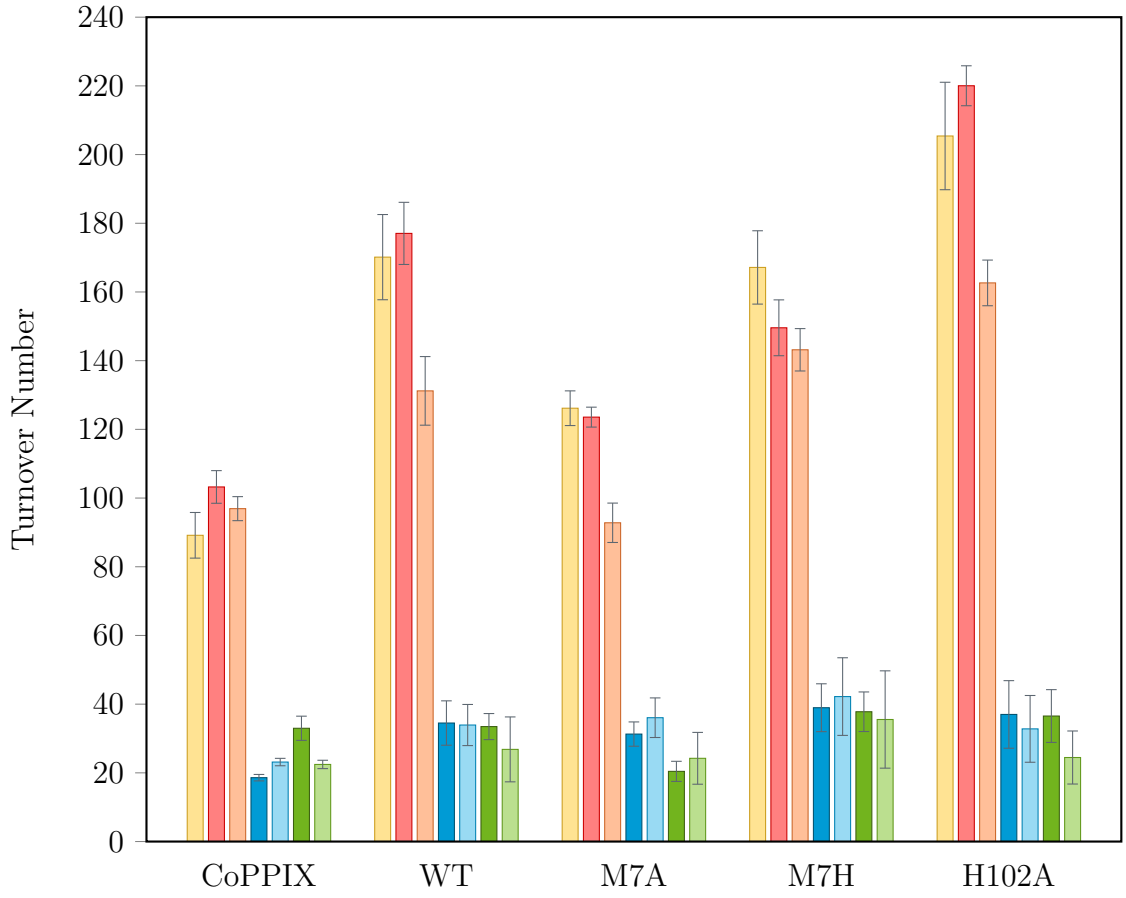

Figure 3.5. Turnover number values obtained for CoPPIX and cobalt cyt b_{562} mutants under irradiation with light for 8 h in 100 mM AscOH, 1 mM $[Ru(bpy)_3]^{2+}$, and 200 mM KP_i. The bars represent the TON of each catalyst at pH 6.0 in absence (H_2: yellow) and presence of CO_2 (H_2: red, CO: dark blue, HCO_2^-: dark green); and in the presence of CO_2 at pH 7.0 (H_2: orange, CO: light blue, HCO_2^-: light green). The error bars represent the standard deviation of the sample.

stabilizing the reduced intermediates that are formed throughout the catalytic cycle. Finally, the difference between the activities of H102A and WT can be due to the opening of a coordination site on one side of the porphyrin, thus increasing the chance of substrate binding to the active site.

In order to investigate if CO_2 reduction was pH dependent, the catalysts were evaluated also at pH 7.0 (Figures B.10 and B.11). The TON for CO did not suffer any considerable changes between the mutants, consistent with the independence of CO_2 binding from proton concentration. Unsurprisingly the H_2 yield for WT, M7A, and H102A decreased by 20 %, which is to be expected when proton concentration is decreased 10-fold. However, no significant change of H_2 TON was observed for free porphyrin or the M7H mutants, suggesting that under these conditions M7H behaves similarly to CoPPIX. Finally, although formate production is in principle dependent on proton reduction, no significant changes in turnover number were observed for this compound, which might indicate that other factors may come into play when it comes to CO_2 reduction by these catalysts in an aqueous environment.

3.4 Conclusions

In summary, this work aimed at the design of cyt b_{562} mutants that incorporate CoPPIX as cofactor and were capable of reducing protons and CO_2 into H_2, CO, and HCO_2^- upon light irradiation in the presence of $[Ru(bpy)_3]^{2+}$ and ascorbic acid as photosensitizer and sacrificial electron donor, respectively. The proteins were designed to investigate the effect of axial mutations on the porphyrin, including the native ligation (WT), removal of a ligand site (M7A, H102A), or change of ligation site (M7H). All proteins bound the porphyrin with similar affinity and exhibited

an increase in folding stability upon binding and remained solubilized in water throughout the experiments.

The findings indicate that CO_2 reduction into CO is slightly increased when incorporated into the protein, whereas HCO_2^- production did not see any changes between free and bound catalyst. On the other hand, proton reduction showed a difference in activities between the mutants, indicating that both electronic and steric effects play an important role throughout the catalytic cycle that leads to H_2 production. Additionally, three of the protein scaffolds (WT, M7A, H102A) showed a dependence of proton reduction activity at higher pH, but M7H and the free porphyrin did not show any noticeable change in activity at the examined pH values. Moreover, no pH dependence of CO_2 reduction activity was observed between the catalysts, indicating that other factors may come into play in the mechanism of CO_2 reduction by these catalysts.

This work shows that it is possible to regulate the hydrogen production activity of CoPPIX by incorporating it into cyt b_{562} and mutating residues involved in the first coordination sphere of the porphyrin. Further work involving the study of other relevant mutations at this site or the second coordination sphere could provide insight into the mechanism(s) of these catalysts in photoinduced reduction of H^+ and CO_2, which in turn could have positive implications in the field of renewable energy and green chemistry.

3.5 References

1. Lacis, A. A.; Schmidt, G. A.; Rind, D.; Ruedy, R. A. Atmospheric CO_2: Principal Control Knob Governing Earth's Temperature. *Science* **2010**, *330*, 356 (cit. on p. 30).

2. Sun, Y.; Gu, L.; Dickinson, R. E.; Norby, R. J.; Pallardy, S. G.; Hoffman, F. M. Impact of mesophyll diffusion on estimated global land CO_2 fertilization. *Proceedings of the National Academy of Sciences* **2014**, 201418075 (cit. on p. 30).

3. Kondo, M.; Ichii, K.; Patra, P. K.; Poulter, B.; Calle, L.; Koven, C.; Pugh, T. A. M.; Kato, E.; Harper, A.; Zaehle, S.; Wiltshire, A. Plant Regrowth as a Driver of Recent Enhancement of Terrestrial CO_2 Uptake. *Geophysical Research Letters* **2018**, *45*, 4820–4830 (cit. on p. 30).

4. Smith, P.; Davis, S. J.; Creutzig, F.; Fuss, S.; Minx, J.; Gabrielle, B.; Kato, E.; Jackson, R. B.; Cowie, A.; Kriegler, E.; van Vuuren, D. P.; Rogelj, J.; Ciais, P.; Milne, J.; Canadell, J. G.; McCollum, D.; Peters, G.; Andrew, R.; Krey, V.; Shrestha, G.; Friedlingstein, P.; Gasser, T.; Grübler, A.; Heidug, W. K.; Jonas, M.; Jones, C. D.; Kraxner, F.; Littleton, E.; Lowe, J.; Moreira, J. R.; Nakicenovic, N.; Obersteiner, M.; Patwardhan, A.; Rogner, M.; Rubin, E.; Sharifi, A.; Torvanger, A.; Yamagata, Y.; Edmonds, J.; Yongsung, C. Biophysical and economic limits to negative CO_2 emissions. *Nature Climate Change* **2015**, *6*, 42 (cit. on p. 30).

5. Fujita, E. Photochemical carbon dioxide reduction with metal complexes. *Coordination Chemistry Reviews* **1999**, *185-186*, 373–384 (cit. on p. 30).

6. Lu, Y.; Yeung, N.; Sieracki, N.; Marshall, N. M. Design of functional metalloproteins. *Nature* **2009**, *460*, 855 (cit. on p. 30).

7. Alcala-Torano, R.; Sommer, D. J.; Bahrami Dizicheh, Z.; Ghirlanda, G. Chapter Seventeen—Design Strategies for Redox Active Metalloenzymes: Applications in Hydrogen Production. In *Methods in Enzymology*, Pecoraro, V. L., Ed.; Academic Press: 2016, pp 389–416 (cit. on p. 30).

8. Schneider, C. R.; Shafaat, H. S. An internal electron reservoir enhances catalytic CO_2 reduction by a semisynthetic enzyme. *Chemical Communications* **2016**, *52*, 9889–9892 (cit. on p. 30).

9. Schneider, C. R.; Manesis, A. C.; Stevenson, M. J.; Shafaat, H. S. A photoactive semisynthetic metalloenzyme exhibits complete selectivity for CO_2

reduction in water. *Chemical Communications* **2018**, *54*, 4681–4684 (cit. on p. 30).

10. Kleingardner, J. G.; Kandemir, B.; Bren, K. L. Hydrogen Evolution from Neutral Water under Aerobic Conditions Catalyzed by Cobalt Microperoxidase-11. *Journal of the American Chemical Society* **2014**, *136*, 4–7 (cit. on p. 31).

11. Sommer, D. J.; Vaughn, M. D.; Ghirlanda, G. Protein secondary-shell interactions enhance the photoinduced hydrogen production of cobalt protoporphyrin IX. *Chemical Communications* **2014**, *50*, 15852–15855 (cit. on p. 31).

12. Sommer, D. J.; Vaughn, M. D.; Clark, B. C.; Tomlin, J.; Roy, A.; Ghirlanda, G. Reengineering cyt b_{562} for hydrogen production: A facile route to artificial hydrogenases. *Biochimica et Biophysica Acta (BBA) - Bioenergetics* **2016**, *1857*, 598–603 (cit. on pp. 31, 37, 38).

13. Manbeck, G. F.; Fujita, E. A review of iron and cobalt porphyrins, phthalocyanines and related complexes for electrochemical and photochemical reduction of carbon dioxide. *Journal of Porphyrins and Phthalocyanines* **2015**, *19*, 45–64 (cit. on p. 31).

14. Mondal, B.; Rana, A.; Sen, P.; Dey, A. Intermediates Involved in the $2\,e^-/2\,H^+$ Reduction of CO_2 to CO by Iron(0) Porphyrin. *Journal of the American Chemical Society* **2015**, *137*, 11214–11217 (cit. on p. 31).

15. Zhang, X.; Wu, Z.; Zhang, X.; Li, L.; Li, Y.; Xu, H.; Li, X.; Yu, X.; Zhang, Z.; Liang, Y.; Wang, H. Highly selective and active CO_2 reduction electrocatalysts based on cobalt phthalocyanine/carbon nanotube hybrid structures. *Nature Communications* **2017**, *8*, 14675 (cit. on p. 31).

16. Birdja, Y. Y.; Vos, R. E.; Wezendonk, T. A.; Jiang, L.; Kapteijn, F.; Koper, M. T. M. Effects of Substrate and Polymer Encapsulation on CO_2 Electroreduction by Immobilized Indium(III) Protoporphyrin. *ACS Catalysis* **2018**, *8*, 4420–4428 (cit. on p. 31).

17. Rao, H.; Lim, C.-H.; Bonin, J.; Miyake, G. M.; Robert, M. Visible-Light-Driven Conversion of CO_2 to CH_4 with an Organic Sensitizer and an Iron Porphyrin Catalyst. *Journal of the American Chemical Society* **2018**, *140*, 17830–17834 (cit. on p. 31).

18. Bhugun, I.; Lexa, D.; Savéant, J.-M. Catalysis of the Electrochemical Reduction of Carbon Dioxide by Iron(0) Porphyrins: Synergystic Effect of Weak

Brönsted Acids. *Journal of the American Chemical Society* **1996**, *118*, 1769–1776 (cit. on p. 31).

19. Lee, C. H.; Dogutan, D. K.; Nocera, D. G. Hydrogen Generation by Hangman Metalloporphyrins. *Journal of the American Chemical Society* **2011**, *133*, 8775–8777 (cit. on p. 31).

20. Costentin, C.; Drouet, S.; Robert, M.; Savéant, J.-M. A Local Proton Source Enhances CO_2; Electroreduction to CO by a Molecular Fe Catalyst. *Science* **2012**, *338*, 90 (cit. on p. 31).

21. Azcarate, I.; Costentin, C.; Robert, M.; Savéant, J.-M. Dissection of Electronic Substituent Effects in Multielectron-Multistep Molecular Catalysis. Electrochemical CO_2-to-CO Conversion Catalyzed by Iron Porphyrins. *The Journal of Physical Chemistry C* **2016**, *120*, 28951–28960 (cit. on p. 31).

22. Azcarate, I.; Costentin, C.; Robert, M.; Savéant, J.-M. Through-Space Charge Interaction Substituent Effects in Molecular Catalysis Leading to the Design of the Most Efficient Catalyst of CO_2-to-CO Electrochemical Conversion. *Journal of the American Chemical Society* **2016**, *138*, 16639–16644 (cit. on p. 31).

23. Call, A.; Cibian, M.; Yamamoto, K.; Nakazono, T.; Yamauchi, K.; Sakai, K. Highly Efficient and Selective Photocatalytic CO_2 Reduction to CO in Water by a Cobalt Porphyrin Molecular Catalyst. *ACS Catalysis* **2019**, *9*, 4867–4874 (cit. on p. 31).

24. Kornienko, N.; Zhao, Y.; Kley, C. S.; Zhu, C.; Kim, D.; Lin, S.; Chang, C. J.; Yaghi, O. M.; Yang, P. Metal-Organic Frameworks for Electrocatalytic Reduction of Carbon Dioxide. *Journal of the American Chemical Society* **2015**, *137*, 14129–14135 (cit. on p. 31).

25. Lin, S.; Diercks, C. S.; Zhang, Y.-B.; Kornienko, N.; Nichols, E. M.; Zhao, Y.; Paris, A. R.; Kim, D.; Yang, P.; Yaghi, O. M.; Chang, C. J. Covalent organic frameworks comprising cobalt porphyrins for catalytic CO_2 reduction in water. *Science* **2015**, *349*, 1208 (cit. on p. 31).

26. Zhang, H.; Wei, J.; Dong, J.; Liu, G.; Shi, L.; An, P.; Zhao, G.; Kong, J.; Wang, X.; Meng, X.; Zhang, J.; Ye, J. Efficient Visible-Light-Driven Carbon Dioxide Reduction by a Single-Atom Implanted Metal-Organic Framework. *Angewandte Chemie International Edition* **2016**, *55*, 14310–14314 (cit. on p. 31).

27. Kramer, W. W.; McCrory, C. C. L. Polymer coordination promotes selective CO_2 reduction by cobalt phthalocyanine. *Chemical Science* **2016**, *7*, 2506–2515 (cit. on p. 31).

28. Morris, A. J.; Meyer, G. J.; Fujita, E. Molecular Approaches to the Photocatalytic Reduction of Carbon Dioxide for Solar Fuels. *Accounts of Chemical Research* **2009**, *42*, 1983–1994 (cit. on pp. 39, 40).

29. Shen, J.; Kolb, M. J.; Göttle, A. J.; Koper, M. T. M. DFT Study on the Mechanism of the Electrochemical Reduction of CO_2 Catalyzed by Cobalt Porphyrins. *The Journal of Physical Chemistry C* **2016**, *120*, 15714–15721 (cit. on p. 40).

30. Nielsen, I. M. B.; Leung, K. Cobalt-Porphyrin Catalyzed Electrochemical Reduction of Carbon Dioxide in Water. 1. A Density Functional Study of Intermediates. *The Journal of Physical Chemistry A* **2010**, *114*, 10166–10173 (cit. on p. 40).

31. Dhanasekaran, T.; Grodkowski, J.; Neta, P.; Hambright, P.; Fujita, E. *p*-Terphenyl-Sensitized Photoreduction of CO_2 with Cobalt and Iron Porphyrins. Interaction between CO and Reduced Metalloporphyrins. *The Journal of Physical Chemistry A* **1999**, *103*, 7742–7748 (cit. on p. 40).

32. Leung, K.; Nielsen, I. M. B.; Sai, N.; Medforth, C.; Shelnutt, J. A. Cobalt-Porphyrin Catalyzed Electrochemical Reduction of Carbon Dioxide in Water. 2. Mechanism from First Principles. *The Journal of Physical Chemistry A* **2010**, *114*, 10174–10184 (cit. on p. 40).

33. Pellegrin, Y.; Odobel, F. Sacrificial electron donor reagents for solar fuel production. *Comptes Rendus Chimie* **2017**, *20*, 283–295 (cit. on p. 40).

CHAPTER 4

A NOVEL DITHIOL AMINO ACID FOR THE INCORPORATION OF [FeFe]-HYDROGENASE ACTIVE SITE MIMICS INTO PROTEIN SCAFFOLDS

4.1 Introduction

The use of hydrogen as an alternative fuel has caught the interest of the scientific community for several reasons, including its abundance, high heat of combustion and its suitability as a green fuel, since the only product of its reaction with oxygen is water (Reaction R-1.1). However, current processes for the production of this gas rely on the use of precious metals or high energy processes.[1,2]

In nature, hydrogen metabolism is regulated by hydrogenases, enzymes that are capable of reversibly reducing protons to hydrogen (Reaction R-1.2) with high efficiency under mild conditions while utilizing earth-abundant metals. Of particular interest are the [FeFe]-hydrogenases, which are biased toward the production of hydrogen gas. The active site in these hydrogenases, the H-cluster, is comprised of a $[Fe_4S_4]$ cluster tethered by a cysteine residue to the proximal iron atom of a peculiar diiron complex. The metal atoms in the latter are coordinated by carbonyl and biologically-unique cyanide ligands, while also being linked together by an aza-dithiolate bridge (Figure 4.1).[3–6]

Recently, a wide variety of small molecule mimics of the H-cluster have been prepared in order to elucidate the enzyme's mechanism, with the hope of reproducing its activity without the need of the complex biological machinery needed for its expression. These studies have shown that the nature of the ligands has an important effect in the proton reduction mechanism, as they regulate the oxidation state of the metals and the geometry of the catalyst, thus determining the binding mode of the hydride and the order of protonation and electron transfer events.[7–12]

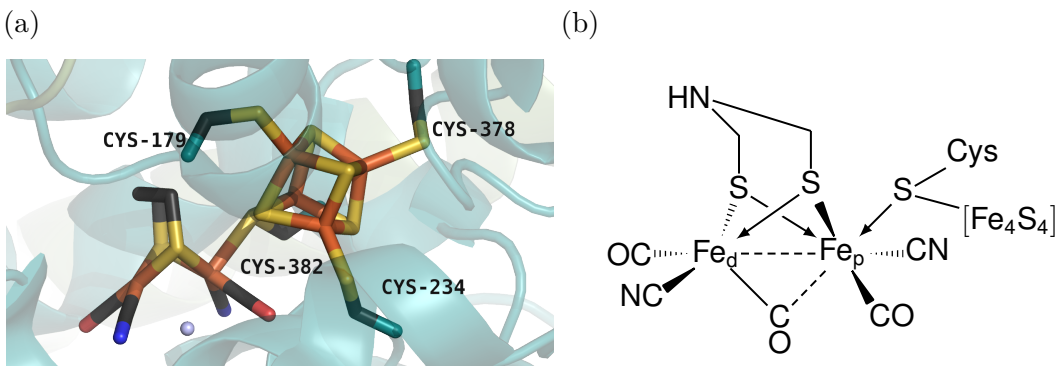

Figure 4.1. (a) Modeled H-cluster of *D. desulfuricans* [FeFe]-hydrogenase, PDB code: 1HFE, and (b) its corresponding line structure representation.

Unfortunately, these organometallic compounds are typically not water soluble, lack the high turnover numbers of the native enzyme, are oxygen sensitive, and often show irreversible events upon electrochemical reduction, thus making them unsuitable for light driven catalysis where electrons must be transferred one-by-one.[7–9,13–15] The reason behind these shortcomings can be attributed to the lack of second-sphere and long-range interactions that the natural enzymes provide. These interactions help stabilize important intermediates during the course of the reaction and alter their redox potential. The protein environment also provides a proton channel that controls the movement of substrates and product to and from the redox center.[16,17] With this in mind, some research groups have ventured into exploring the utilization of a variety scaffolds to mimic the role of the protein during catalysis and study proton reduction by this diiron complex.[18]

Different strategies have been utilized to incorporate mimics of the active site of [FeFe]-hydrogenases into supramolecular structures; however, most of them are not easily amenable to modification and offer a narrow variety of functional groups, making it difficult to reproduce the chemically rich environment that proteins offer.[19–23]

Some examples can be found in the literature that make use of proteins and peptide scaffolds, the main strategy being the use of the dithiol bridge to anchor the diiron complex. For instance, the thiol groups of cysteine residues have been used as anchoring points to incorporate the diiron mimic into proteins and peptides.[24–27]

Other synthetic approaches have involved specifically targeting a particular residue in a peptide or protein by using orthogonal groups. In the case of peptides made through SPPS, for instance, it is possible to use an orthogonal protecting group that can be selectively deprotected on-resin to incorporate a dithiol functionality, which after cleavage of the peptide can be used to anchor a diiron complex.[28] For proteins, the use of the bioorthogonal maleimide-thiol reaction has been utilized to incorporate the diiron catalyst in a similar fashion into the cavity of a protein bearing a single cysteine residue.[29]

Perhaps more interestingly, our laboratory has explored the alternative of utilizing non-natural amino acids that bear the dithiol bridge as a side chain. In previous work, our group reported the preparation of an amino acid with a 1,3-propanedithiol side chain that was suitable for SPPS. This amino acid was then incorporated into a helical peptide where a diiron hexacarbonyl mimic of [FeFe]-hydrogenase was tethered through the dithiol groups resulting in aqueous proton reduction catalysis in a photosensitized experiment.[30] Additionally, phosphine amino acids have also been utilized to tether the diiron complex asymmetrically, more in line with the native cofactor.[31]

However, no work has been done to explore the incorporation of [FeFe]-hydrogenase mimics that could be more suitable for photocatalysis. Studies done on (μ-1,2-benzenedithiolato-1$\kappa^2 S$:2$\kappa^2 S$)bis(tricarbonyliron)(Fe—Fe) have shown that upon irradiation in presence of a photosensitizer and a sacrificial electron

donor, complexes bearing a 1,2-benzenedithiolate bridge have a higher activity as compared to those containing an azadithiolate bridge found in the native cofactor.[13,32–34] DFT calculations suggest this may be due to a different mechanism in which the bridging ligand plays a crucial role in stabilizing the reduced intermediates throughout the reaction.[32]

In order to evaluate this type of [FeFe]-hydrogenase mimics in aqueous conditions, and with particular interest in studying how protein interactions may come into play with the proposed mechanism, this work presents the enantioselective synthesis a novel amino acid bearing 1,2-benzenedithiol as a side-chain and suitable protecting groups for its use in Fmoc SPPS (Figure 4.2).

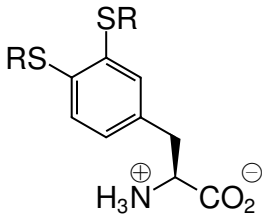

Figure 4.2. Structure of target compound **4-1**.

4.2 Retrosynthetic Analysis

Several synthetic routes were assayed to prepare the target molecule involving the use of alternative ways of controlling the stereochemistry of the final reaction. The results from these attempts were not successful and are not discussed in this chapter, but a brief overview is presented in Appendix D. The most promising strategy that was followed makes use of a nickel-based chiral auxiliary, [(*N*-benzyl-L-prolyl-κN)(2-{(*E*)-[(carboxylato-κO-methyl)imino-κN](phenyl)methyl}phenyl)azanido-κN]nickel (NiCA, Figure 4.3), which can be alkylated with a modified Mitsunobu reaction on the corresponding benzyl alcohol.[35,36] The preparation of the benzyl alcohol could be carried from the reduction of the benzaldehyde derivative, which

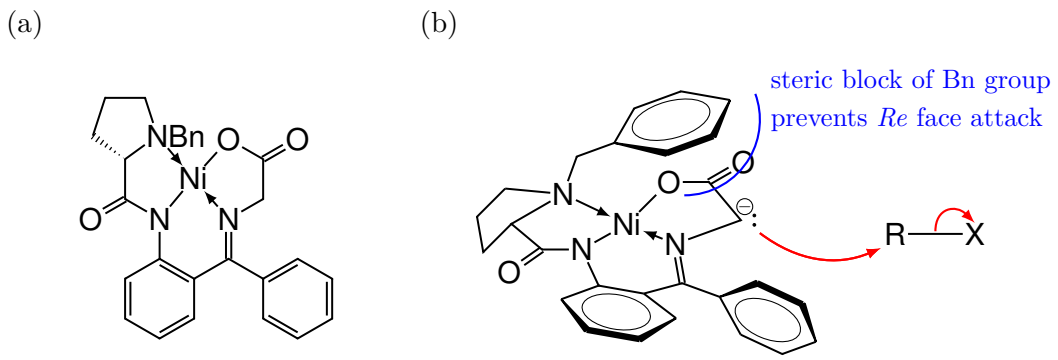

Figure 4.3. (a) Structure of NiCA and (b) rationale behind its stereospecificity.

could also be obtained from the reduction of a nitrile group. The nitrile group activates the ring toward nucleophilic aromatic substitution, thus 3,4-dichlorobenzonitrile (**4-2**) was chosen as a starting material for this synthesis (Scheme 4.1).

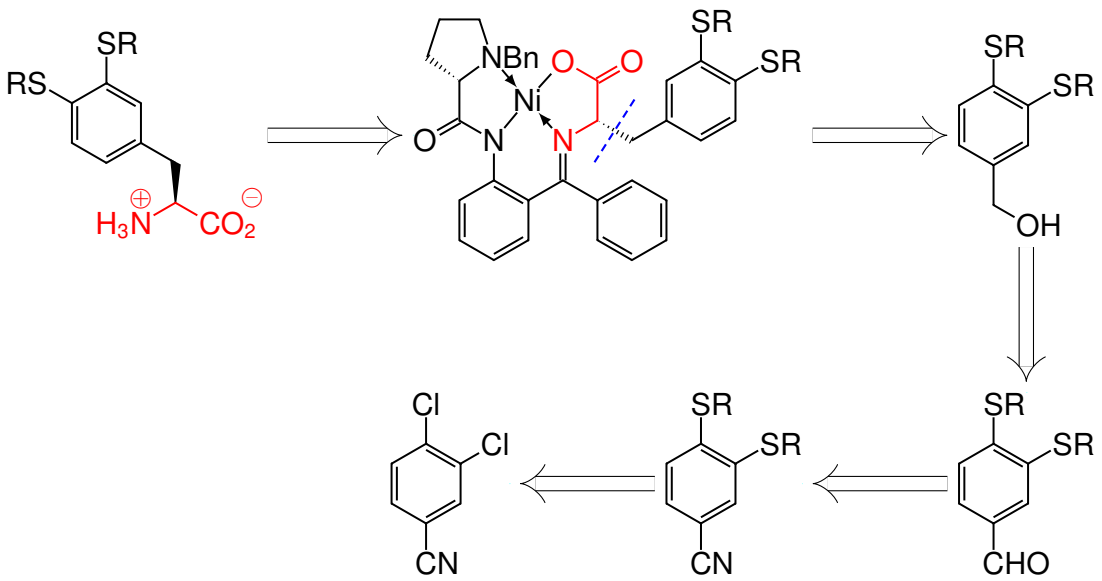

Scheme 4.1. Retrosynthetic analysis for the synthesis of compound **4-1**.

4.3 Results and Discussion

The synthetic route followed for the synthesis of the target compound is shown on Scheme 4.2. Two different sulfur nucleophiles were evaluated to introduce the thiol

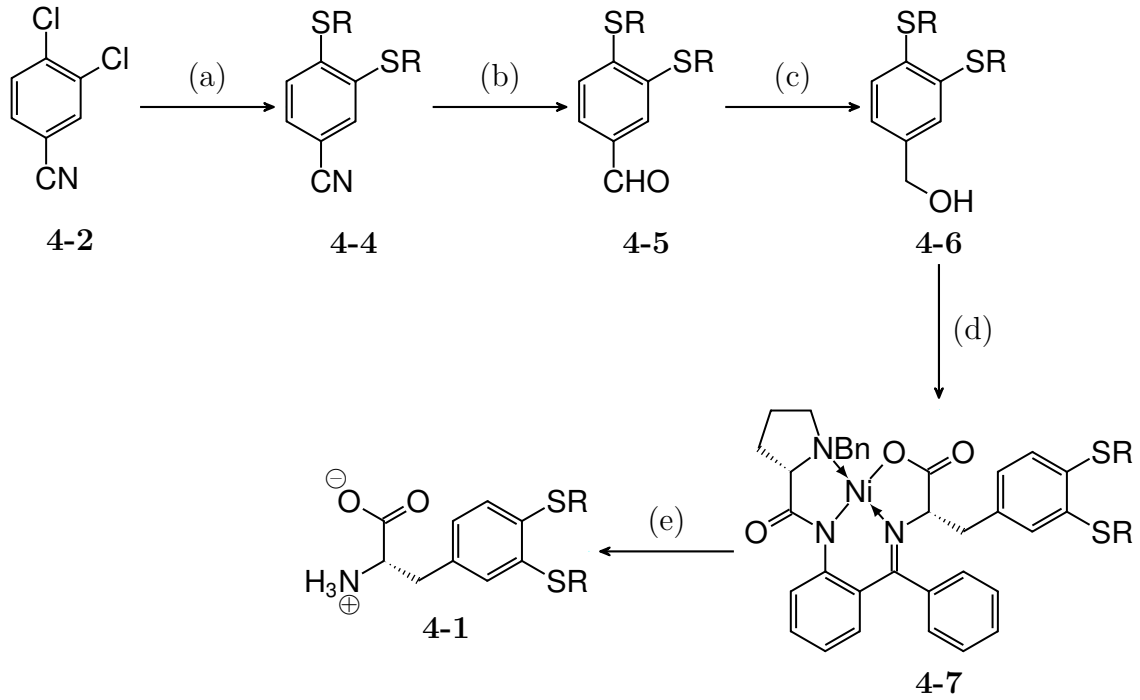

Scheme 4.2. Synthetic route for compound **4-1**. (a) **4-3a** or **4-3b**, NaH, DMF, 0 °C to r. t.; (b) DIBAL, toluene, 0 °C; (c) $NaBH_4$, EtOH; (d) NiCA, CMBP, toluene, 110 °C; (e) MeOH, HCl, reflux.

groups on the basis of their nucleophilicity and lability as protecting groups. The thiols thus chosen were (4-methoxyphenyl)methanethiol (**4-3a**), and 2-(trimethylsilyl)ethanethiol (**4-3b**).

The nucleophilic substitution of **4-2** to obtain compounds **4-4a**,**b** was carried out by using the sodium thiolate salt of the thiols, formed *in situ* by their irreversible deprotonation using NaH in DMF. Low to moderate yields were obtained when **4-3a** was used as compared to **4-3b**, likely due to the bulkiness of the former. Purification of **4-4a** was very demanding, indicating that a number of side reactions occurred when (4-methoxyphenyl)methyl (PMB) was used as protecting group, which could involve the monosubstituted products, demethylation of the methoxy group by the thiolate nucleophile, or other side products that can result from the latter. In contrast, there was little difficulty on when the 2-(trimethylsi-

lyl)ethyl (TMSE) group was used, in line with the lower steric hindrance and more inert nature of this group.

Selective reduction of the nitrile with DIBAL in THF yielded the desired aldehydes **4-5a**,**b** in moderate to high yields with no detectable side products. Further reduction to alcohols **4-6a**,**b** with $NaBH_4$ in an ethanol:water mixture also went smoothly for all compounds in good yields.

The NiCA was prepared as reported in the literature[35,37,38] and the coupling to the obtained alcohols using CMBP in refluxing toluene was carried out without major complications and the NiCA complexes **4-7a**,**b** were obtained in moderate yields. The structure of the complexes was determined by 2D NMR experiments (PMB: Figures C.15 to C.18; TMSE: Figures C.21 to C.24).

The free amino acid with the protected thiols was recovered after acidic hydrolysis of the NiCA complex in methanol. Surprisingly, the amino acid was recovered in the organic phase, likely due to the high hydrophobicity of the side chains, albeit along with the other part of the ligand as a result from the imine hydrolysis. Due to the ionic nature of the amino acid, column chromatography using silica gel proved complicated, as it is difficult to elute the amino acid once it is adsorbed onto the stationary phase. An alternative is to use ion exchange chromatography with an anion exchange resin, as at high pH values the amino groups in both, the amino acid and the ligand, will be the deprotonated (neutral), and the carboxylate in the amino acid will have a negative charge, thus making it possible to elute the ligand first, and then switch to an acidic solvent to elute the desired amino acid.

The removal of the protecting groups on **4-1** was not successful for either protecting group. The PMB groups have proven stable on acidic cleavage using TFA, both in DCM and neat, and to the use of mercury salts ($Hg(OAc)_2$) in this

same acid.[39,40] Other unsuccessful attempts include the use of $AgBF_4$ in TFA[41] and TMSCl with Ph_2SO in the same solvent.[42] Alternative methods that can be still assayed include anhydrous HF or reduction of the protecting group with sodium metal in ammonia.[43]

Similarly, the TMSE deprotection with tetrabutylammonium fluoride (TBAF) in THF[44] has not been successful in the deprotection of the thiol groups, despite the fact that **4-4b** did show signs of deprotection in the same conditions. A possible explanation of this fact is that the thiolate anion that acts as leaving group is better stabilized by the cyano group, suggesting that a stronger driving force may be necessary for a successful reaction on the amino acid. This could be accomplished by using a different source of fluoride ions in a less polar solvent, or by making use of a different deprotection mechanism that simultaneously protects the thiols from other side reactions, such as dimethyl(methylsulfanyl)sulfonium tetrafluoroborate ($(MeSSMe_2)BF_4$).[45]

4.4 Conclusions

This project aimed at developing a novel artificial amino acid bearing a 1,2-benzenedithiol side chain that could serve as anchoring point for embedding [FeFe]-hydrogenase mimics into peptide and protein scaffolds. Two versions of the desired amino acid were prepared with different protecting groups on the thiols, namely (4-methoxyphenyl)methyl and 2-(trimethylsilyl)ethyl. Product stereochemistry was controlled by using a nickel-based chiral auxiliary in a Mitsunobu-like reaction.

The use of this amino acid will allow future work into investigating the effect of [FeFe]-hydrogenase organometallic mimics that may be more suitable for the photoinduced reduction of protons, which could have important implications as we move toward a green fuel-based society. Additionally, this amino acid can be

used for the incorporation of other organometallic complexes, thus allowing a high throughput exploration of the effect of the protein environment on catalysts that are not close in structure or activity to those found in nature.[46,47] Further, the chelating nature of this particular ligand could be taken advantage of on the fields of metal-mediated self-assembly and the design of novel protein-based materials.

4.5 Experimental Details

All reagents were purchased from Acros Organics, Alfa Aesar, Oakwood Chemicals, Sigma Aldrich, or TCI America and used as received. All reactions were carried out under an atmosphere of argon gas using traditional Schlenk techniques. Dry DMF and toluene were purchased from Sigma Aldrich in SureSeal bottles and used as received. Thin Layer Chromatography (TLC) was performed on silica plates with a fluorescent marker (Analtech) and visualized under UV light, or by exposing to iodine vapors, a $KMnO_4$ stain solution, a 2,4-dinitrophenylhydrazine staining solution, an Ellman's reagent solution (for thiols), or a ninhydrin solution. Column chromatography was performed using 230–400 mesh silica gel (SiliaCycle). The compounds were characterized by NMR in a Varian 400 MHz or a Bruker 500 MHz spectrometer.

4.5.1 Synthesis of substituted benzonitriles (**4-4**)

3,4-Bis{[(4-methoxyphenyl)methyl]sulfanyl}benzaldehyde (4-4a). To a suspension of NaH (1.05 g, 43.6 mmol) in DMF (15 mL) was added **4-3a** (6.1 mL) in DMF (15 mL) dropwise while keeping the reaction in a water-ice bath. The suspension became clear and was stirred for 30 min at the same temperature. A solution of **4-2** (3.0 g) in DMF (10 mL) was then added dropwise through an addition funnel. The reaction mixture quickly turned to a yellow color. The water-ice bath

was removed and the mixture was stirred overnight at room temperature. The solvent was removed under reduced pressure and the residue diluted with water (15 mL). The suspension was extracted with $CHCl_3$ (3 × 25 mL), the organic layers washed with water (3 × 25 mL), dried over $MgSO_4$, and the solvent removed under reduced pressure. The pure product was purified by column chromatography using a hexanes:ethoxyethane (Et_2O) 3:2 as a mobile phase and obtained as a white solid (2.95 g, 35 %). m. p. 90–92 °C. R_f (hexanes:Et_2O 3:2) 0.1. ^{1}H NMR (400 MHz, $CDCl_3$): δ 7.34 (d, 1 H, J = 1.4 Hz), 7.30 (dd, 1 H, J = 8.2, 1.2 Hz), 7.24 (d, 2 H, J = 8.5 Hz), 7.15 (m, 3 H), 6.86 (m, 4 H), 4.14 (s, 2 H), 4.07 (s, 2 H), 3.80 (s, 3 H), 3.79 (s, 3 H). ^{13}C NMR (100 MHz, $CDCl_3$): δ 159.10, 159.02, 145.94, 137.78, 135.93, 132.93, 130.10, 130.03, 130.03, 129.91, 129.00, 128.19, 127.77, 127.04, 126.37, 125.27, 113.11, 113.97, 108.54, 55.23, 55.22, 37.71, 36.66.

3,4-Bis{[(2(trimethylsilyl)ethyl]sulfanyl}benzonitrile (4-4b). The procedure was similar to the one used for **4-4a**, using 1.79 mL (11.2 mmol) of **4-3b** as thiolate, 286 mg (11.9 mmol) of NaH, and 640 mg (3.72 mmol) of **4-2**. The compound was purified through column chromatography using hexanes:Et_2O 92.5:7.5 as mobile phase, and obtained as a clear oil (937 mg, 68 %). R_f (hexanes:Et_2O 92.5:7.5) 0.43. ^{1}H NMR (400 MHz, $CDCl_3$): δ 7.42 (d, 1 H, J = 1.7 Hz), 7.38 (dd, 1 H, J = 8.2, 1.7 Hz), 7.17 (d, 1 H, J = 8.2 Hz), 2.96 (m, 4 H), 0.96 (m, 4 H), 0.07 (s, 9 H), 0.06 (s, 9 H). ^{13}C NMR (100 MHz, $CDCl_3$): δ 145.65, 137.19, 131.04, 129.17, 125.61, 118.97, 108.30, 29.54, 28.53, 16.46, 16.00, −1.66.

4.5.2 Synthesis of substituted benzaldehydes (**4-5**)

3,4-Bis{[(4-methoxyphenyl)methyl]sulfanyl}benzaldehyde (4-5a). To a stirred solution of **4-4a** (2.95 g, 7.2 mmol) in dry toluene (70 mL) at 0 °C, DIBAL in toluene (25 % w/v in toluene, 9.9 mL, 14.5 mmol) was added dropwise through

an addition funnel. After the addition was completed, the reaction was stirred for 3 h at 0 °C, and then quenched by the dropwise addition of 3 mL of acetone, followed by the dropwise addition of half-saturated aqueous solution of Rochelle's salt (sodium potassium tartrate, 25 mL). The reaction was let warm up to room temperature and stirred overnight until the layers were separated. The aqueous layer was extracted with ethyl acetate (EtOAc) (3 × 50 mL), the organic fractions combined, and washed with brine (50 mL), dried over $MgSO_4$, and the solvent was removed *in vacuo*. The product was purified through column chromatography using hexanes:EtOAc 1:1 as mobile phase and obtained as a yellow oil (2.81 g, 95 %). R_f (hexanes:EtOAc 1:1) 0.56. ^{1}H NMR (400 MHz, $CDCl_3$): δ 9.72 (s, 1 H), 7.58 (d, 1 H, $J = 1.6$ Hz), 7.49 (dd, 1 H, $J = 8.1, 1.6$ Hz), 7.20 (d, 3 H, $J = 8.5$ Hz), 7.09 (d, 2 H, $J = 8.6$ Hz), 6.76 (d, 2 H, $J = 8.6$ Hz), 6.70 (d, 2 H, $J = 8.6$ Hz), 4.06 (s, 2 H), 4.01 (s, 2 H), 3.69 (s, 3 H), 3.67 (s, 3 H). ^{13}C NMR (100 MHz, $CDCl_3$): δ 191.03, 159.25, 159.10, 148.15, 135.39, 133.54, 131.41, 130.34, 130.25, 128.46, 128.30, 127.43, 126.16, 114.28, 114.09, 55.44, 55.41, 38.05, 36.89.

3,4-Bis{[(2-(trimethylsilyl)ethyl]sulfanyl}benzaldehyde (4-5b). This compound was synthesized using the same procedure as outlined for **4-5a** using 937 mg (2.55 mmol) of **4-4b** and 3.48 mL (5.10 mmol) of DIBAL (25 % w/v in toluene) in 25 mL of toluene. The compound was obtained after purification via column chromatography (hexanes:Et_2O 9:1), yielding a yellow oil (819 mg, 87 %). R_f (hexanes:Et_2O) 0.46. ^{1}H NMR (400 MHz, $CDCl_3$): δ 9.90 (s, 1 H), 7.72 (d, 1 H, $J = 1.7$ Hz), 7.61 (dd, 1 H, $J = 8.1, 1.7$ Hz), 7.25 (d, 1 H, $J = 8.1$ Hz), 3.03 (m, 4 H), 0.98 (m, 4 H), 0.08 (s, 9 H), 0.05 (s, 9 H). ^{13}C NMR (100 MHz, $CDCl_3$): δ 191.18, 147.92, 136.35, 133.24, 129.15, 127.83, 125.20, 29.49, 28.50, 16.70, 16.05, −1.62.

4.5.3 Synthesis of substituted benzyl alcohols (**4-6**)

(3,4-Bis{[(4-methoxyphenyl)methyl]sulfanyl}phenyl)methanol (4-6a). To a solution of **4-5a** (2.82 g, 6.9 mmol) in THF:EtOH 2:3 (25 mL) cooled at 0 °C was added $NaBH_4$ (628 mg, 2.4 mmol) in portions. The reaction was stirred for 3 h at room temperature and then poured onto HCl 2 N (25 mL) containing ice (30 g). The suspension was then extracted with $CHCl_3$ (3 × 50 mL), the organic layers dried with $MgSO_4$, and the solvent removed with a rotary evaporator. The compound is purified through column chromatography using hexanes:EtOAc 1:2 to obtain an off-white solid (2.29 g, 81 %). R_f (hexanes:EtOAc 1:2) 0.50. ^{1}H NMR (400 MHz, $(CD_3)_2CO$): δ 7.37 (d, 1 H, $J = 1.3$ Hz), 7.72 (m, 5 H), 7.11 (dd, 1 H, $J = 8.0, 1.3$ Hz), 6.84 (m, 4 H), 4.57 (d, 2 H, $J = 3.8$ Hz), 4.22 (br, 1 H), 4.13 (s, 2 H), 4.10 (s, 2 H), 3.76 (s, 3 H), 3.75 (s, 3 H). ^{13}C NMR (100 MHz, $CDCl_3$): δ 159.95, 159.89, 142.29, 138.52, 135.44, 131.14, 131.05, 130.91, 130.19, 129.93, 128.10, 125.41, 114.71, 114.66, 64.17, 55.58, 55.57, 38.05, 37.79.

(3,4-Bis{[2-(trimethylsilyl)ethyl]sulfanyl}phenyl)methanol (4-6b). The same procedure as for the preparation of **4-6a** was followed using 762 mg (2.06 mmol) of **4-5b** and 156 mg (4.12 mmol) of $NaBH_4$ in 8.2 mL of ethanol. After purification by column chromatography (hexanes:EtOAc 4:1) the compound was obtained as a yellow oil (732 mg, 96 %). R_f (hexanes:EtOAc 4:1) 0.44. ^{1}H NMR (400 MHz, $CDCl_3$): δ 7.25 (m, 2 H), 7.12 (dd, 1 H, $J = 8.0, 1.9$ Hz), 4.66 (s, 2 H), 2.95 (m, 4 H), 1.67 (br, 1 H), 0.95 (m, 4 H), 0.05 (s, 9 H), 0.04 (s, 9 H). ^{13}C NMR (100 MHz, $CDCl_3$): δ 138.98, 138.28, 136.56, 129.22, 127.09, 124.71, 65.09, 29.45, 29.14, 16.70, 16.60, −1.58, −1.61.

4.5.4 Synthesis of alkylated NiCA complexes (**4-7**)

[(*N*-Benzyl-L-prolyl-*κN*){2-[{(*E*)-[(*2S*)-(3,4-bis{[(4-methoxyphenyl)-methyl]sulfanyl}phenyl)-1-carboxylato-*κO*-ethyl]imino-*κN*}(phenyl)-methyl]phenyl}azanido-*κN*]nickel (4-7a). A solution of **4-6a** (596 mg, 1.45 mmol), NiCA (1.44 g, 2.89 mmol), and CMBP (380 µL), 1.45 mmol) in dry toluene (725 µL) was stirred and refluxed at 120 °C overnight. After the reaction was complete, the solvent was evaporated under reduced pressure and the crude mixture was purified through column chromatography using DCM 9:1 as mobile phase. The compound was obtained as a crystalline orange-red powder (714 mg, 55 %). When 2 eq of **4-5a** and CMBP where used in the presence of 1 eq of NiCA the yield was 96 % based on NiCA. R_f (DCM:acetone 9:1) 0.3. ^{1}H NMR (500 MHz, $CDCl_3$): δ 8.34 (dd, 1 H, $J = 8.8, 1.2$ Hz), 8.01 (d, 2 H, $J = 6.8$ Hz), 7.50 (m, 2 H), 7.39 (m, 1 H), 7.28 (m, 6 H), 7.16 (m, 2 H), 7.00 (d, 2 H, $J = 8.6$ Hz), 6.90 (m, 2 H), 6.81 (m, 2 H), 6.68 (m, 4 H), 6.43 (dd, 1 H, $J = 7.6, 1.7$ Hz), 4.23 (m, 2 H), 4.10 (d, 2 H, $J = 3.2$ Hz), 3.84 (m, 2 H), 3.78 (s, 3 H), 3.76 (s, 3 H), 3.43 (d, 1 H, $J = 12.6$ Hz), 3.31 (dd, 1 H, $J = 9.8, 7.2$ Hz), 3.05 (m, 1 H), 2.92 (dd, 1 H, $J = 13.8, 4.2$ Hz), 2.61 (dd, 1 H, $J = 13.8, 5.6$ Hz); 2.33 (m, 3 H), 1.93 (m, 1 H), 1.61 (m, 1 H) . ^{13}C NMR (125 MHz, $CDCl_3$): δ 180.54, 178.40, 171.13, 158.85, 158.66, 143.04, 139.65, 134.68, 134.11, 133.63, 133.41, 132.52, 131.50, 130.62, 130.13, 130.10, 129.91, 129.79, 129.06, 128.85, 128.77, 128.10, 127.91, 127.88, 127.03, 125.92, 123.54, 120.51, 113.94, 113.86, 113.83, 71.13, 70.30, 63.40, 57.53, 55.28, 55.25, 38.84, 37.86, 36.25, 30.82, 23.13.

[(*N*-Benzyl-L-prolyl-*κN*){2-[{(*E*)-[(*2S*)-(3,4-bis{[2-(trimethylsilyl)-ethyl]sulfanyl}phenyl)-1-carboxylato-*κO*-ethyl]imino-*κN*}(phenyl)methyl]-phenyl}azanido-*κN*]nickel (4-7b). A mixture of **4-6b** (732 mg, 1.96 mmol), NiCA (1.97 g), 3.93 mmol), and CMBP (515 µL, 1.96 µL) in dry toluene (4 mL) was

stirred and refluxed at 120 °C overnight. The solvent was then removed under reduced pressure and the crude mixture was purified via column chromatography using a gradient from DCM:acetone 99:1 to DCM:acetone 95:5 to obtain a red-orange oil (826 mg, 49 %). R_f (DCM:acetone 99:1) 0.26. ^{1}H NMR (500 MHz, $CDCl_3$): δ 8.23 (d, 1 H, J = 8.7 Hz), 8.03 (d, 2 H, J = 7.0 Hz), 7.51 (m, 2 H), 7.40 (m, 1 H), 7.27 (m, 4 H), 7.14 (m, 2 H) 6.96 (m, 2 H), 6.66 (m, 3 H), 4.28 (m, 2 H), 3.43 (d, 1 H, J = 12.7 Hz), 3.33 (dd, 1 H, J = 10.0, 7.1 Hz), 3.15 (m, 2 H), 2.95 (m, 2 H), 2.79 (m, 3 H), 2.53 (m, 1), 2.38 (m, 2 H), 2.00 (m, 1 H), 1.77 (m, 1 H), 0.93 (m, 4 H), 0.03 (s, 9 H), −0.01 (s, 9 H). ^{13}C NMR (125 MHz, $CDCl_3$): δ 180.53, 178.53, 171.16, 143.06, 138.85, 135.88, 134.19, 133.65, 133.43, 132.50, 131.61, 129.79, 129.09, 129.05, 128.88, 128.88, 128.51, 127.97, 127.72, 127.30, 126.16, 123.56, 120.65, 71.53, 70.48, 63.44, 57.65, 39.78, 30.99, 29.20, 28.58, 23.37, 16.59, 16.18, −1.62, −1.64.

4.5.5 General procedure for the synthesis of **4-1**

(*S*)-2-Amino-3-(3,4-bis{[(4-methoxyphenyl)methyl]sulfanyl}phenyl)-propanoic acid (4-1a). Compound **4-7a** (52 mg, 58 µmol) was refluxed in methanol (1.2 mL) in presence of HCl (60 µL, 120 µmol) for 2 h to obtain a blue-green solution. The solvent was then removed under reduced pressure. The crude product was redissolved in water (5 mL), and extracted with DCM (3 × 5 mL). The organic extracts were dried over $MgSO_4$ and the solvent evaporated. The product was not isolated.

(*S*)-2-Amino-3-(3,4-bis{[2-(trimethylsilyl)ethyl]sulfanyl}phenyl)-propanoic acid (4-1b). A mixture of **4-7b** (150 mg, 0.176 mmol) and HCl 2 M (1.76 mL, 3.52 mmol) in methanol (3.5 mL) was refluxed for 2 h and the solvent then removed under reduced pressure. The residue was treated with water (10 mL) and

extracted with DCM ($3 \times 10\,\mathrm{mL}$). The organic fractions were combined and dried over $MgSO_4$, and the solvent removed *in vacuo*. The product was not isolated.

4.6 References

1. Schlapbach, L.; Züttel, A. Hydrogen-storage materials for mobile applications. *Nature* **2001**, *414*, 353 (cit. on p. 51).

2. Chu, S.; Majumdar, A. Opportunities and challenges for a sustainable energy future. *Nature* **2012**, *488*, 294 (cit. on p. 51).

3. Vignais, P. M.; Billoud, B. Occurrence, Classification, and Biological Function of Hydrogenases: An Overview. *Chemical Reviews* **2007**, *107*, 4206–4272 (cit. on p. 51).

4. Faiella, M.; Roy, A.; Sommer, D.; Ghirlanda, G. De novo design of functional proteins: Toward artificial hydrogenases. *Peptide Science* **2013**, *100*, 558–571 (cit. on p. 51).

5. Adams, M. W. W. The structure and mechanism of iron-hydrogenases. *Biochimica et Biophysica Acta (BBA) - Bioenergetics* **1990**, *1020*, 115–145 (cit. on p. 51).

6. Nicolet, Y.; Piras, C.; Legrand, P.; Hatchikian, C. E.; Fontecilla-Camps, J. C. *Desulfovibrio desulfuricans* iron hydrogenase: the structure shows unusual coordination to an active site Fe binuclear center. *Structure* **1999**, *7*, 13–23 (cit. on p. 51).

7. Wang, N.; Wang, M.; Chen, L.; Sun, L. Reactions of [FeFe]-hydrogenase models involving the formation of hydrides related to proton reduction and hydrogen oxidation. *Dalton Transactions* **2013**, *42*, 12059–12071 (cit. on pp. 51, 52).

8. Capon, J.-F.; Gloaguen, F.; Pétillon, F. Y.; Schollhammer, P.; Talarmin, J. Electron and proton transfers at diiron dithiolate sites relevant to the catalysis of proton reduction by the [FeFe]-hydrogenases. *Coordination Chemistry Reviews* **2009**, *253*, 1476–1494 (cit. on pp. 51, 52).

9. Felton, G. A. N.; Mebi, C. A.; Petro, B. J.; Vannucci, A. K.; Evans, D. H.; Glass, R. S.; Lichtenberger, D. L. Review of electrochemical studies of complexes containing the Fe_2S_2 core characteristic of [FeFe]-hydrogenases including catalysis by these complexes of the reduction of acids to form dihydrogen. *Journal of Organometallic Chemistry* **2009**, *694*, 2681–2699 (cit. on pp. 51, 52).

10. Camara, J. M.; Rauchfuss, T. B. Combining acid-base, redox and substrate binding functionalities to give a complete model for the [FeFe]-hydrogenase. *Nature Chemistry* **2011**, *4*, 26 (cit. on p. 51).

11. Tard, C.; Pickett, C. J. Structural and Functional Analogues of the Active Sites of the [Fe]-, [NiFe]-, and [FeFe]-Hydrogenases. *Chemical Reviews* **2009**, *109*, 2245–2274 (cit. on p. 51).

12. DuBois, D. L.; Bullock, R. M. Molecular Electrocatalysts for the Oxidation of Hydrogen and the Production of Hydrogen—The Role of Pendant Amines as Proton Relays. *European Journal of Inorganic Chemistry* **2011**, *2011*, 1017–1027 (cit. on p. 51).

13. Lomoth, R.; Ott, S. Introducing a dark reaction to photochemistry: photocatalytic hydrogen from [FeFe] hydrogenase active site model complexes. *Dalton Transactions* **2009**, 9952–9959 (cit. on pp. 52, 54).

14. Wang, M.; Chen, L.; Li, X.; Sun, L. Approaches to efficient molecular catalyst systems for photochemical H_2 production using [FeFe]-hydrogenase active site mimics. *Dalton Transactions* **2011**, *40*, 12793–12800 (cit. on p. 52).

15. Wang, F.; Wang, W.-G.; Wang, H.-Y.; Si, G.; Tung, C.-H.; Wu, L.-Z. Artificial Photosynthetic Systems Based on [FeFe]-Hydrogenase Mimics: the Road to High Efficiency for Light-Driven Hydrogen Evolution. *ACS Catalysis* **2012**, *2*, 407–416 (cit. on p. 52).

16. Knörzer, P.; Silakov, A.; Foster, C. E.; Armstrong, F. A.; Lubitz, W.; Happe, T. Importance of the Protein Framework for Catalytic Activity of [FeFe]-Hydrogenases. *Journal of Biological Chemistry* **2012**, *287*, 1489–1499 (cit. on p. 52).

17. Winkler, M.; Esselborn, J.; Happe, T. Molecular basis of [FeFe]-hydrogenase function: An insight into the complex interplay between protein and catalytic cofactor. *Biochimica et Biophysica Acta (BBA) - Bioenergetics* **2013**, *1827*, 974–985 (cit. on p. 52).

18. Alcala-Torano, R.; Sommer, D. J.; Bahrami Dizicheh, Z.; Ghirlanda, G. Chapter Seventeen—Design Strategies for Redox Active Metalloenzymes: Applications in Hydrogen Production. In *Methods in Enzymology*, Pecoraro, V. L., Ed.; Academic Press: 2016, pp 389–416 (cit. on p. 52).

19. Singleton, M. L.; Reibenspies, J. H.; Darensbourg, M. Y. A Cyclodextrin Host/Guest Approach to a Hydrogenase Active Site Biomimetic Cavity. *Journal of the American Chemical Society* **2010**, *132*, 8870–8871 (cit. on p. 52).

20. Jian, J.-X.; Liu, Q.; Li, Z.-J.; Wang, F.; Li, X.-B.; Li, C.-B.; Liu, B.; Meng, Q.-Y.; Chen, B.; Feng, K.; Tung, C.-H.; Wu, L.-Z. Chitosan confinement enhances hydrogen photogeneration from a mimic of the diiron subsite of [FeFe]-hydrogenase. *Nature Communications* **2013**, *4*, 2695 (cit. on p. 52).

21. Pullen, S.; Fei, H.; Orthaber, A.; Cohen, S. M.; Ott, S. Enhanced Photochemical Hydrogen Production by a Molecular Diiron Catalyst Incorporated into a Metal-Organic Framework. *Journal of the American Chemical Society* **2013**, *135*, 16997–17003 (cit. on p. 52).

22. Wang, F.; Liang, W.-J.; Jian, J.-X.; Li, C.-B.; Chen, B.; Tung, C.-H.; Wu, L.-Z. Exceptional Poly(acrylic acid)-Based Artificial [FeFe]-Hydrogenases for Photocatalytic H_2 Production in Water. *Angewandte Chemie International Edition* **2013**, *52*, 8134–8138 (cit. on p. 52).

23. Yu, T.; Zeng, Y.; Chen, J.; Li, Y.-Y.; Yang, G.; Li, Y. Exceptional Dendrimer-Based Mimics of Diiron Hydrogenase for the Photochemical Production of Hydrogen. *Angewandte Chemie International Edition* **2013**, *52*, 5631–5635 (cit. on p. 52).

24. Jones, A. K.; Lichtenstein, B. R.; Dutta, A.; Gordon, G.; Dutton, P. L. Synthetic Hydrogenases: Incorporation of an Iron Carbonyl Thiolate into a Designed Peptide. *Journal of the American Chemical Society* **2007**, *129*, 14844–14845 (cit. on p. 53).

25. Apfel, U.-P.; Rudolph, M.; Apfel, C.; Robl, C.; Langenegger, D.; Hoyer, D.; Jaun, B.; Ebert, M.-O.; Alpermann, T.; Seebach, D.; Weigand, W. Reaction of $Fe_3(CO)_{12}$ with octreotide—chemical, electrochemical and biological investigations. *Dalton Transactions* **2010**, *39*, 3065–3071 (cit. on p. 53).

26. Sano, Y.; Onoda, A.; Hayashi, T. A hydrogenase model system based on the sequence of cytochrome *c*: photochemical hydrogen evolution in aqueous media. *Chemical Communications* **2011**, *47*, 8229–8231 (cit. on p. 53).

27. Sano, Y.; Onoda, A.; Hayashi, T. Photocatalytic hydrogen evolution by a diiron hydrogenase model based on a peptide fragment of cytochrome c_{556} with an attached diiron carbonyl cluster and an attached ruthenium photosensitizer. *Journal of Inorganic Biochemistry* **2012**, *108*, 159–162 (cit. on p. 53).

28. Roy, S.; Shinde, S.; Hamilton, G. A.; Hartnett, H. E.; Jones, A. K. Artificial [FeFe]-Hydrogenase: On Resin Modification of an Amino Acid to Anchor a Hexacarbonyldiiron Cluster in a Peptide Framework. *European Journal of Inorganic Chemistry* **2011**, *2011*, 1050–1055 (cit. on p. 53).

29. Onoda, A.; Kihara, Y.; Fukumoto, K.; Sano, Y.; Hayashi, T. Photoinduced Hydrogen Evolution Catalyzed by a Synthetic Diiron Dithiolate Complex Embedded within a Protein Matrix. *ACS Catalysis* **2014**, *4*, 2645–2648 (cit. on p. 53).

30. Roy, A.; Madden, C.; Ghirlanda, G. Photo-induced hydrogen production in a helical peptide incorporating a [FeFe] hydrogenase active site mimic. *Chemical Communications* **2012**, *48*, 9816–9818 (cit. on p. 53).

31. Roy, S.; Nguyen, T.-A. D.; Gan, L.; Jones, A. K. Biomimetic peptide-based models of [FeFe]-hydrogenases: utilization of phosphine-containing peptides. *Dalton Transactions* **2015**, *44*, 14865–14876 (cit. on p. 53).

32. Felton, G. A. N.; Vannucci, A. K.; Chen, J.; Lockett, L. T.; Okumura, N.; Petro, B. J.; Zakai, U. I.; Evans, D. H.; Glass, R. S.; Lichtenberger, D. L. Hydrogen Generation from Weak Acids: Electrochemical and Computational Studies of a Diiron Hydrogenase Mimic. *Journal of the American Chemical Society* **2007**, *129*, 12521–12530 (cit. on p. 54).

33. Capon, J.-F.; Gloaguen, F.; Schollhammer, P.; Talarmin, J. Activation of proton by the two-electron reduction of a di-iron organometallic complex. *Journal of Electroanalytical Chemistry* **2006**, *595*, 47–52 (cit. on p. 54).

34. Streich, D.; Astuti, Y.; Orlandi, M.; Schwartz, L.; Lomoth, R.; Hammarström, L.; Ott, S. High-Turnover Photochemical Hydrogen Production Catalyzed by a Model Complex of the [FeFe]-Hydrogenase Active Site. *Chemistry – A European Journal* **2010**, *16*, 60–63 (cit. on p. 54).

35. Belokon, Y. N.; Bakhmutov, V. I.; Chernoglazova, N. I.; Kochetkov, K. A.; Vitt, S. V.; Garbalinskaya, N. S.; Belikov, V. M. General method for the asymmetric synthesis of α-amino acids via alkylation of the chiral nickel(II) Schiff base complexes of glycine and alanine. *Journal of the Chemical Society, Perkin Transactions 1* **1988**, 305–312 (cit. on pp. 54, 57).

36. Noisier, A. F. M.; Harris, C. S.; Brimble, M. A. Novel preparation of chiral α-amino acids using the Mitsunobu-Tsunoda reaction. *Chemical Communications* **2013**, *49*, 7744–7746 (cit. on p. 54).

37. Belokon, Y. N.; Tararov, V. I.; Maleev, V. I.; Savel'eva, T. F.; Ryzhov, M. G. Improved procedures for the synthesis of (*S*)-2-[*N*-(*N′*-benzylprolyl)amino]-benzophenone (BPB) and Ni(II) complexes of Schiff's bases derived from BPB and amino acids. *Tetrahedron: Asymmetry* **1998**, *9*, 4249–4252 (cit. on p. 57).

38. Ueki, H.; Ellis, T. K.; Martin, C. H.; Boettiger, T. U.; Bolene, S. B.; Soloshonok, V. A. Improved Synthesis of Proline-Derived Ni(II) Complexes of Glycine: Versatile Chiral Equivalents of Nucleophilic Glycine for General Asymmetric Synthesis of α-Amino Acids. *The Journal of Organic Chemistry* **2003**, *68*, 7104–7107 (cit. on p. 57).

39. Shiro, A.; Shumpei, S.; Yasutsugu, S.; Yoshifumi, N. A New Method for the Protection of the Sulfhydryl Group during Peptide Synthesis. *Bulletin of the Chemical Society of Japan* **1964**, *37*, 433–434 (cit. on p. 58).

40. Nishimura, O.; Kitada, C.; Fujino, M. New Method for Removing the S-*p*-Methoxybenzyl and S-*t*-Butyl Groups of Cysteine Residues with Mercuric Trifluoroacetate. *Chemical & Pharmaceutical Bulletin* **1978**, *26*, 1576–1585 (cit. on p. 58).

41. Yoshida, M.; Tatsumi, T.; Fujiwara, Y.; Iinuma, S.; Kimura, T.; Akaji, K.; Kiso, Y. Deprotection of the S-Trimetylacetamidomethyl (Tacm) Group Using Silver Tetrafluoroborate: Application to the Synthesis of Porcine Brain Natriuretic Peptide-32 (pBNP-32). *Chemical & Pharmaceutical Bulletin* **1990**, *38*, 1551–1557 (cit. on p. 58).

42. Akaji, K.; Tatsumi, T.; Yoshida, M.; Kimura, T.; Fujiwara, Y.; Kiso, Y. Synthesis of cystine-peptide by a new disulphide bond-forming reaction using the siiyl chloride–sulphoxide system. *Journal of the Chemical Society, Chemical Communications* **1991**, 167–168 (cit. on p. 58).

43. Corrie, J. E. T.; Hlubucek, J. R.; Lowe, G. Synthesis of a cephalosporin analogue. *Journal of the Chemical Society, Perkin Transactions 1* **1977**, 1421–1425 (cit. on p. 58).

44. Koreeda, M.; Yang, W. Chemistry of 1,2-Dithiins. Synthesis of the Potent Antibiotic Thiarubrine A. *Journal of the American Chemical Society* **1994**, *116*, 10793–10794 (cit. on p. 58).

45. Anderson, M. B.; Ranasinghe, M. G.; Palmer, J. T.; Fuchs, P. L. Cytochalasin support studies. 10. Nucleophilic and electrophilic mercaptanylations via 2-(trimethylsilyl)ethanethiol-derived reagents. *The Journal of Organic Chemistry* **1988**, *53*, 3125–3127 (cit. on p. 58).

46. Huynh, H. V.; Schulze-Isfort, C.; Seidel, W. W.; Lügger, T.; Fröhlich, R.; Kataeva, O.; Hahn, F. E. Dinuclear Complexes with Bis(benzenedithiolate) Ligands. *Chemistry – A European Journal* **2002**, *8*, 1327–1335 (cit. on p. 59).

47. McNamara, W. R.; Han, Z.; Yin, C.-J.; Brennessel, W. W.; Holland, P. L.; Eisenberg, R. Cobalt-dithiolene complexes for the photocatalytic and electrocatalytic reduction of protons in aqueous solutions. *Proceedings of the National Academy of Sciences* **2012**, *109*, 15594–15599 (cit. on p. 59).

CHAPTER 5

CONCLUDING REMARKS AND FUTURE OUTLOOK

Over millions of years of evolution, nature has selected a rich variety of metalloenzymes that make use of earth-abundant metals embedded in a protein architecture in order to catalyze a wide array of redox reactions. As such, studying the effect that the protein plays in regulating the activity of these metal-based catalytic centers has become a growing field of study. In particular, the design of artificial metalloenzymes with tailored activities has become the objective of many research groups, as current methodologies to carry out the production of valuable goods—such as renewable fuels—typically involve the use of expensive and energy intensive methodologies.

This thesis explored the design of metalloproteins with aims at building a multicomponent system that could integrate the several parts of a light-driven redox catalytic reaction, such as the light absorbing component, an electron transport chain, and the catalytic center. Further, it also discussed the use of two strategies to incorporate catalytic centers into protein and peptide environments in order to enhance their catalytic properties in the reduction of protons into hydrogen gas and carbon dioxide into other reduced carbon species.

Since each part of the redox process has its own particular requirements, the best approach would be to develop a strategy that can be used to bring each of the elements together. The first part of this dissertation makes use of 2,2′-bipyridine as a ligand to template the metal-driven trimerization of peptides. By covalently attaching this ligand to DSD, a robust protein scaffold that forms dimers in solution, it was shown that addition of divalent metals results in the trimerization of these dimers, effectively forming a hexameric supramolecular architecture. The results

also indicate that the degree of oligomerization strongly depends on the sequence of the peptide and the nature of the metal ion, as thermodynamics and kinetics of the formation of the tris(bpy) complexes has an effect in the folding of the designed peptides.

In particular, this strategy can be not only utilized for the assembly of the desired components into a supramolecular machinery, but the use of the tris(bpy) functionality opens up the door for the formation of photoactive complexes, which may be utilized as the light absorbing centers of the system. Future experiments with this strategy would then aim at incorporating the electron transfer and catalytic modules into a single structure, as well as introducing a photoactive species into the architecture, whether it be by integration of a third subunit, or by making use of photoactive tris(bpy) moieties.

With a system capable of combining the necessary components into a single entity, this dissertation then explores the use and development of strategies that make use of proteins or peptides as scaffolds that incorporate earth-abundant organometallic complexes in order to enhance their properties through the effect of the surrounding environment.

The first of these strategies made use of a host-guest approach by incorporating the cobalt version of heme, cobalt protoporphyrin IX, into cytochrome b_{562}, a natural heme-binding protein. In this particular enzyme, the protein not only serves as a support for the metal complex, but it also provides two coordinating ligands that can alter the properties of the bare compound. Taking this into consideration, the underlying hypothesis of this work was that modification of these particular ligands would have an effect in the catalytic properties of this complex. Further, in order to evaluate their potential use as catalysts for the target reactions in an environmentally friendly fashion, the activity of these constructs was assayed

in the presence of a photosensitizer/sacrificial electron donor; consequently, light was the primary energy source to drive these catalytic reactions.

There are three key aspects that are worth highlighting. First, incorporation of the porphyrin into any of the studied protein structures resulted in active catalysts that remained water soluble throughout the time span of the experiments, as opposed to the porphyrin which quickly precipitated in water. Additionally, all of the designed metalloenzymes were active toward proton and CO_2 reduction, producing molecular hydrogen from the former, and carbon monoxide and formic acid from the latter, and total turnover number was enhanced for the production of hydrogen and carbon monoxide upon reconstitution of the protein with the cobalt porphyrin. Finally, the total activity for hydrogen production varied between the analyzed mutants, while that of CO and HCO_2H remained the same. This important finding supports the hypothesis that modification of the axial ligands would result in modification of the catalytic activity. Interestingly, these results also suggest that although the observed effect of the studied mutations may operate on certain reactions, it may not be as evident in others.

This last statement presents an opportunity for future work with this system. Exploring the functional groups that can be incorporated into the protein sequence—and now not only limited to natural amino acids but also a library of artificial ones—future endeavors may seek to characterize the effect of other residues that may act as ligands in order to observe an effect on the catalytic reduction of CO_2 or to further improve on the activity of hydrogen generation. Moving forward, modification of residues surrounding the active site might offer not only better catalysts, but also insight into the mechanism of the reactions at play, thus resulting in a better foundation for the rational design of this and other metalloenzymes.

While this approach has proven useful for incorporating a catalyst that is not found in nature to a guest protein, it is limited in the sense that this and related proteins are designed to bind the same type of cofactors due to the nature of the binding pocket. In order to expand the range of organometallic complexes that could be incorporated into the protein environment a different strategy has been developed. This dissertation has also presented a suitable alternative to incorporate another class of catalysts by describing the preparation of an unnatural amino acid bearing a 1,2-benzenedithiol side chain. Two versions of the amino acids have been prepared through an enantioselective route that yielded the amino acid in the same configuration as natural amino acids. The two amino acids differ in the protecting groups for the thiol groups, one with PMB and TMSE, respectively.

This novel amino acid resembles the dithiol bridge present in the unique active site of [FeFe]-hydrogenases, thus it is suitable for the incorporation of mimics of this catalytic center. Moreover, complexes bearing this non-innocent ligand have been shown to have enhanced catalytic activity when used during the light driven reduction of protons, likely due to the stabilization of the one-electron reduced species that are inherently formed throughout the process.

Non-natural amino acids are a powerful tool when it comes to conferring new functionality to proteins. This particular functional group is interesting in the metalloenzyme field as it offers a new chelating ligand capable of binding metals, particularly in lower redox states due to the soft nature of the thiolate groups, and stabilizing radical intermediates. Moving forward, two general pathways for the use of this amino acid can be outlined. First, the incorporation of the amino acid into small peptides by automated solid phase synthesis should be straightforward from the Fmoc protected compound. In this way organometallic complexes can be reconstituted to form water soluble versions thereof. Perhaps of interest could be to

take advantage of the orthogonality of the protecting groups that have been used, as this would allow the introduction of different metal functionalities on different positions of the same structure.

The second pathway would be the introduction of the amino acid into protein scaffolds by making use of amber codon suppression technology, which allows the incorporation of non-natural amino acids into protein sequences by using a tRNA/tRNA aminoacyl synthase pair that is orthogonal to the cell expression system. The success of this approach would greatly broaden the scope not only of protein environments that can be used to analyze their effects on organometallic mimics, but also for the high-throughput screening for finding the best scaffolds for a particular complex, or even directed evolution methods to select for them.

Ultimately, this thesis has contributed to the field of metalloprotein design by offering strategies to incorporate catalysts into proteins, exploring the effect of protein environment on catalysts, and providing a methodology for the assembly of components of a multi-domain protein based redox system. Overall, the results of this thesis are compatible with current research efforts as they expand on the interaction between proteins and metals upon catalysis, while setting the starting point for future projects in the area. The mechanistic insight gathered through these projects will help with the development of new and better protein-based catalysts and the chemical principles behind them could also further be applied to other materials, thus playing an important role in the development of new technologies that can satisfy our society's growing energetic demand in a sustainable way.

REFERENCES

Adams, M. W. W. The structure and mechanism of iron-hydrogenases. *Biochimica et Biophysica Acta (BBA) - Bioenergetics* **1990**, *1020*, 115–145 (cit. on p. 51).

Akaji, K.; Tatsumi, T.; Yoshida, M.; Kimura, T.; Fujiwara, Y.; Kiso, Y. Synthesis of cystine-peptide by a new disulphide bond-forming reaction using the siiyl chloride–sulphoxide system. *Journal of the Chemical Society, Chemical Communications* **1991**, 167–168 (cit. on p. 58).

Alcala-Torano, R.; Sommer, D. J.; Bahrami Dizicheh, Z.; Ghirlanda, G. Chapter Seventeen—Design Strategies for Redox Active Metalloenzymes: Applications in Hydrogen Production. In *Methods in Enzymology*, Pecoraro, V. L., Ed.; Academic Press: 2016, pp 389–416 (cit. on pp. 30, 52).

Alcala-Torano, R.; Walther, M.; Sommer, D. J.; Park, C. K.; Ghirlanda, G. Rational design of a hexameric protein assembly stabilized by metal chelation. *Biopolymers* **2018**, *109*, e23233 (cit. on p. 4).

Allen, M.; Dube, O.; Solecki, W.; Aragón-Durand, F.; Cramer, W.; Humphreys, S.; Kainuma, M.; Kala, J.; Mahowald, N.; Mulugetta, Y.; Perez, R.; M.Wairiu; Zickfeld, K. Framing and Context. In *Global Warming of 1.5°C. An IPCC Special Report on the impacts of global warming of 1.5°C above pre-industrial levels and related global greenhouse gas emission pathways, in the context of strengthening the global response to the threat of climate change, sustainable development, and efforts to eradicate poverty*, Masson-Delmotte, V., Zhai, P., Pörtner, H.-O., Roberts, D., Skea, J., Shukla, P., Pirani, A., Moufouma-Okia, W., Péan, C., Pidcock, R., Connors, S., Matthews, J., Chen, Y., Zhou, X., Gomis, M., Lonnoy, E., Maycock, T., Tignor, M., Waterfield, T., Eds.; In Press: 2018 (cit. on p. 1).

Anderson, M. B.; Ranasinghe, M. G.; Palmer, J. T.; Fuchs, P. L. Cytochalasin support studies. 10. Nucleophilic and electrophilic mercaptanylations via 2-(trimethylsilyl)ethanethiol-derived reagents. *The Journal of Organic Chemistry* **1988**, *53*, 3125–3127 (cit. on p. 58).

Apfel, U.-P.; Rudolph, M.; Apfel, C.; Robl, C.; Langenegger, D.; Hoyer, D.; Jaun, B.; Ebert, M.-O.; Alpermann, T.; Seebach, D.; Weigand, W. Reaction of $Fe_3(CO)_{12}$ with octreotide—chemical, electrochemical and biological investigations. *Dalton Transactions* **2010**, *39*, 3065–3071 (cit. on p. 53).

Aussignargues, C.; Pandelia, M.-E.; Sutter, M.; Plegaria, J. S.; Zarzycki, J.; Turmo, A.; Huang, J.; Ducat, D. C.; Hegg, E. L.; Gibney, B. R.; Kerfeld, C. A.

Structure and function of a bacterial microcompartment shell protein engineered to bind a [4Fe-4S] cluster. *Journal of the American Chemical Society* **2016**, *138*, 5262–5270 (cit. on p. 8).

Azcarate, I.; Costentin, C.; Robert, M.; Savéant, J.-M. Dissection of Electronic Substituent Effects in Multielectron-Multistep Molecular Catalysis. Electrochemical CO_2-to-CO Conversion Catalyzed by Iron Porphyrins. *The Journal of Physical Chemistry C* **2016**, *120*, 28951–28960 (cit. on p. 31).

Azcarate, I.; Costentin, C.; Robert, M.; Savéant, J.-M. Through-Space Charge Interaction Substituent Effects in Molecular Catalysis Leading to the Design of the Most Efficient Catalyst of CO_2-to-CO Electrochemical Conversion. *Journal of the American Chemical Society* **2016**, *138*, 16639–16644 (cit. on p. 31).

Bale, J. B.; Gonen, S.; Liu, Y.; Sheffler, W.; Ellis, D.; Thomas, C.; Cascio, D.; Yeates, T. O.; Gonen, T.; King, N. P.; Baker, D. Accurate design of megadalton-scale two-component icosahedral protein complexes. *Science* **2016**, *353*, 389–394 (cit. on p. 8).

Barelli, L.; Bidini, G.; Gallorini, F.; Servili, S. Hydrogen production through sorption-enhanced steam methane reforming and membrane technology: A review. *Energy* **2008**, *33*, 554–570 (cit. on p. 2).

Belokon, Y. N.; Bakhmutov, V. I.; Chernoglazova, N. I.; Kochetkov, K. A.; Vitt, S. V.; Garbalinskaya, N. S.; Belikov, V. M. General method for the asymmetric synthesis of α-amino acids via alkylation of the chiral nickel(II) Schiff base complexes of glycine and alanine. *Journal of the Chemical Society, Perkin Transactions 1* **1988**, 305–312 (cit. on pp. 54, 57).

Belokon, Y. N.; Tararov, V. I.; Maleev, V. I.; Savel'eva, T. F.; Ryzhov, M. G. Improved procedures for the synthesis of (*S*)-2-[*N*-(*N′*-benzylprolyl)amino]-benzophenone (BPB) and Ni(II) complexes of Schiff's bases derived from BPB and amino acids. *Tetrahedron: Asymmetry* **1998**, *9*, 4249–4252 (cit. on p. 57).

Bhugun, I.; Lexa, D.; Savéant, J.-M. Catalysis of the Electrochemical Reduction of Carbon Dioxide by Iron(0) Porphyrins: Synergystic Effect of Weak Brönsted Acids. *Journal of the American Chemical Society* **1996**, *118*, 1769–1776 (cit. on p. 31).

Birdja, Y. Y.; Vos, R. E.; Wezendonk, T. A.; Jiang, L.; Kapteijn, F.; Koper, M. T. M. Effects of Substrate and Polymer Encapsulation on CO_2 Electrore-

duction by Immobilized Indium(III) Protoporphyrin. *ACS Catalysis* **2018**, *8*, 4420–4428 (cit. on p. 31).

Boyle, A. L.; Woolfson, D. N. De novo designed peptides for biological applications. *Chemical Society Reviews* **2011**, *40*, 4295–4306 (cit. on p. 8).

Brodin, J. D.; Carr, J. R.; Sontz, P. A.; Tezcan, F. A. Exceptionally stable, redox-active supramolecular protein assemblies with emergent properties. *Proceedings of the National Academy of Sciences of the United States of America* **2014**, *111*, 2897–2902 (cit. on pp. 8, 9).

Call, A.; Cibian, M.; Yamamoto, K.; Nakazono, T.; Yamauchi, K.; Sakai, K. Highly Efficient and Selective Photocatalytic CO_2 Reduction to CO in Water by a Cobalt Porphyrin Molecular Catalyst. *ACS Catalysis* **2019**, *9*, 4867–4874 (cit. on p. 31).

Camara, J. M.; Rauchfuss, T. B. Combining acid-base, redox and substrate binding functionalities to give a complete model for the [FeFe]-hydrogenase. *Nature Chemistry* **2011**, *4*, 26 (cit. on p. 51).

Capon, J.-F.; Gloaguen, F.; Pétillon, F. Y.; Schollhammer, P.; Talarmin, J. Electron and proton transfers at diiron dithiolate sites relevant to the catalysis of proton reduction by the [FeFe]-hydrogenases. *Coordination Chemistry Reviews* **2009**, *253*, 1476–1494 (cit. on pp. 51, 52).

Capon, J.-F.; Gloaguen, F.; Schollhammer, P.; Talarmin, J. Activation of proton by the two-electron reduction of a di-iron organometallic complex. *Journal of Electroanalytical Chemistry* **2006**, *595*, 47–52 (cit. on p. 54).

Case, M. A.; McLendon, G. L. Metal-assembled modular proteins: Toward functional protein design. *Accounts of Chemical Research* **2004**, *37*, 754–762 (cit. on p. 9).

Chu, S.; Majumdar, A. Opportunities and challenges for a sustainable energy future. *Nature* **2012**, *488*, 294 (cit. on p. 51).

Corrie, J. E. T.; Hlubucek, J. R.; Lowe, G. Synthesis of a cephalosporin analogue. *Journal of the Chemical Society, Perkin Transactions 1* **1977**, 1421–1425 (cit. on p. 58).

Costentin, C.; Drouet, S.; Robert, M.; Savéant, J.-M. A Local Proton Source Enhances CO_2; Electroreduction to CO by a Molecular Fe Catalyst. *Science* **2012**, *338*, 90 (cit. on p. 31).

Dang, B.; Wu, H.; Mulligan, V. K.; Mravic, M.; Wu, Y.; Lemmin, T.; Ford, A.; Silva, D.-A.; Baker, D.; DeGrado, W. F. De novo design of covalently constrained mesosize protein scaffolds with unique tertiary structures. *Proceedings of the National Academy of Sciences of the United States of America* **2017**, *114*, 10852–10857 (cit. on p. 8).

Dhanasekaran, T.; Grodkowski, J.; Neta, P.; Hambright, P.; Fujita, E. *p*-Terphenyl-Sensitized Photoreduction of CO_2 with Cobalt and Iron Porphyrins. Interaction between CO and Reduced Metalloporphyrins. *The Journal of Physical Chemistry A* **1999**, *103*, 7742–7748 (cit. on p. 40).

DuBois, D. L.; Bullock, R. M. Molecular Electrocatalysts for the Oxidation of Hydrogen and the Production of Hydrogen—The Role of Pendant Amines as Proton Relays. *European Journal of Inorganic Chemistry* **2011**, *2011*, 1017–1027 (cit. on p. 51).

Faiella, M.; Roy, A.; Sommer, D.; Ghirlanda, G. De novo design of functional proteins: Toward artificial hydrogenases. *Peptide Science* **2013**, *100*, 558–571 (cit. on p. 51).

Fedorova, A.; Chaudhari, A.; Ogawa, M. Y. Photoinduced electron-transfer along alpha-helical and coiled-coil metallopeptides. *Journal of the American Chemical Society* **2003**, *125*, 357–362 (cit. on p. 9).

Fedorova, A.; Ogawa, M. Y. Site-specific modification of de novo designed coiled-coil polypeptides with inorganic redox complexes. *Bioconjugate Chemistry* **2002**, *13*, 150–154 (cit. on p. 9).

Felton, G. A. N.; Mebi, C. A.; Petro, B. J.; Vannucci, A. K.; Evans, D. H.; Glass, R. S.; Lichtenberger, D. L. Review of electrochemical studies of complexes containing the Fe_2S_2 core characteristic of [FeFe]-hydrogenases including catalysis by these complexes of the reduction of acids to form dihydrogen. *Journal of Organometallic Chemistry* **2009**, *694*, 2681–2699 (cit. on pp. 51, 52).

Felton, G. A. N.; Vannucci, A. K.; Chen, J.; Lockett, L. T.; Okumura, N.; Petro, B. J.; Zakai, U. I.; Evans, D. H.; Glass, R. S.; Lichtenberger, D. L. Hydrogen Generation from Weak Acids: Electrochemical and Computational Studies of a Diiron Hydrogenase Mimic. *Journal of the American Chemical Society* **2007**, *129*, 12521–12530 (cit. on p. 54).

Fujita, E. Photochemical carbon dioxide reduction with metal complexes. *Coordination Chemistry Reviews* **1999**, *185-186*, 373–384 (cit. on pp. 2, 30).

Ghadiri, M. R.; Soares, C.; Choi, C. A convergent approach to protein design. Metal ion-assisted spontaneous self-assembly of a polypeptide into a triple-helix bundle protein. *Journal of the American Chemical Society* **1992**, *114*, 825–831 (cit. on pp. 9, 22).

Ghirlanda, G.; Lear, J. D.; Ogihara, N. L.; Eisenberg, D.; DeGrado, W. F. A hierarchic approach to the design of hexameric helical barrels. *Journal of Molecular Biology* **2002**, *319*, 243–253 (cit. on pp. 10, 21, 22).

Hauser, A.; Mader, M.; Robinson, W. T.; Murugesan, R.; Ferguson, J. Electronic and molecular-structure of Cr(2,2'-bipyridine)$_3^{3+}$. *Inorganic Chemistry* **1987**, *26*, 1331–1338 (cit. on p. 18).

Howorka, S. Rationally engineering natural protein assemblies in nanobiotechnology. *Current Opinion in Biotechnology* **2011**, *22*, 485–491 (cit. on p. 8).

Huynh, H. V.; Schulze-Isfort, C.; Seidel, W. W.; Lügger, T.; Fröhlich, R.; Kataeva, O.; Hahn, F. E. Dinuclear Complexes with Bis(benzenedithiolate) Ligands. *Chemistry – A European Journal* **2002**, *8*, 1327–1335 (cit. on p. 59).

International Energy Agency. World Energy Outlook 2018. https://www.iea.org/weo/ (accessed 02/12/2019) (cit. on p. 1).

Irving, H.; Mellor, D. H. 1002. The stability of metal complexes of 1,10-phenanthroline and its analogues. Part I. 1,10-Phenanthroline and 2,2′-bipyridyl. *Journal of the Chemical Society* **1962**, 5222–5237 (cit. on p. 21).

Jian, J.-X.; Liu, Q.; Li, Z.-J.; Wang, F.; Li, X.-B.; Li, C.-B.; Liu, B.; Meng, Q.-Y.; Chen, B.; Feng, K.; Tung, C.-H.; Wu, L.-Z. Chitosan confinement enhances hydrogen photogeneration from a mimic of the diiron subsite of [FeFe]-hydrogenase. *Nature Communications* **2013**, *4*, 2695 (cit. on p. 52).

Jones, A. K.; Lichtenstein, B. R.; Dutta, A.; Gordon, G.; Dutton, P. L. Synthetic Hydrogenases: Incorporation of an Iron Carbonyl Thiolate into a Designed Peptide. *Journal of the American Chemical Society* **2007**, *129*, 14844–14845 (cit. on p. 53).

Jones, E. Y. Structure and function in complex macromolecular assemblies: Some evolutionary themes. *Current Opinion in Structural Biology* **2012**, *22*, 197–199 (cit. on p. 8).

Kang, M.; Light, K.; Ai, H.-w.; Shen, W.; Kim, C. H.; Chen, P. R.; Lee, H. S.; Solomon, E. I.; Schultz, P. G. Evolution of iron(II)-finger peptides by using a bipyridyl amino acid. *Chembiochem* **2014**, *15*, 822–825 (cit. on p. 9).

King, N. P.; Bale, J. B.; Sheffler, W.; McNamara, D. E.; Gonen, S.; Gonen, T.; Yeates, T. O.; Baker, D. Accurate design of co-assembling multi-component protein nanomaterials. *Nature* **2014**, *510*, 103–108 (cit. on p. 8).

King, N. P.; Sheffler, W.; Sawaya, M. R.; Vollmar, B. S.; Sumida, J. P.; Andre, I.; Gonen, T.; Yeates, T. O.; Baker, D. Computational design of self-assembling protein nanomaterials with atomic level accuracy. *Science* **2012**, *336*, 1171–1174 (cit. on p. 8).

Kleingardner, J. G.; Kandemir, B.; Bren, K. L. Hydrogen Evolution from Neutral Water under Aerobic Conditions Catalyzed by Cobalt Microperoxidase-11. *Journal of the American Chemical Society* **2014**, *136*, 4–7 (cit. on p. 31).

Knörzer, P.; Silakov, A.; Foster, C. E.; Armstrong, F. A.; Lubitz, W.; Happe, T. Importance of the Protein Framework for Catalytic Activity of [FeFe]-Hydrogenases. *Journal of Biological Chemistry* **2012**, *287*, 1489–1499 (cit. on p. 52).

Kobayashi, N.; Yanase, K.; Sato, T.; Unzai, S.; Hecht, M. H.; Arai, R. Self-assembling nano-architectures created from a protein nano-building block using an intermolecularly folded dimeric de novo protein. *Journal of the American Chemical Society* **2015**, *137*, 11285–11293 (cit. on p. 8).

Koide, T.; Yuguchi, M.; Kawakita, M.; Konno, H. Metal-assisted stabilization and probing of collagenous triple helices. *Journal of the American Chemical Society* **2002**, *124*, 9388–9389 (cit. on p. 9).

Kondo, M.; Ichii, K.; Patra, P. K.; Poulter, B.; Calle, L.; Koven, C.; Pugh, T. A. M.; Kato, E.; Harper, A.; Zaehle, S.; Wiltshire, A. Plant Regrowth as a Driver of Recent Enhancement of Terrestrial CO_2 Uptake. *Geophysical Research Letters* **2018**, *45*, 4820–4830 (cit. on p. 30).

Koreeda, M.; Yang, W. Chemistry of 1,2-Dithiins. Synthesis of the Potent Antibiotic Thiarubrine A. *Journal of the American Chemical Society* **1994**, *116*, 10793–10794 (cit. on p. 58).

Kornienko, N.; Zhao, Y.; Kley, C. S.; Zhu, C.; Kim, D.; Lin, S.; Chang, C. J.; Yaghi, O. M.; Yang, P. Metal-Organic Frameworks for Electrocatalytic Reduction of Carbon Dioxide. *Journal of the American Chemical Society* **2015**, *137*, 14129–14135 (cit. on p. 31).

Kramer, W. W.; McCrory, C. C. L. Polymer coordination promotes selective CO_2 reduction by cobalt phthalocyanine. *Chemical Science* **2016**, *7*, 2506–2515 (cit. on p. 31).

Lacis, A. A.; Schmidt, G. A.; Rind, D.; Ruedy, R. A. Atmospheric CO_2: Principal Control Knob Governing Earth's Temperature. *Science* **2010**, *330*, 356 (cit. on p. 30).

Lai, Y.-T.; King, N. P.; Yeates, T. O. Principles for designing ordered protein assemblies. *Trends in Cell Biology* **2012**, *22*, 653–661 (cit. on p. 8).

Lee, C. H.; Dogutan, D. K.; Nocera, D. G. Hydrogen Generation by Hangman Metalloporphyrins. *Journal of the American Chemical Society* **2011**, *133*, 8775–8777 (cit. on p. 31).

Leung, K.; Nielsen, I. M. B.; Sai, N.; Medforth, C.; Shelnutt, J. A. Cobalt-Porphyrin Catalyzed Electrochemical Reduction of Carbon Dioxide in Water. 2. Mechanism from First Principles. *The Journal of Physical Chemistry A* **2010**, *114*, 10174–10184 (cit. on p. 40).

Lieberman, M.; Sasaki, T. Iron(II) organizes a synthetic peptide into 3-helix bundles. *Journal of the American Chemical Society* **1991**, *113*, 1470–1471 (cit. on p. 9).

Lin, S.; Diercks, C. S.; Zhang, Y.-B.; Kornienko, N.; Nichols, E. M.; Zhao, Y.; Paris, A. R.; Kim, D.; Yang, P.; Yaghi, O. M.; Chang, C. J. Covalent organic frameworks comprising cobalt porphyrins for catalytic CO_2 reduction in water. *Science* **2015**, *349*, 1208 (cit. on p. 31).

Ljubetič, A.; Gradišar, H.; Jerala, R. Advances in design of protein folds and assemblies. *Current Opinion in Chemical Biology* **2017**, *40*, 65–71 (cit. on p. 8).

Ljubetič, A.; Lapenta, F.; Gradišar, H.; Drobnak, I.; Aupič, J.; Strmšek, Ž.; Lainšček, D.; Hafner-Bratkovič, I.; Majerle, A.; Krivec, N.; Benčina, M.; Pisanski, T.; Veličković, T. Ć.; Round, A.; Carazo, J. M.; Melero, R.; Jerala, R. Design of coiled-coil protein-origami cages that self-assemble in vitro and in vivo. *Nature Biotechnology* **2017**, *35*, 1094–1101 (cit. on p. 8).

Lomoth, R.; Ott, S. Introducing a dark reaction to photochemistry: photocatalytic hydrogen from [FeFe] hydrogenase active site model complexes. *Dalton Transactions* **2009**, 9952–9959 (cit. on pp. 52, 54).

Lu, Y.; Yeung, N.; Sieracki, N.; Marshall, N. M. Design of functional metalloproteins. *Nature* **2009**, *460*, 855 (cit. on p. 30).

Luo, Q.; Hou, C.; Bai, Y.; Wang, R.; Liu, J. Protein assembly: Versatile approaches to construct highly ordered nanostructures. *Chemical Reviews* **2016**, *116*, 13571–13632 (cit. on p. 8).

Luo, X.; Wang, T.-S. A.; Zhang, Y.; Wang, F.; Schultz, P. G. Stabilizing protein motifs with a genetically encoded metal-ion chelator. *Cell Chemical Biology* **2016**, *23*, 1098–1102 (cit. on p. 9).

Manbeck, G. F.; Fujita, E. A review of iron and cobalt porphyrins, phthalocyanines and related complexes for electrochemical and photochemical reduction of carbon dioxide. *Journal of Porphyrins and Phthalocyanines* **2015**, *19*, 45–64 (cit. on p. 31).

Mason, S. F. The electronic spectra and optical activity of phenanthroline and dipyridyl metal complexes. *Inorganica Chimica Acta Reviews* **1968**, *2*, 89–109 (cit. on pp. 19, 21).

McNamara, W. R.; Han, Z.; Yin, C.-J.; Brennessel, W. W.; Holland, P. L.; Eisenberg, R. Cobalt-dithiolene complexes for the photocatalytic and electrocatalytic reduction of protons in aqueous solutions. *Proceedings of the National Academy of Sciences* **2012**, *109*, 15594–15599 (cit. on p. 59).

Mikkelsen, M.; Jørgensen, M.; Krebs, F. C. The teraton challenge. A review of fixation and transformation of carbon dioxide. *Energy & Environmental Science* **2010**, *3*, 43–81 (cit. on p. 2).

Mills, J. H.; Khare, S. D.; Bolduc, J. M.; Forouhar, F.; Mulligan, V. K.; Lew, S.; Seetharaman, J.; Tong, L.; Stoddard, B. L.; Baker, D. Computational design of an unnatural amino acid dependent metalloprotein with atomic level accuracy. *Journal of the American Chemical Society* **2013**, *135*, 13393–13399 (cit. on p. 9).

Mills, J. H.; Sheffler, W.; Ener, M. E.; Almhjell, P. J.; Oberdorfer, G.; Pereira, J. H.; Parmeggiani, F.; Sankaran, B.; Zwart, P. H.; Baker, D. Computational design of a homotrimeric metalloprotein with a trisbipyridyl core. *Proceedings of the National Academy of Sciences of the United States of America* **2016**, *113*, 15012–15017 (cit. on pp. 9, 22).

Mocny, C. S.; Pecoraro, V. L. De novo protein design as a methodology for synthetic bioinorganic chemistry. *Accounts of Chemical Research* **2015**, *48*, 2388–2396 (cit. on p. 9).

Mondal, B.; Rana, A.; Sen, P.; Dey, A. Intermediates Involved in the $2\,e^-/2\,H^+$ Reduction of CO_2 to CO by Iron(0) Porphyrin. *Journal of the American Chemical Society* **2015**, *137*, 11214–11217 (cit. on p. 31).

Moore, G. F.; Brudvig, G. W. Energy Conversion in Photosynthesis: A Paradigm for Solar Fuel Production. *Annual Review of Condensed Matter Physics* **2011**, *2*, 303–327 (cit. on p. 3).

Morris, A. J.; Meyer, G. J.; Fujita, E. Molecular Approaches to the Photocatalytic Reduction of Carbon Dioxide for Solar Fuels. *Accounts of Chemical Research* **2009**, *42*, 1983–1994 (cit. on pp. 39, 40).

Ni, T. W.; Tezcan, F. A. Structural characterization of a microperoxidase inside a metal-directed protein cage. *Angewandte Chemie-International Edition* **2010**, *49*, 7014–7018 (cit. on p. 9).

Nicolet, Y.; Piras, C.; Legrand, P.; Hatchikian, C. E.; Fontecilla-Camps, J. C. *Desulfovibrio desulfuricans* iron hydrogenase: the structure shows unusual coordination to an active site Fe binuclear center. *Structure* **1999**, *7*, 13–23 (cit. on p. 51).

Nielsen, I. M. B.; Leung, K. Cobalt-Porphyrin Catalyzed Electrochemical Reduction of Carbon Dioxide in Water. 1. A Density Functional Study of Intermediates. *The Journal of Physical Chemistry A* **2010**, *114*, 10166–10173 (cit. on p. 40).

Nishimura, O.; Kitada, C.; Fujino, M. New Method for Removing the S-*p*-Methoxybenzyl and S-*t*-Butyl Groups of Cysteine Residues with Mercuric Trifluoroacetate. *Chemical & Pharmaceutical Bulletin* **1978**, *26*, 1576–1585 (cit. on p. 58).

Noisier, A. F. M.; Harris, C. S.; Brimble, M. A. Novel preparation of chiral α-amino acids using the Mitsunobu-Tsunoda reaction. *Chemical Communications* **2013**, *49*, 7744–7746 (cit. on p. 54).

Ogihara, N. L.; Ghirlanda, G.; Bryson, J. W.; Gingery, M.; DeGrado, W. F.; Eisenberg, D. Design of three-dimensional domain-swapped dimers and fibrous oligomers. *Proceedings of the National Academy of Sciences of the United States of America* **2001**, *98*, 1404–1409 (cit. on pp. 10, 21, 22, 24).

Onoda, A.; Kihara, Y.; Fukumoto, K.; Sano, Y.; Hayashi, T. Photoinduced Hydrogen Evolution Catalyzed by a Synthetic Diiron Dithiolate Complex Embedded within a Protein Matrix. *ACS Catalysis* **2014**, *4*, 2645–2648 (cit. on p. 53).

Park, C. K.; Stiteler, A. P.; Shah, S.; Ghare, M. I.; Bitinaite, J.; Horton, N. C. Activation of DNA cleavage by oligomerization of DNA-bound SgrAI. *Biochemistry* **2010**, *49*, 8818–8830 (cit. on pp. 16, 17).

Pellegrin, Y.; Odobel, F. Sacrificial electron donor reagents for solar fuel production. *Comptes Rendus Chimie* **2017**, *20*, 283–295 (cit. on p. 40).

Plegaria, J. S.; Pecoraro, V. L. De Novo Design of Metalloproteins and Metalloenzymes in a Three-Helix Bundle. In *Computational Design of Ligand Binding Proteins*, Stoddard, B. L., Ed.; Methods in Molecular Biology, Vol. 1414; Humana Press: New York, NY, 2016, pp 187–196 (cit. on p. 9).

Pullen, S.; Fei, H.; Orthaber, A.; Cohen, S. M.; Ott, S. Enhanced Photochemical Hydrogen Production by a Molecular Diiron Catalyst Incorporated into a Metal-Organic Framework. *Journal of the American Chemical Society* **2013**, *135*, 16997–17003 (cit. on p. 52).

Rao, H.; Lim, C.-H.; Bonin, J.; Miyake, G. M.; Robert, M. Visible-Light-Driven Conversion of CO_2 to CH_4 with an Organic Sensitizer and an Iron Porphyrin Catalyst. *Journal of the American Chemical Society* **2018**, *140*, 17830–17834 (cit. on p. 31).

Roy, A.; Madden, C.; Ghirlanda, G. Photo-induced hydrogen production in a helical peptide incorporating a [FeFe] hydrogenase active site mimic. *Chemical Communications* **2012**, *48*, 9816–9818 (cit. on p. 53).

Roy, A.; Sarrou, I.; Vaughn, M. D.; Astashkin, A. V.; Ghirlanda, G. De novo design of an artificial bis [4Fe-4S] binding protein. *Biochemistry* **2013**, *52*, 7586–7594 (cit. on pp. 10, 24).

Roy, A.; Sommer, D. J.; Schmitz, R. A.; Brown, C. L.; Gust, D.; Astashkin, A.; Ghirlanda, G. A de novo designed 2 [4Fe-4S] ferredoxin mimic mediates electron transfer. *Journal of the American Chemical Society* **2014**, *136*, 17343–17349 (cit. on pp. 9, 10, 24).

Roy, L.; Case, M. A. Electrostatic determinants of stability in parallel 3-stranded coiled coils. *Chemical Communications* **2009**, 192–194 (cit. on p. 9).

Roy, S.; Nguyen, T.-A. D.; Gan, L.; Jones, A. K. Biomimetic peptide-based models of [FeFe]-hydrogenases: utilization of phosphine-containing peptides. *Dalton Transactions* **2015**, *44*, 14865–14876 (cit. on p. 53).

Roy, S.; Shinde, S.; Hamilton, G. A.; Hartnett, H. E.; Jones, A. K. Artificial [FeFe]-Hydrogenase: On Resin Modification of an Amino Acid to Anchor a Hexacarbonyldiiron Cluster in a Peptide Framework. *European Journal of Inorganic Chemistry* **2011**, *2011*, 1050–1055 (cit. on p. 53).

Salgado, E. N.; Lewis, R. A.; Mossin, S.; Rheingold, A. L.; Tezcan, F. A. Control of protein oligomerization symmetry by metal coordination: C_2 and C_3 symmetrical assemblies through Cu^{II} and Ni^{II} coordination. *Inorganic Chemistry* **2009**, *48*, 2726–2728 (cit. on p. 9).

Salgado, E. N.; Radford, R. J.; Tezcan, F. A. Metal-directed protein self-assembly. *Accounts of Chemical Research* **2010**, *43*, 661–672 (cit. on p. 9).

Sano, Y.; Onoda, A.; Hayashi, T. A hydrogenase model system based on the sequence of cytochrome *c*: photochemical hydrogen evolution in aqueous media. *Chemical Communications* **2011**, *47*, 8229–8231 (cit. on p. 53).

Sano, Y.; Onoda, A.; Hayashi, T. Photocatalytic hydrogen evolution by a diiron hydrogenase model based on a peptide fragment of cytochrome c_{556} with an attached diiron carbonyl cluster and an attached ruthenium photosensitizer. *Journal of Inorganic Biochemistry* **2012**, *108*, 159–162 (cit. on p. 53).

Savage, S. A.; Smith, A. P.; Fraser, C. L. Efficient synthesis of 4-, 5-, and 6-methyl-2,2'-bipyridine by a Negishi cross-coupling strategy followed by high-yield conversion to bromo- and chloromethyl-2,2'-bipyridines. *Journal of Organic Chemistry* **1998**, *63*, 10048–10051 (cit. on pp. 12, 19).

Schlapbach, L.; Züttel, A. Hydrogen-storage materials for mobile applications. *Nature* **2001**, *414*, 353 (cit. on pp. 1, 2, 51).

Schneider, C. R.; Manesis, A. C.; Stevenson, M. J.; Shafaat, H. S. A photoactive semisynthetic metalloenzyme exhibits complete selectivity for CO_2 reduction in water. *Chemical Communications* **2018**, *54*, 4681–4684 (cit. on p. 30).

Schneider, C. R.; Shafaat, H. S. An internal electron reservoir enhances catalytic CO_2 reduction by a semisynthetic enzyme. *Chemical Communications* **2016**, *52*, 9889–9892 (cit. on p. 30).

Shen, J.; Kolb, M. J.; Göttle, A. J.; Koper, M. T. M. DFT Study on the Mechanism of the Electrochemical Reduction of CO_2 Catalyzed by Cobalt Porphyrins. *The Journal of Physical Chemistry C* **2016**, *120*, 15714–15721 (cit. on p. 40).

Shiro, A.; Shumpei, S.; Yasutsugu, S.; Yoshifumi, N. A New Method for the Protection of the Sulfhydryl Group during Peptide Synthesis. *Bulletin of the Chemical Society of Japan* **1964**, *37*, 433–434 (cit. on p. 58).

Singleton, M. L.; Reibenspies, J. H.; Darensbourg, M. Y. A Cyclodextrin Host/Guest Approach to a Hydrogenase Active Site Biomimetic Cavity.

Journal of the American Chemical Society **2010**, *132*, 8870–8871 (cit. on p. 52).

Smith, P.; Davis, S. J.; Creutzig, F.; Fuss, S.; Minx, J.; Gabrielle, B.; Kato, E.; Jackson, R. B.; Cowie, A.; Kriegler, E.; van Vuuren, D. P.; Rogelj, J.; Ciais, P.; Milne, J.; Canadell, J. G.; McCollum, D.; Peters, G.; Andrew, R.; Krey, V.; Shrestha, G.; Friedlingstein, P.; Gasser, T.; Grübler, A.; Heidug, W. K.; Jonas, M.; Jones, C. D.; Kraxner, F.; Littleton, E.; Lowe, J.; Moreira, J. R.; Nakicenovic, N.; Obersteiner, M.; Patwardhan, A.; Rogner, M.; Rubin, E.; Sharifi, A.; Torvanger, A.; Yamagata, Y.; Edmonds, J.; Yongsung, C. Biophysical and economic limits to negative CO_2 emissions. *Nature Climate Change* **2015**, *6*, 42 (cit. on p. 30).

Sommer, D. J.; Roy, A.; Astashkin, A.; Ghirlanda, G. Modulation of cluster incorporation specificity in a de novo iron-sulfur cluster binding peptide. *Biopolymers* **2015**, *104*, 412–418 (cit. on pp. 9, 10, 24).

Sommer, D. J.; Vaughn, M. D.; Clark, B. C.; Tomlin, J.; Roy, A.; Ghirlanda, G. Reengineering cyt b_{562} for hydrogen production: A facile route to artificial hydrogenases. *Biochimica et Biophysica Acta (BBA) - Bioenergetics* **2016**, *1857*, 598–603 (cit. on pp. 31, 37, 38).

Sommer, D. J.; Vaughn, M. D.; Ghirlanda, G. Protein secondary-shell interactions enhance the photoinduced hydrogen production of cobalt protoporphyrin IX. *Chemical Communications* **2014**, *50*, 15852–15855 (cit. on p. 31).

Song, W. J.; Tezcan, F. A. A designed supramolecular protein assembly with in vivo enzymatic activity. *Science* **2014**, *346*, 1525–1528 (cit. on pp. 8, 9).

Sontz, P. A.; Song, W. J.; Tezcan, F. A. Interfacial metal coordination in engineered protein and peptide assemblies. *Current Opinion in Chemical Biology* **2014**, *19*, 42–49 (cit. on p. 9).

Stips, A.; Macias, D.; Coughlan, C.; Garcia-Gorriz, E.; Liang, X. S. On the causal structure between CO_2 and global temperature. *Scientific Reports* **2016**, *6*, 21691 (cit. on p. 1).

Streich, D.; Astuti, Y.; Orlandi, M.; Schwartz, L.; Lomoth, R.; Hammarström, L.; Ott, S. High-Turnover Photochemical Hydrogen Production Catalyzed by a Model Complex of the [FeFe]-Hydrogenase Active Site. *Chemistry – A European Journal* **2010**, *16*, 60–63 (cit. on p. 54).

Sun, Y.; Gu, L.; Dickinson, R. E.; Norby, R. J.; Pallardy, S. G.; Hoffman, F. M. Impact of mesophyll diffusion on estimated global land CO_2 fertilization.

Proceedings of the National Academy of Sciences **2014**, 201418075 (cit. on p. 30).

Tard, C.; Pickett, C. J. Structural and Functional Analogues of the Active Sites of the [Fe]-, [NiFe]-, and [FeFe]-Hydrogenases. *Chemical Reviews* **2009**, *109*, 2245–2274 (cit. on p. 51).

Tezcan, F. A.; Crane, B. R.; Winkler, J. R.; Gray, H. B. Electron tunneling in protein crystals. *Proceedings of the National Academy of Sciences of the United States of America* **2001**, *98*, 5002–5006 (cit. on p. 9).

Turner, J. A. Sustainable Hydrogen Production. *Science* **2004**, *305*, 972 (cit. on p. 1).

Ueki, H.; Ellis, T. K.; Martin, C. H.; Boettiger, T. U.; Bolene, S. B.; Soloshonok, V. A. Improved Synthesis of Proline-Derived Ni(II) Complexes of Glycine: Versatile Chiral Equivalents of Nucleophilic Glycine for General Asymmetric Synthesis of α-Amino Acids. *The Journal of Organic Chemistry* **2003**, *68*, 7104–7107 (cit. on p. 57).

Vignais, P. M.; Billoud, B. Occurrence, Classification, and Biological Function of Hydrogenases: An Overview. *Chemical Reviews* **2007**, *107*, 4206–4272 (cit. on p. 51).

Wang, F.; Liang, W.-J.; Jian, J.-X.; Li, C.-B.; Chen, B.; Tung, C.-H.; Wu, L.-Z. Exceptional Poly(acrylic acid)-Based Artificial [FeFe]-Hydrogenases for Photocatalytic H_2 Production in Water. *Angewandte Chemie International Edition* **2013**, *52*, 8134–8138 (cit. on p. 52).

Wang, F.; Wang, W.-G.; Wang, H.-Y.; Si, G.; Tung, C.-H.; Wu, L.-Z. Artificial Photosynthetic Systems Based on [FeFe]-Hydrogenase Mimics: the Road to High Efficiency for Light-Driven Hydrogen Evolution. *ACS Catalysis* **2012**, *2*, 407–416 (cit. on p. 52).

Wang, M.; Chen, L.; Li, X.; Sun, L. Approaches to efficient molecular catalyst systems for photochemical H_2 production using [FeFe]-hydrogenase active site mimics. *Dalton Transactions* **2011**, *40*, 12793–12800 (cit. on p. 52).

Wang, N.; Wang, M.; Chen, L.; Sun, L. Reactions of [FeFe]-hydrogenase models involving the formation of hydrides related to proton reduction and hydrogen oxidation. *Dalton Transactions* **2013**, *42*, 12059–12071 (cit. on pp. 51, 52).

Winkler, M.; Esselborn, J.; Happe, T. Molecular basis of [FeFe]-hydrogenase function: An insight into the complex interplay between protein and catalytic

cofactor. *Biochimica et Biophysica Acta (BBA) - Bioenergetics* **2013**, *1827*, 974–985 (cit. on p. 52).

Woolfson, D. N.; Mahmoud, Z. N. More than just bare scaffolds: Towards multicomponent and decorated fibrous biomaterials. *Chemical Society Reviews* **2010**, *39*, 3464–3479 (cit. on p. 8).

Yoshida, M.; Tatsumi, T.; Fujiwara, Y.; Iinuma, S.; Kimura, T.; Akaji, K.; Kiso, Y. Deprotection of the S-Trimetylacetamidomethyl (Tacm) Group Using Silver Tetrafluoroborate: Application to the Synthesis of Porcine Brain Natriuretic Peptide-32 (pBNP-32). *Chemical & Pharmaceutical Bulletin* **1990**, *38*, 1551–1557 (cit. on p. 58).

Yu, T.; Zeng, Y.; Chen, J.; Li, Y.-Y.; Yang, G.; Li, Y. Exceptional Dendrimer-Based Mimics of Diiron Hydrogenase for the Photochemical Production of Hydrogen. *Angewandte Chemie International Edition* **2013**, *52*, 5631–5635 (cit. on p. 52).

Zastrow, M. L.; Peacock, A. F. A.; Stuckey, J. A.; Pecoraro, V. L. Hydrolytic catalysis and structural stabilization in a designed metalloprotein. *Nature Chemistry* **2012**, *4*, 118–123 (cit. on p. 9).

Zastrow, M. L.; Pecoraro, V. L. Designing functional metalloproteins: From structural to catalytic metal sites. *Coordination Chemistry Reviews* **2013**, *257*, 2565–2588 (cit. on p. 9).

Zhang, H.; Wei, J.; Dong, J.; Liu, G.; Shi, L.; An, P.; Zhao, G.; Kong, J.; Wang, X.; Meng, X.; Zhang, J.; Ye, J. Efficient Visible-Light-Driven Carbon Dioxide Reduction by a Single-Atom Implanted Metal-Organic Framework. *Angewandte Chemie International Edition* **2016**, *55*, 14310–14314 (cit. on p. 31).

Zhang, J.; Zheng, F.; Grigoryan, G. Design and designability of protein-based assemblies. *Current Opinion in Structural Biology* **2014**, *27*, 79–86 (cit. on p. 8).

Zhang, X.; Wu, Z.; Zhang, X.; Li, L.; Li, Y.; Xu, H.; Li, X.; Yu, X.; Zhang, Z.; Liang, Y.; Wang, H. Highly selective and active CO_2 reduction electrocatalysts based on cobalt phthalocyanine/carbon nanotube hybrid structures. *Nature Communications* **2017**, *8*, 14675 (cit. on p. 31).

APPENDIX A

SUPPORTING INFORMATION FOR CHAPTER 2

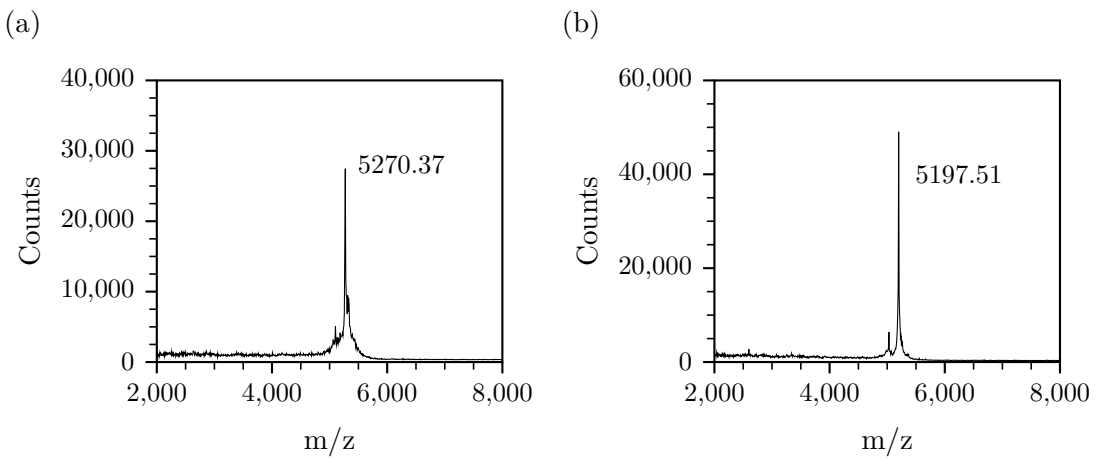

Figure A.1. MALDI-TOF-MS spectra of (a) HB1 and (b) HB2.

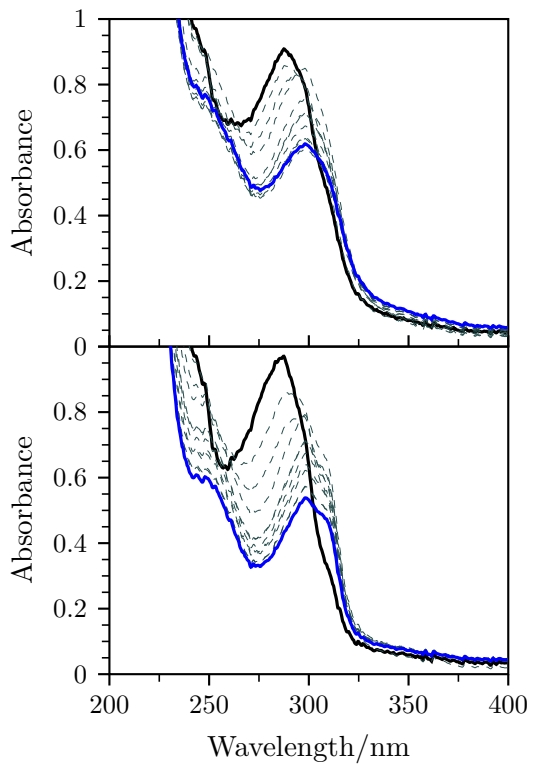

Figure A.2. UV-Vis traces for the titration of HB1 (black trace) with $CoCl_2$ (top) or $NiCl_2$ (blue traces).

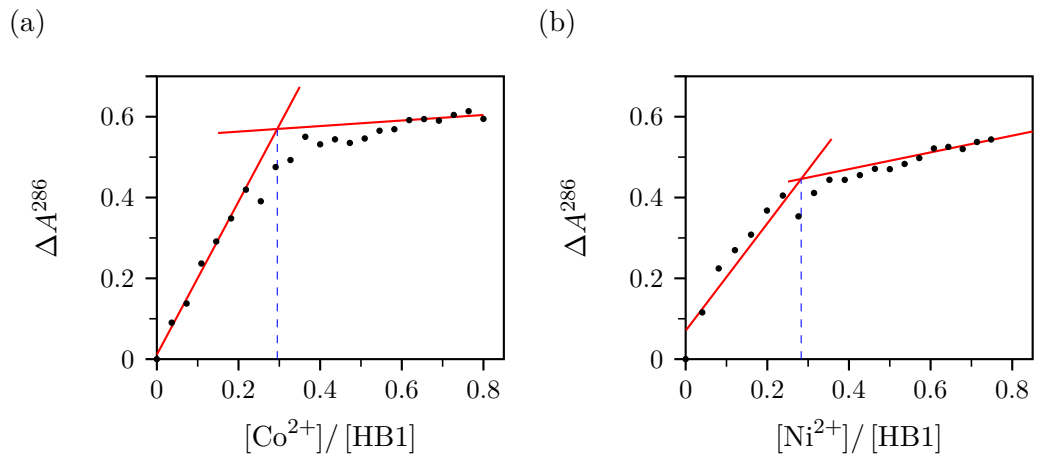

Figure A.3. Binding curves of HB1 titrated with $CoCl_2$ (left) and $NiCl_2$ (right) as monitored by UV-Vis. The calculated binding stoichiometry was (a) 3.4 peptides per metal ion, (b) 3.5 peptides per metal ion.

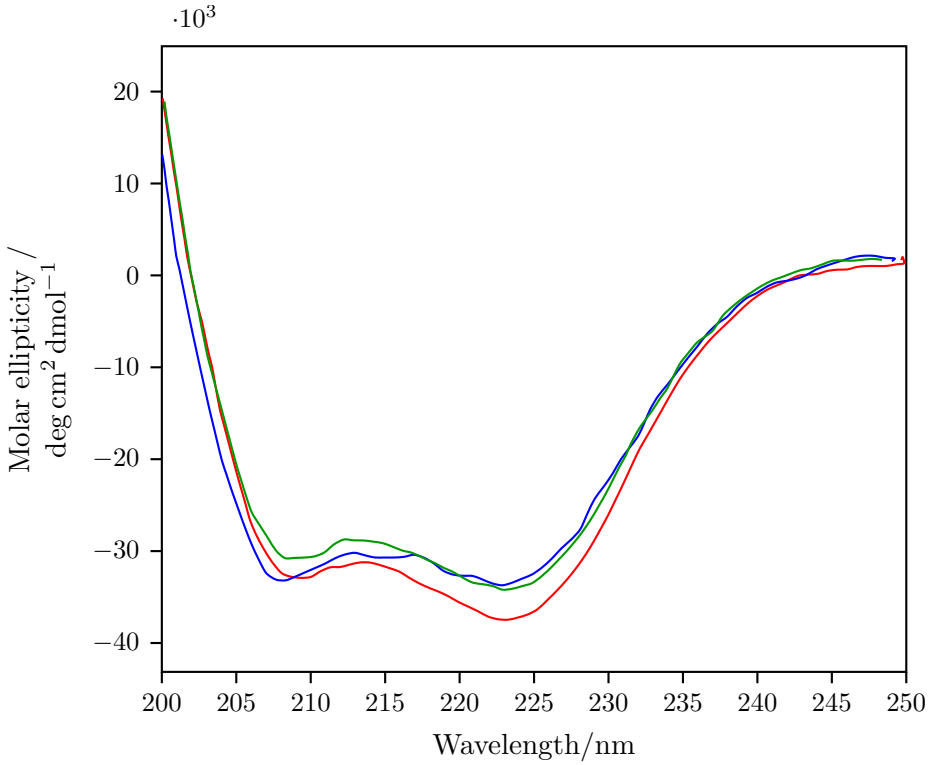

Figure A.4. CD spectra of HB1 (red), CoHB1 (blue), and NiHB1 (green).

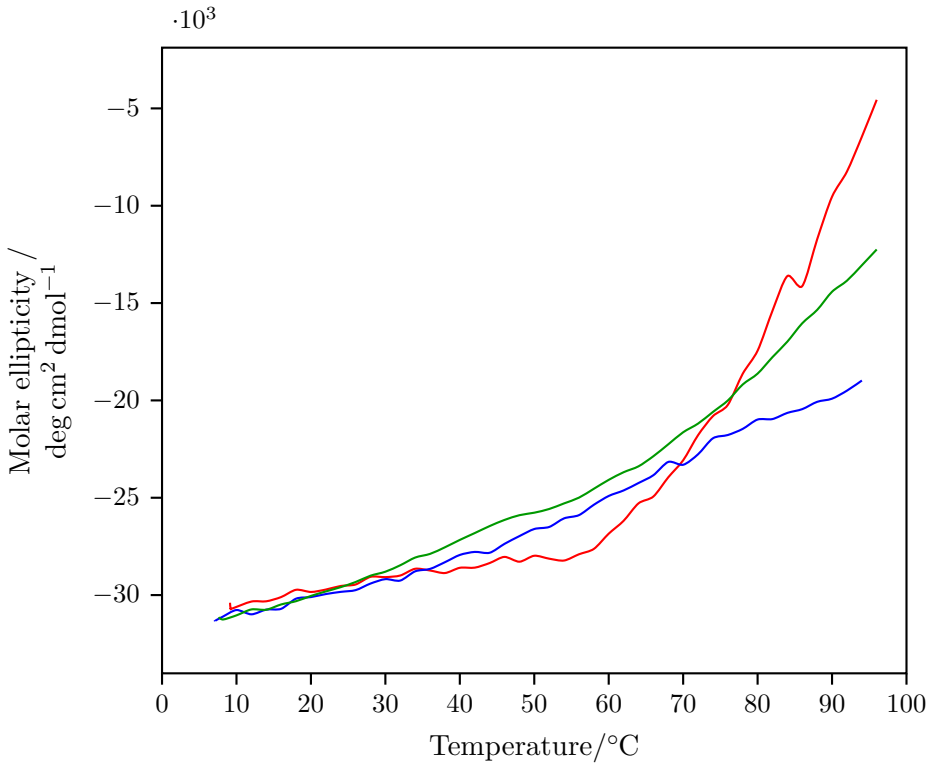

Figure A.5. Thermal denaturation curves of HB2 (red), CoHB2 (blue), and NiHB2 (green). Molar ellipticity was followed at 222 nm.

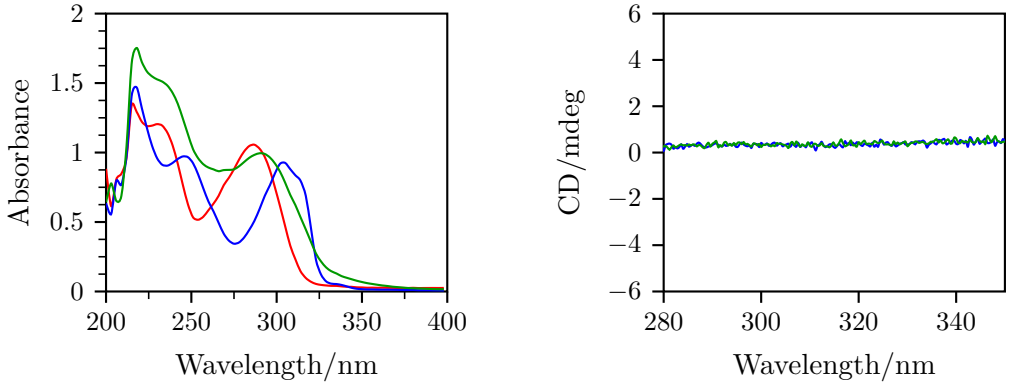

Figure A.6. UV-Vis (left) and CD (right) data for bpy-4-CO_2H ((2,2'-bipyridine)-6-carboxylic acid, red trace), $[Co(bpy\text{-}4\text{-}CO_2H)_3]^{2+}$ (blue traces), and $[Ni(bpy\text{-}4\text{-}CO_2H)_3]^{2+}$ (green traces). Spectra obtained in 100 mM Tris · HCl buffer at pH 8.5. The $[Co(bpy\text{-}4\text{-}CO_2H)_3]^{2+}$ sample contains total concentrations of $[CoCl_2]$ = 41.3 µM and [bpy-4-CO_2H] = 187 µM; the $[Ni(bpy\text{-}4\text{-}CO_2H)_3]^{2+}$ sample was prepared with a total concentration of $[Ni(OAc)_2]$ = 30.6 µM and [bpy-4-CO_2H] = 140 µM. The [bpy-4-CO_2H] in the red trace was 187 µM.

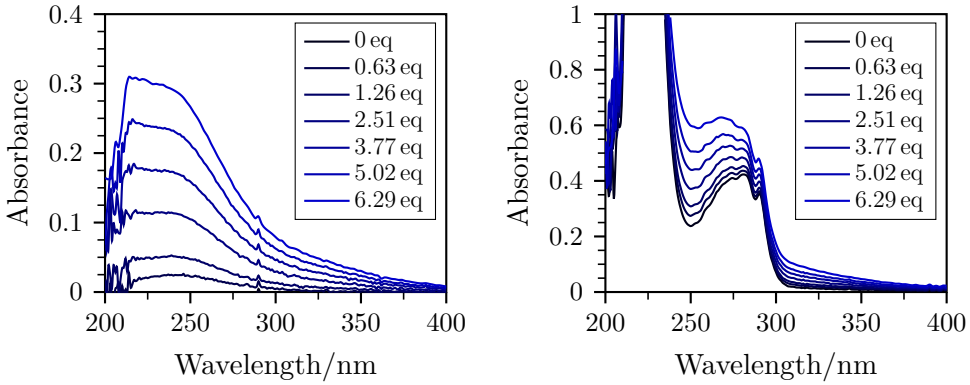

Figure A.7. Titration of 10 mM Tris buffer pH 8.0 (left) and 76.5 µM Hex-Phe (right) in the same buffer with $CoCl_2$.

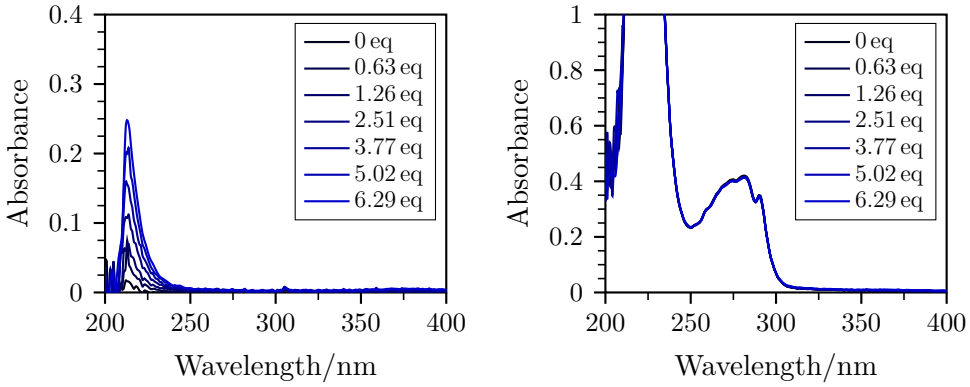

Figure A.8. Titration of 10 mM Tris buffer pH 8.0 (left) and 76.5 µM Hex-Phe (right) in the same buffer with $NiCl_2$.

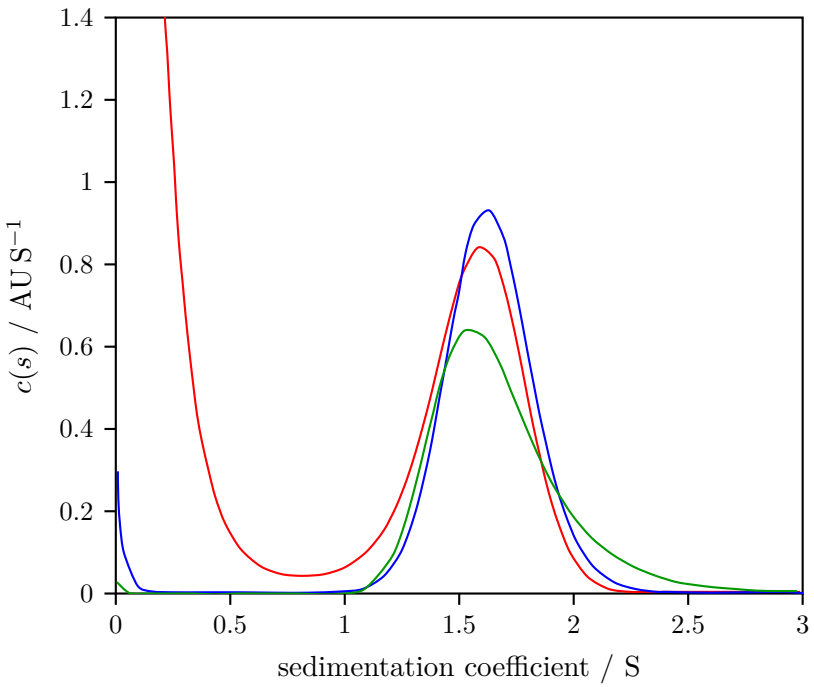

Figure A.9. Sedimentation AUC of Hex-Phe alone (red) and in the presence of Co(II) (blue) or Ni(II) (green). The three species sediment with the same coefficient indicating no changes to the oligomerization state.

APPENDIX B

SUPPORTING INFORMATION FOR CHAPTER 3

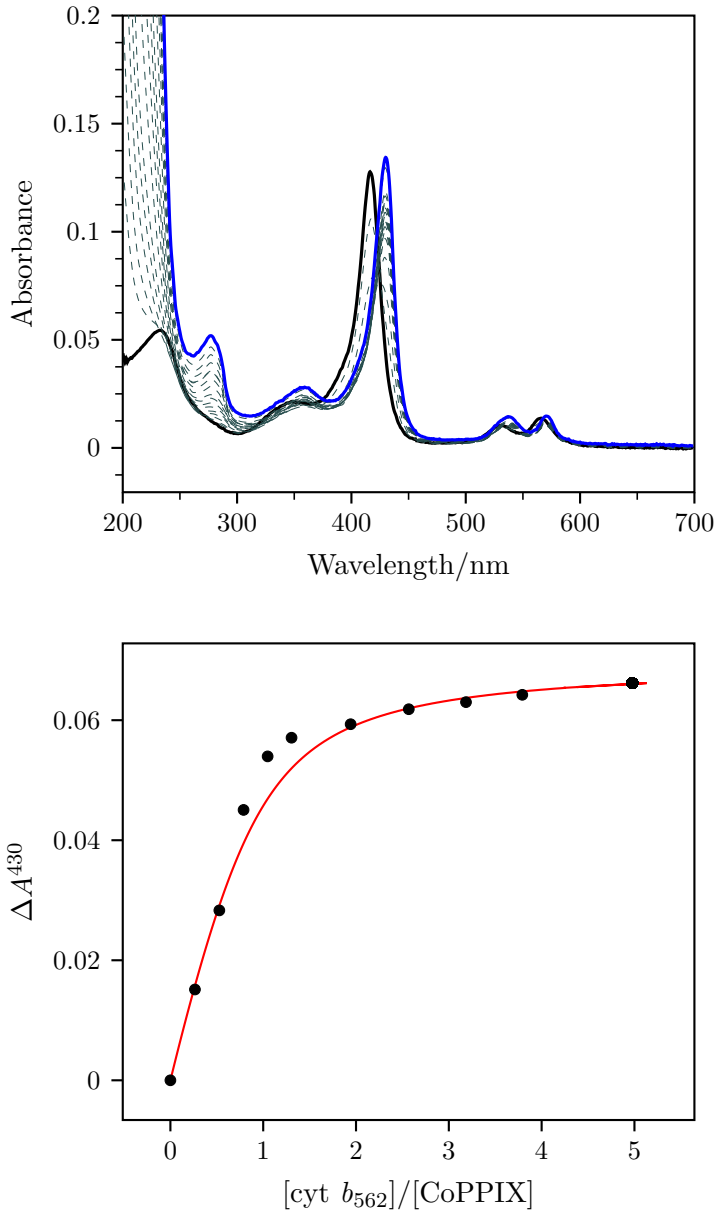

Figure B.1. UV-Vis traces (top) and fitted binding isotherm (bottom) for the titration of CoPPIX (0.89 µM, black trace) with cyt b_{562} WT in 1 M KP_i pH 6.0.

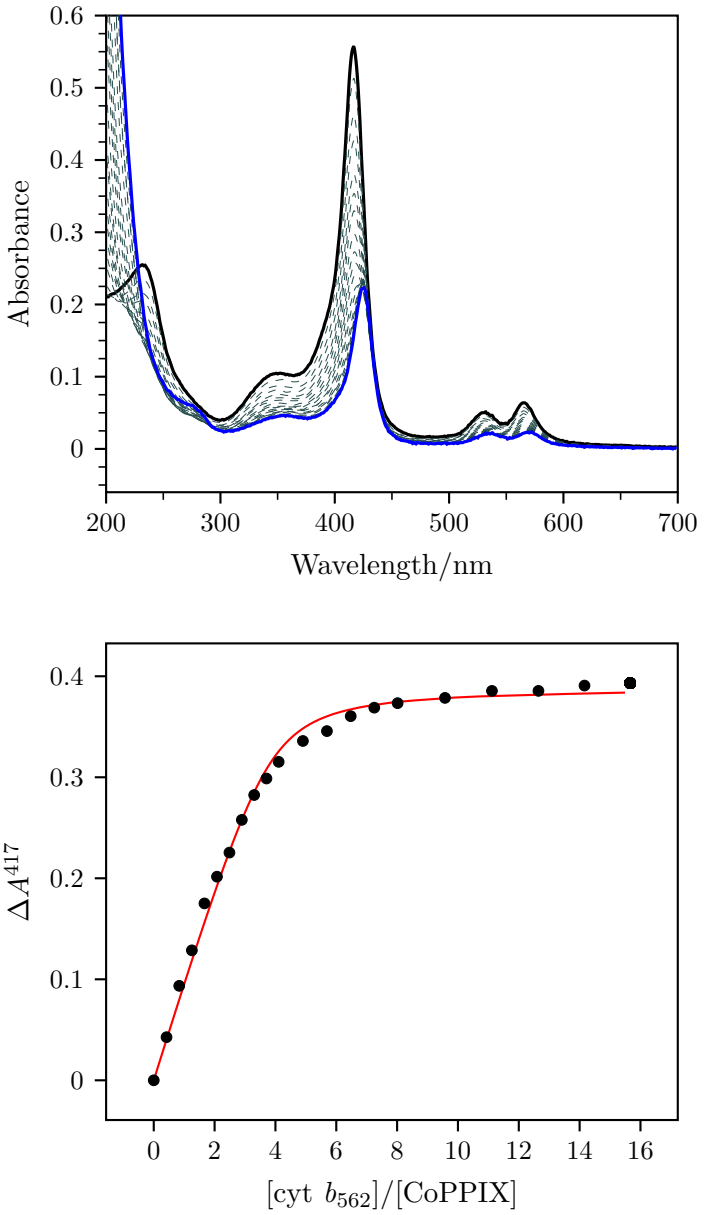

Figure B.2. UV-Vis traces (top) and fitted binding isotherm (bottom) for the titration of CoPPIX (3.86 µM, black trace) with cyt b_{562} M7A in 1 M KP_i pH 6.0.

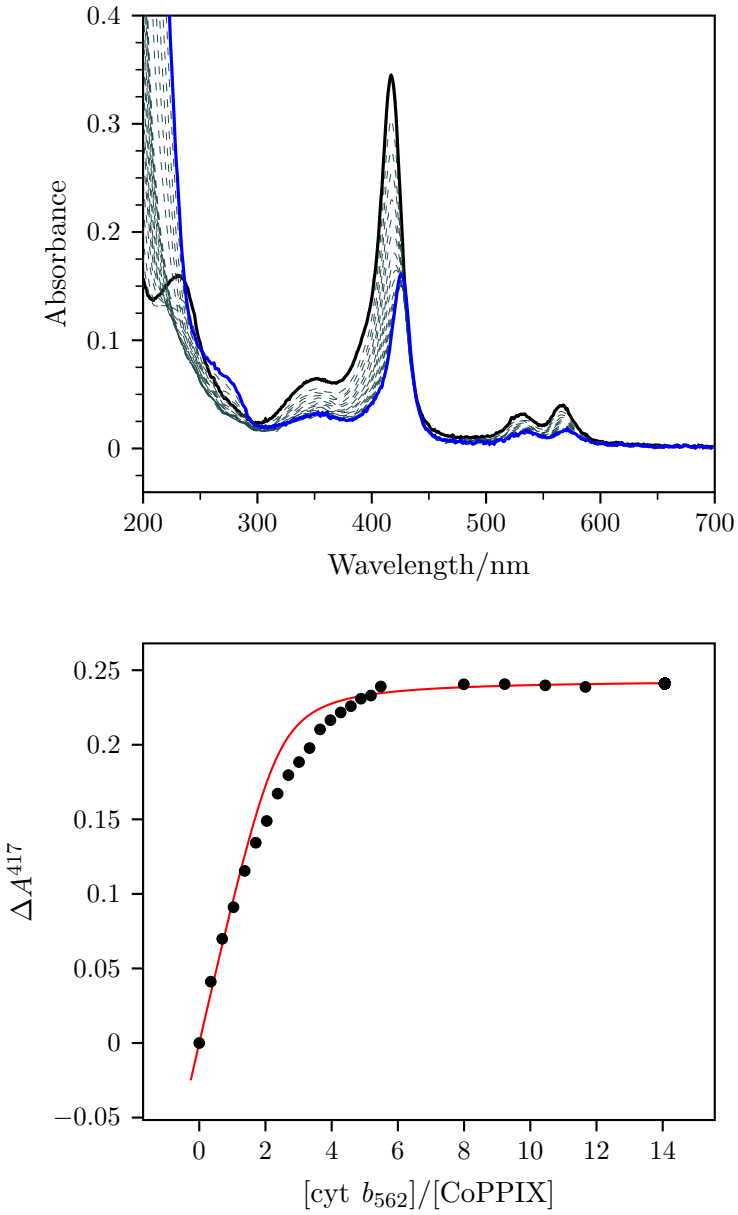

Figure B.3. UV-Vis traces (top) and fitted binding isotherm (bottom) for the titration of CoPPIX (2.40 µM, black trace) with cyt b_{562} M7H in 1 M KP_i pH 6.0.

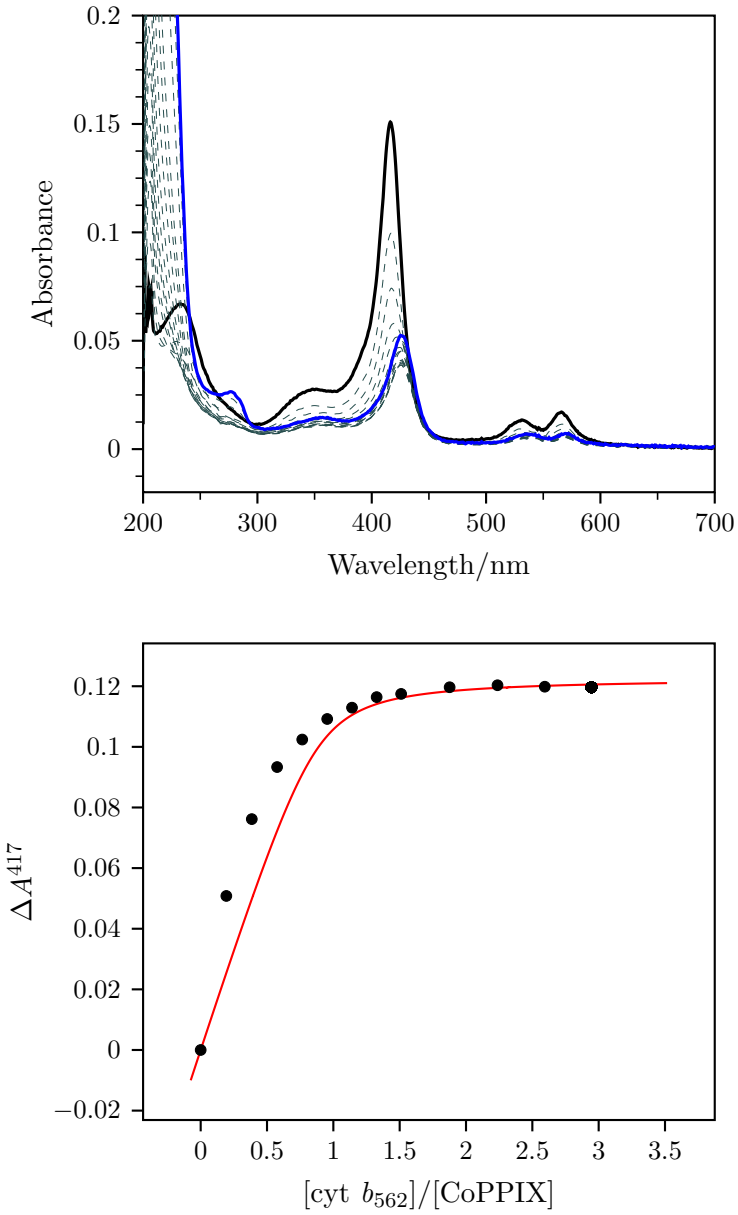

Figure B.4. UV-Vis traces (top) and fitted binding isotherm (bottom) for the titration of CoPPIX (1.05 µM, black trace) with cyt b_{562} H102A in 1 M KP_i pH 6.0.

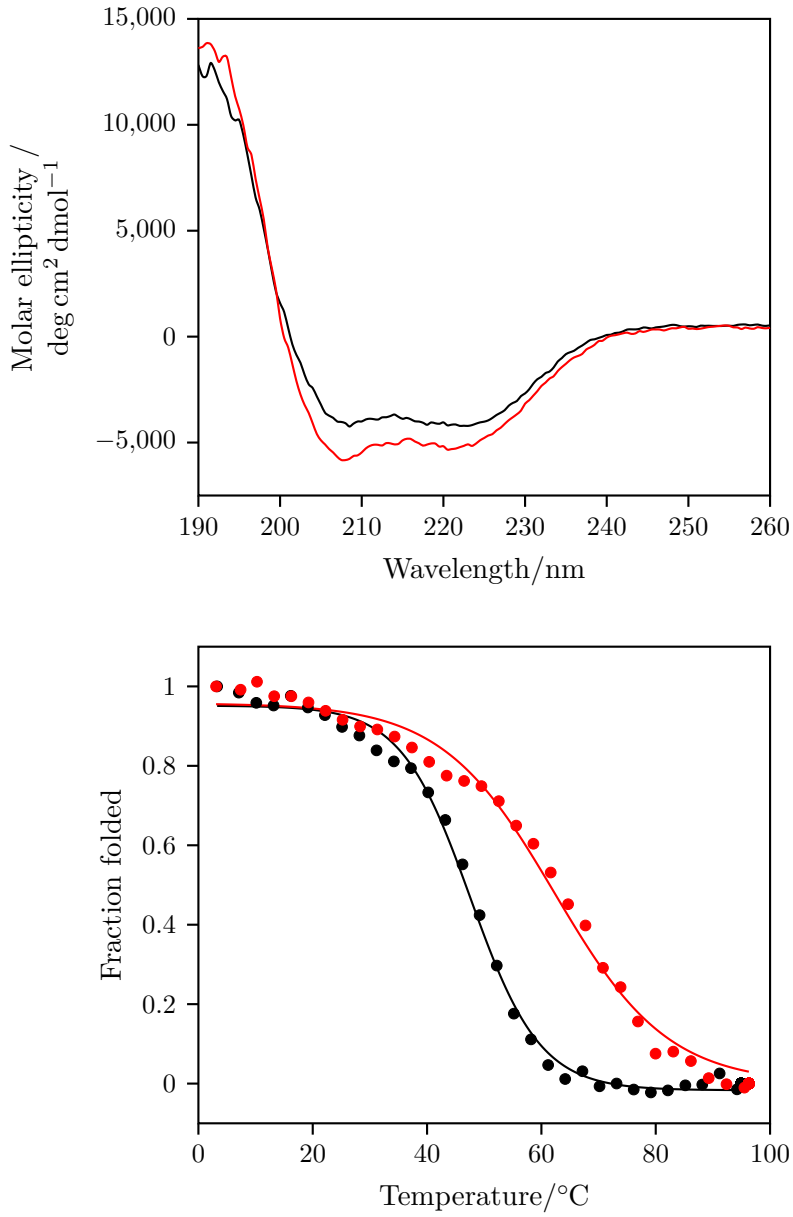

Figure B.5. CD spectra (top) and thermal denaturation curves (bottom) of apo (black) and holo (red) cobalt cyt b_{562} M7H.

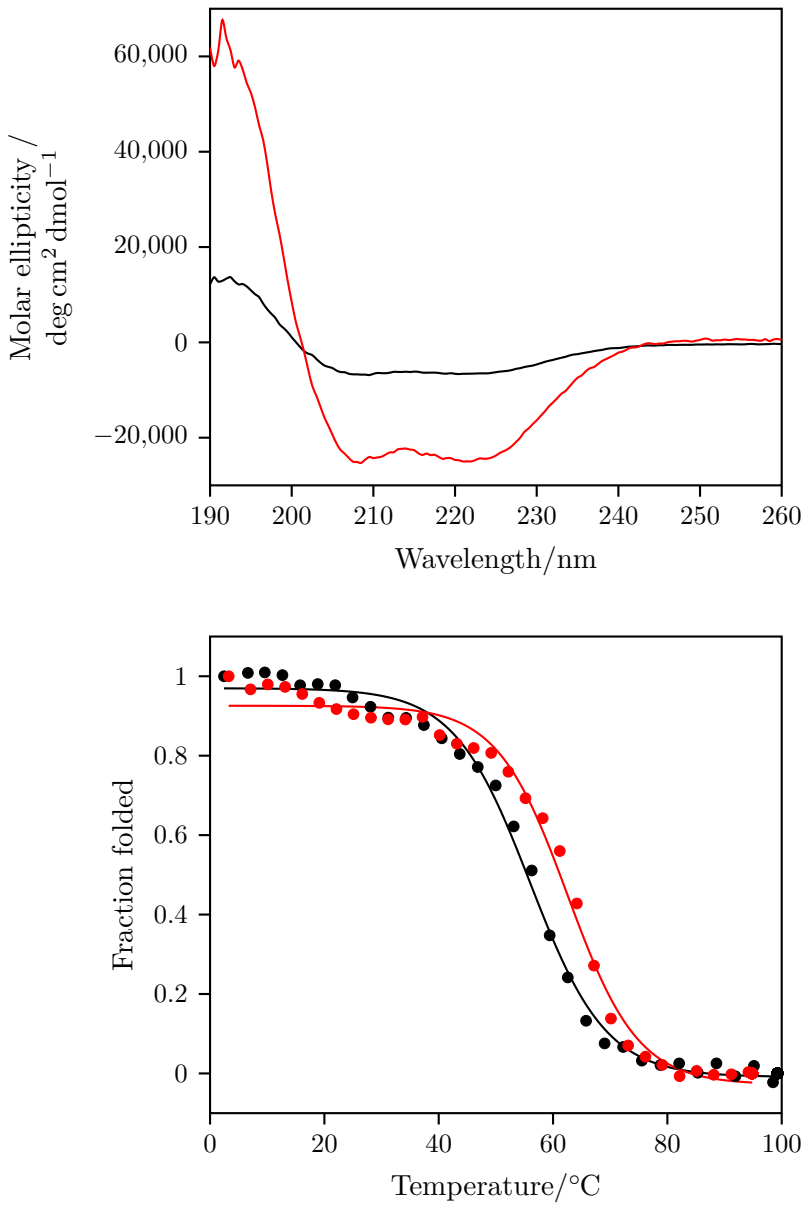

Figure B.6. CD spectra (top) and thermal denaturation curves (bottom) of apo (black) and holo (red) cobalt cyt b_{562} H102A.

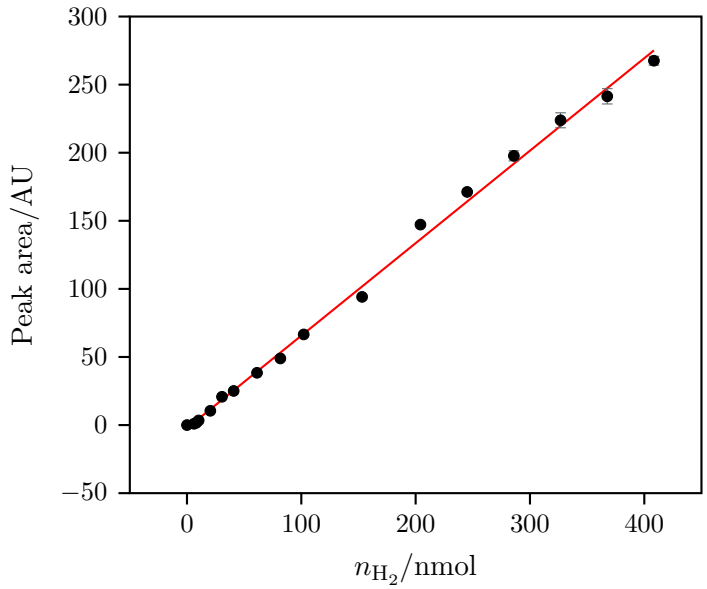

Figure B.7. Calibration curve for H_2. The data was fitted to the linear equation $y = 0.679 - 2.27$, with an adjusted $R^2 = 0.9970$.

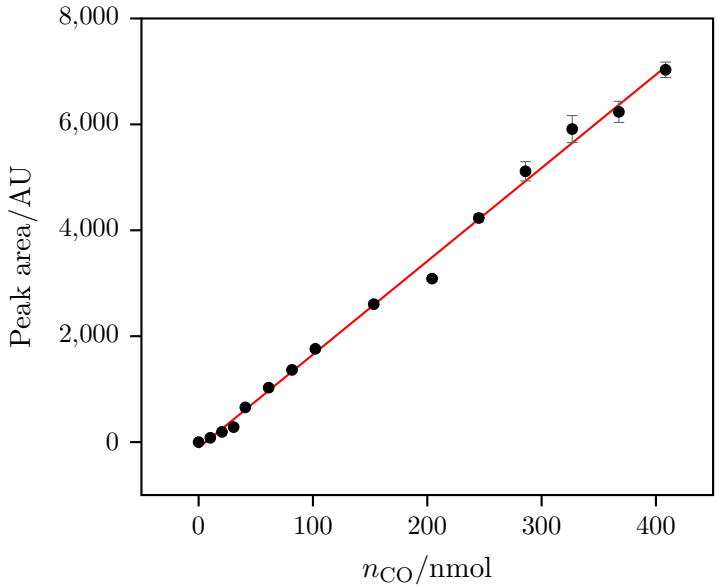

Figure B.8. Calibration curve for CO. The data was fitted to the linear equation $y = 17.62x - 107.97$, with an adjusted $R^2 = 0.9958$.

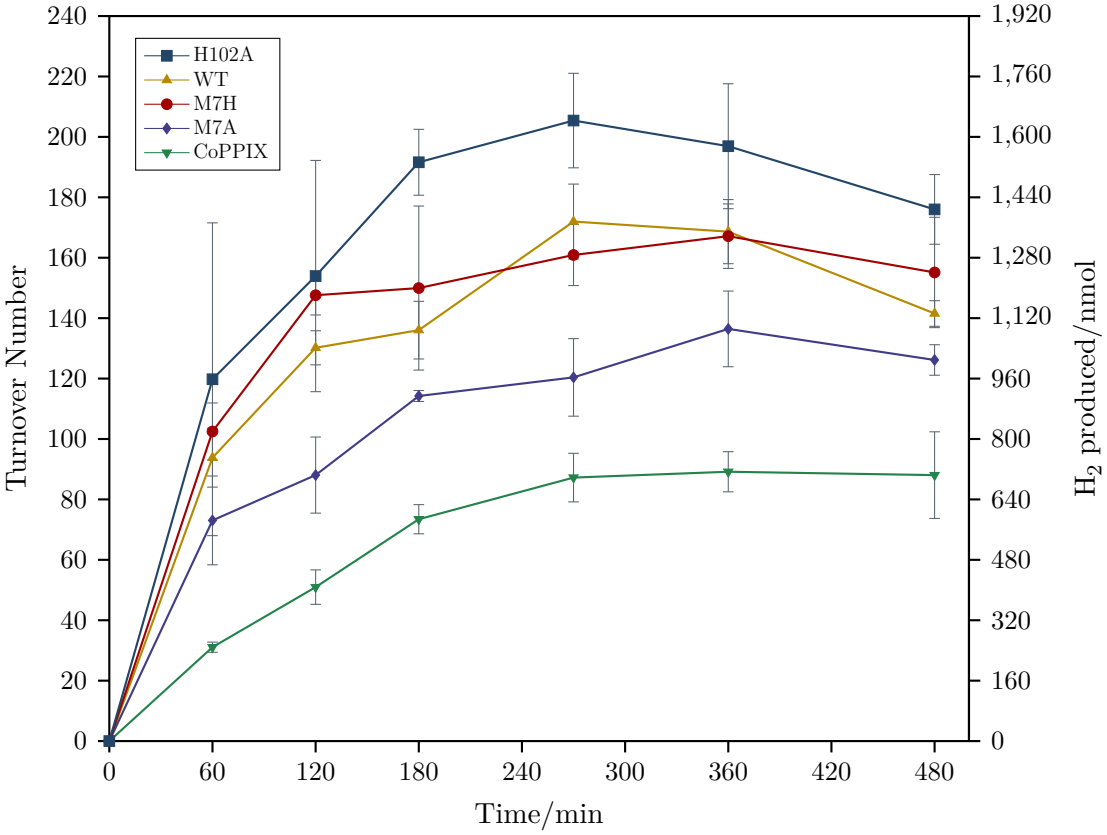

Figure B.9. Produced H_2 over time from the photoinduced reduction of protons by CoPPIX and cobalt cyt b_{562} mutants at pH 6.0 under Ar. The experiments were carried out in 100 mM AscOH, 1 mM $[Ru(bpy)_3]^{2+}$, 200 mM KP_i, and 20 µM catalyst. The error bars represent the standard deviation of the sample.

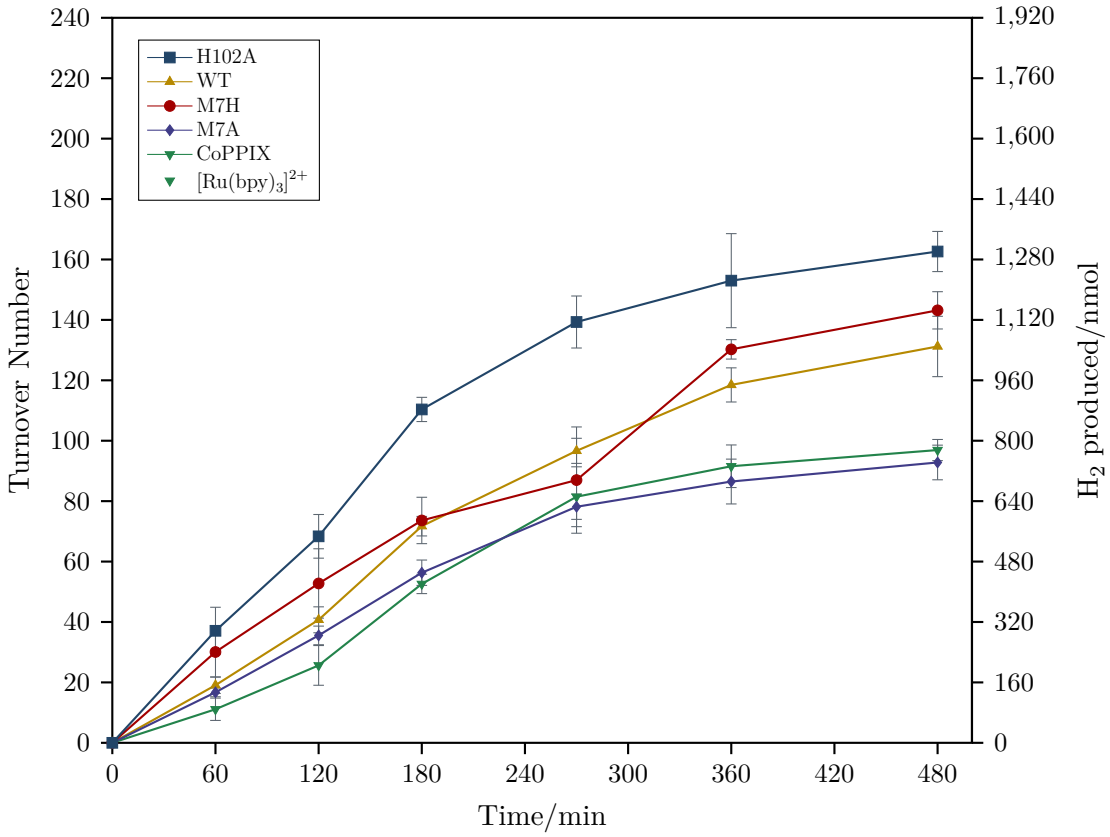

Figure B.10. Produced H_2 over time from the photoinduced reduction of protons by CoPPIX and cobalt cyt b_{562} mutants at pH 7.0 under 1 atm CO_2. The experiments were carried out in 100 mM AscOH, 1 mM $[Ru(bpy)_3]^{2+}$, 200 mM KP_i, and 20 µM catalyst (when appropriate). The error bars represent the standard deviation of the sample.

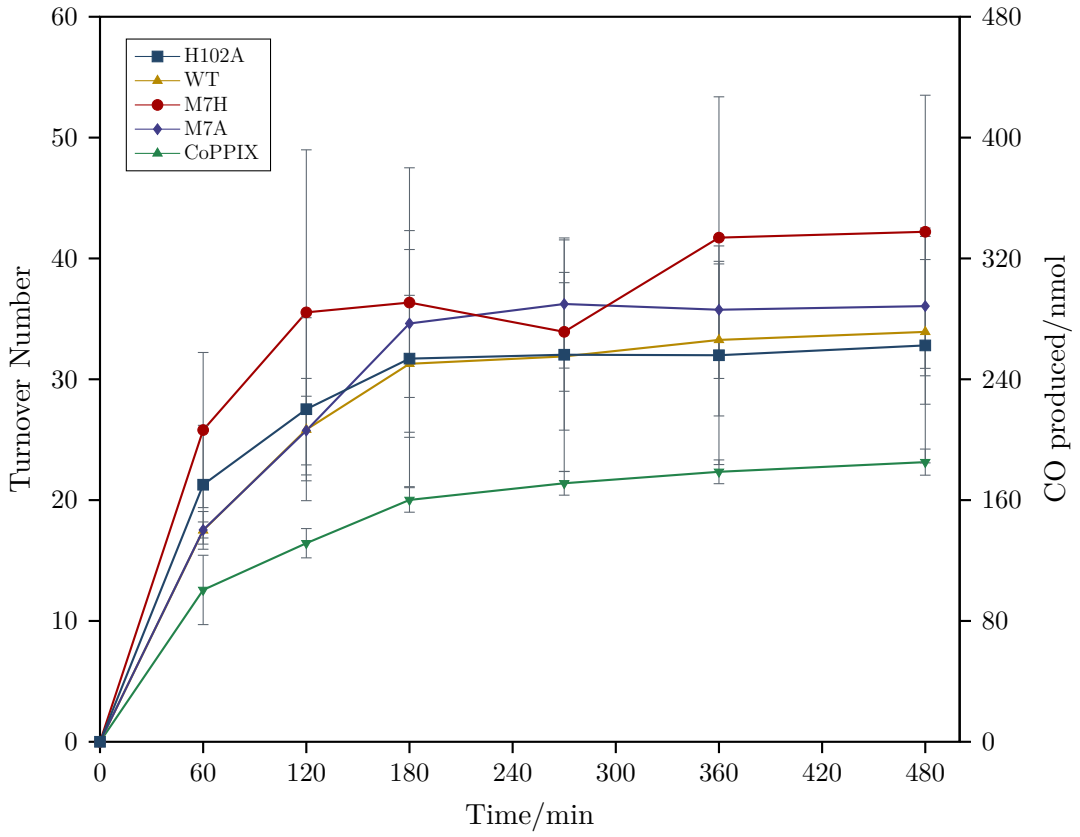

Figure B.11. Produced CO over time from the photoinduced reduction of protons by CoPPIX and cobalt cyt b_{562} mutants at pH 7.0 under 1 atm CO_2. The experiments were carried out in 100 mM AscOH, 1 mM $[Ru(bpy)_3]^{2+}$, 200 mM KP_i, and 20 µM catalyst. The error bars represent the standard deviation of the sample.

APPENDIX C

SUPPORTING INFORMATION FOR CHAPTER 4

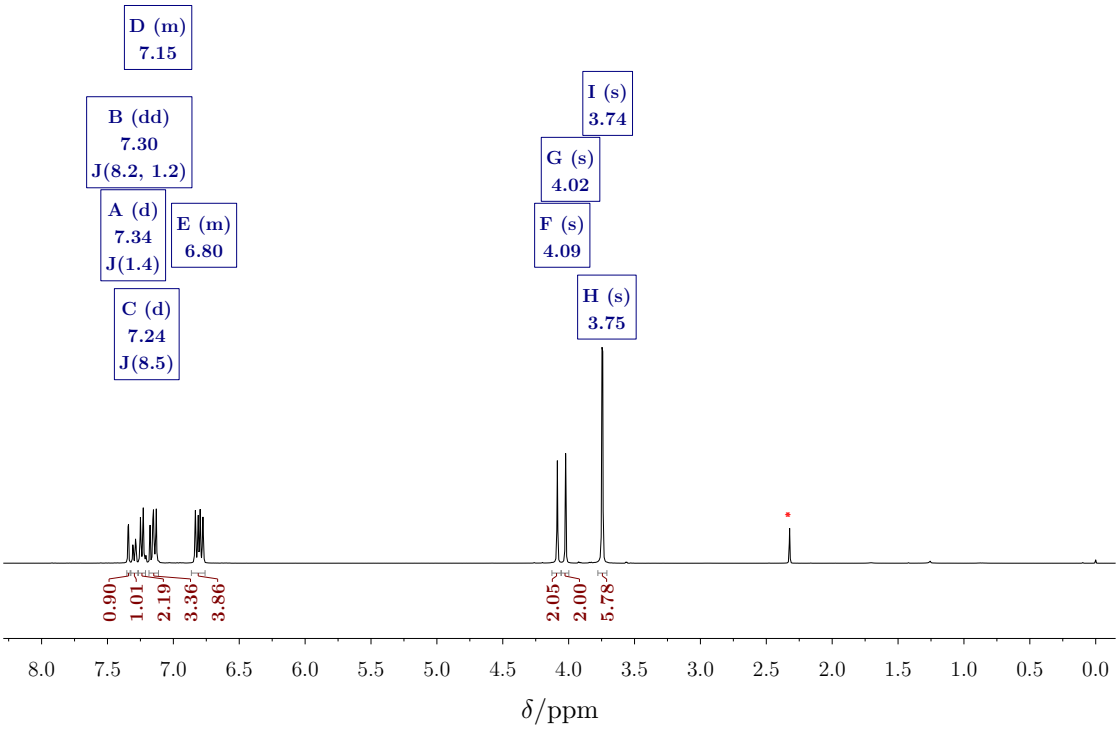

Figure C.1. ^{1}H NMR spectrum of compound **4-4a**. The red star indicates traces of toluene as impurity.

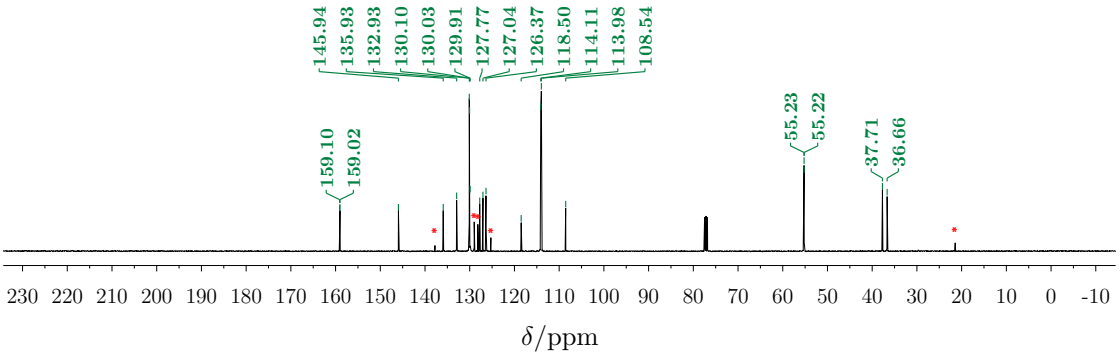

Figure C.2. ^{13}C NMR spectrum of compound **4-4a**. The red stars indicate traces of toluene as impurity.

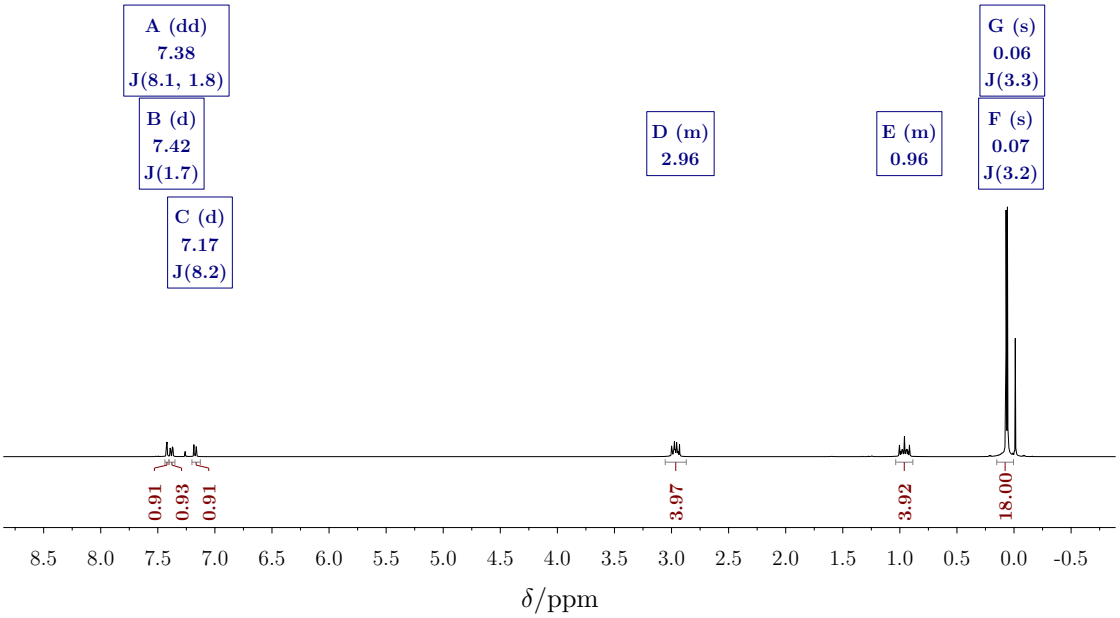

Figure C.3. ^{1}H NMR spectrum of compound **4-4b**.

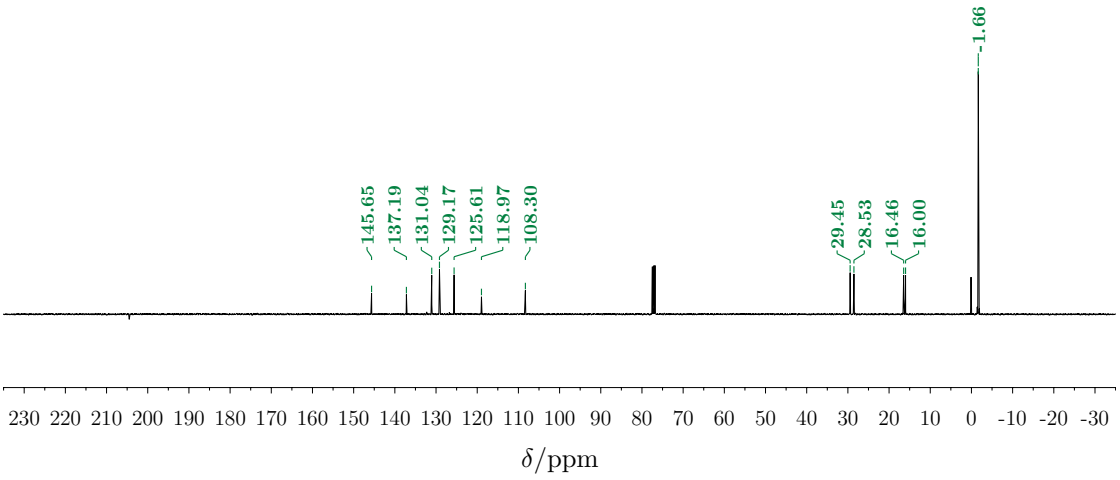

Figure C.4. ^{13}C NMR spectrum of compound **4-4b**.

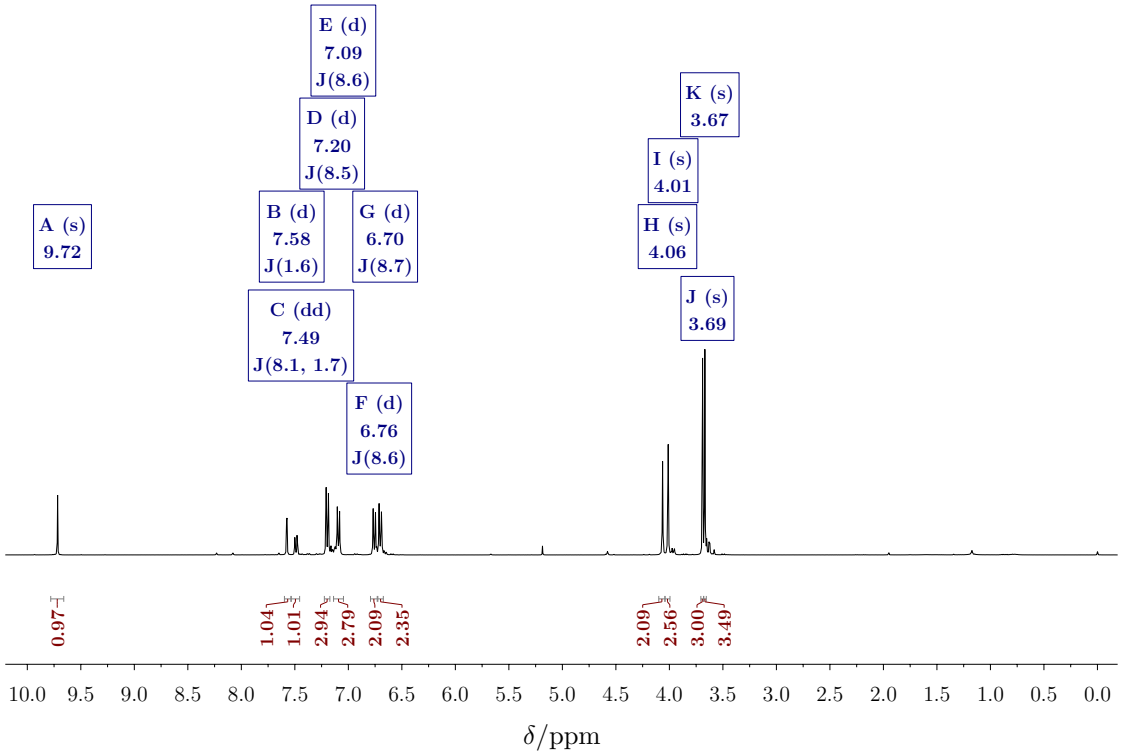

Figure C.5. ^{1}H NMR spectrum of compound **4-5a**.

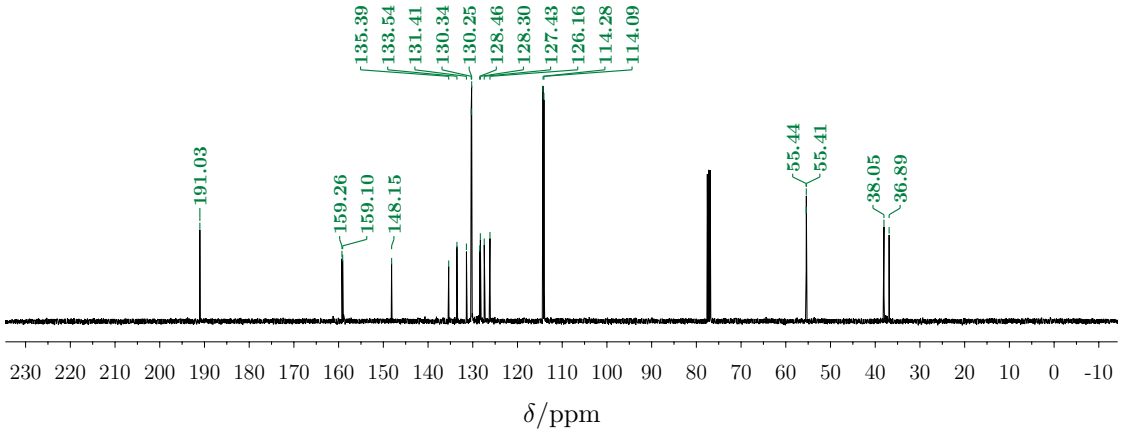

Figure C.6. ^{13}C NMR spectrum of compound **4-5a**.

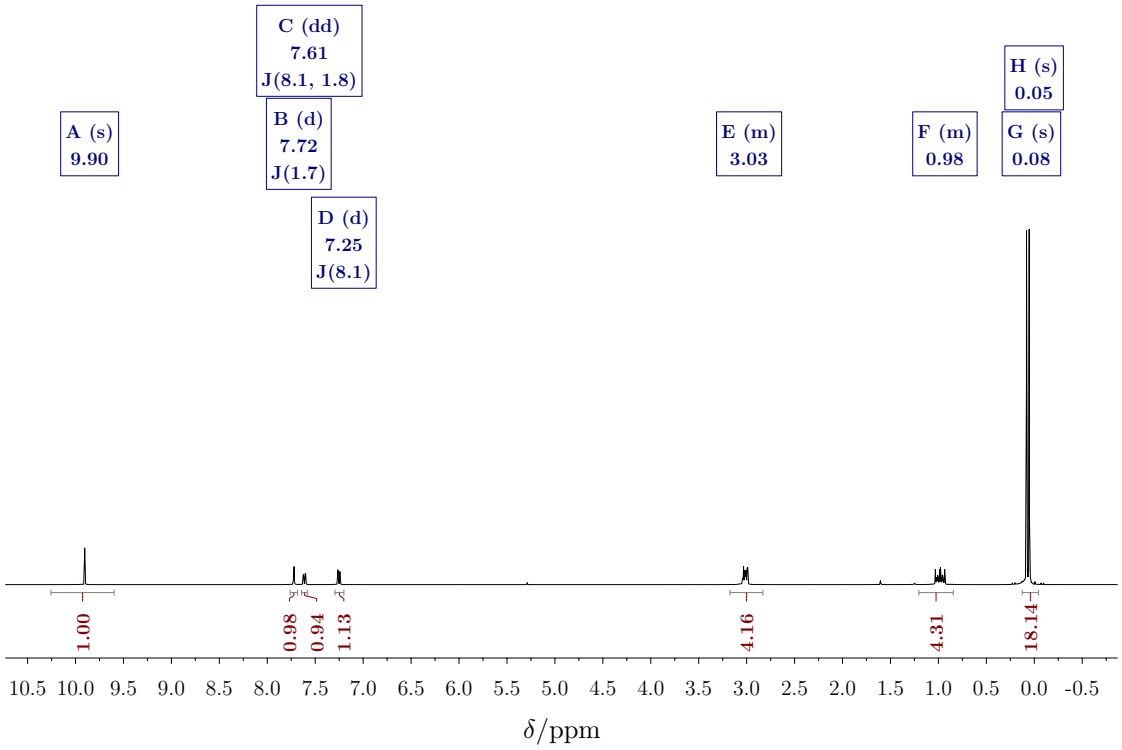

Figure C.7. ^{1}H NMR spectrum of compound **4-5b**.

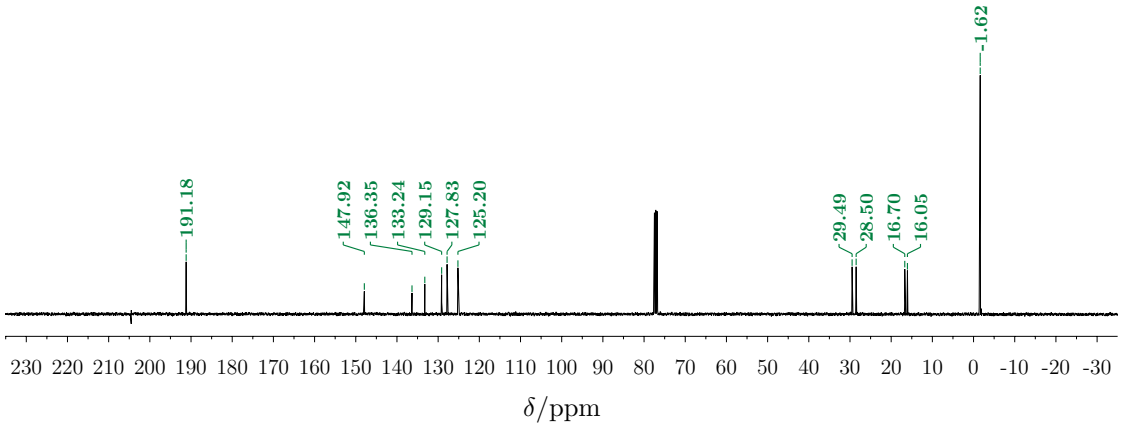

Figure C.8. ^{13}C NMR spectrum of compound **4-5b**.

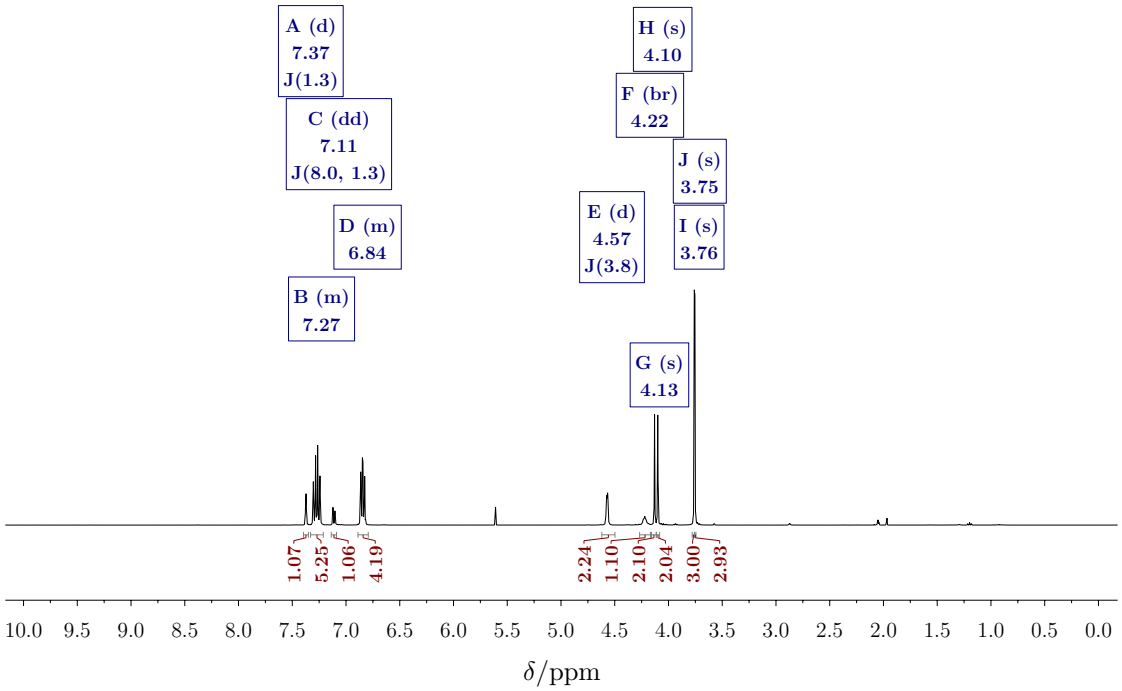

Figure C.9. ^{1}H NMR spectrum of compound **4-6a**.

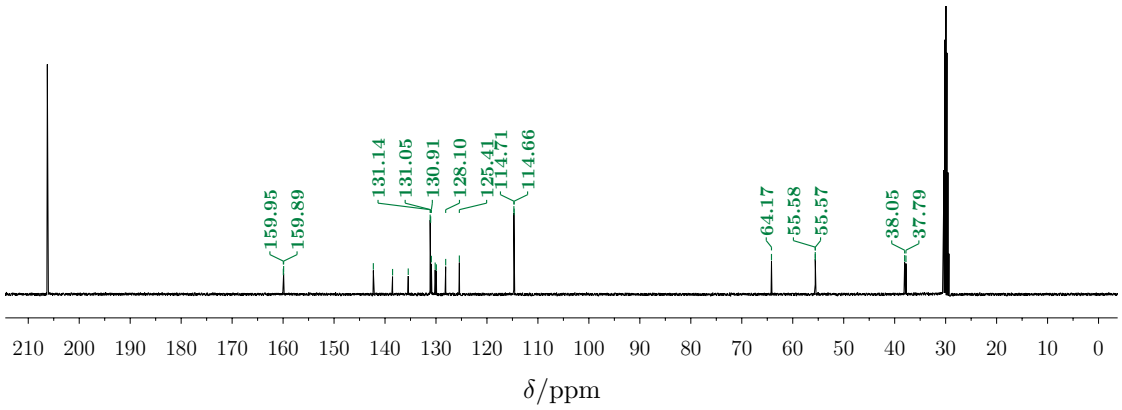

Figure C.10. ^{13}C NMR spectrum of compound **4-6a**.

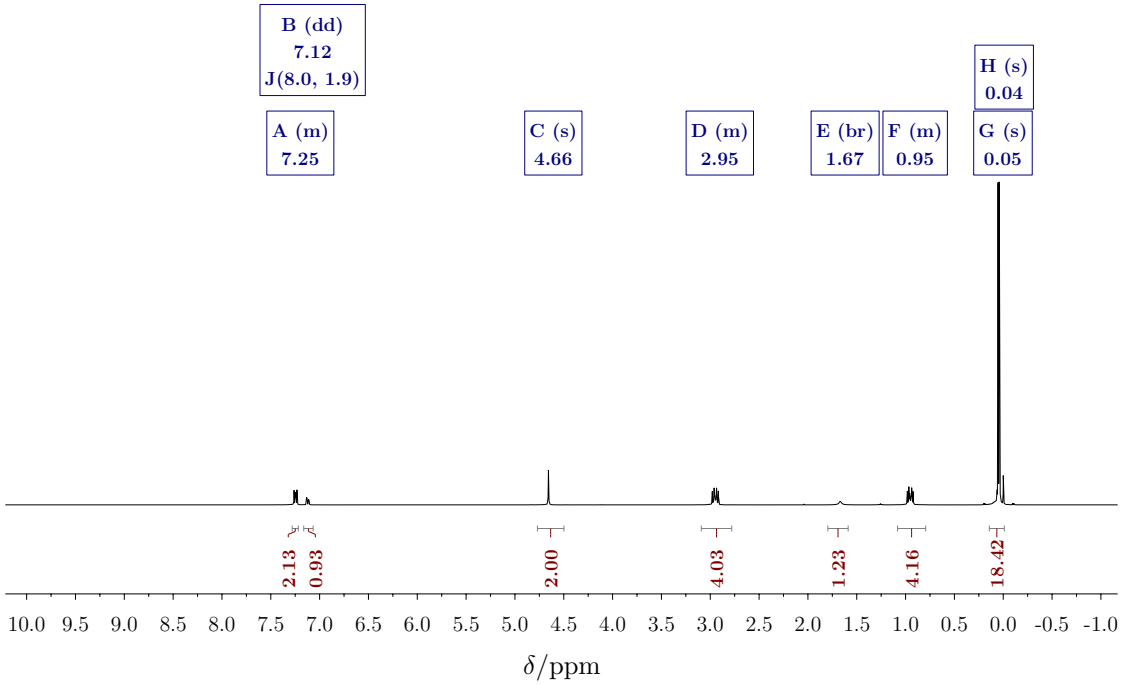

Figure C.11. ^{1}H NMR spectrum of compound **4-6b**.

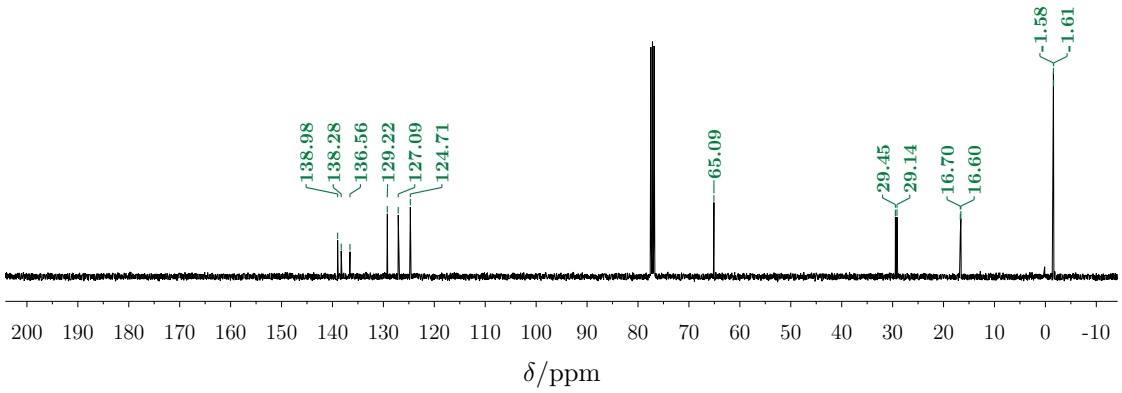

Figure C.12. ^{13}C NMR spectrum of compound **4-6b**.

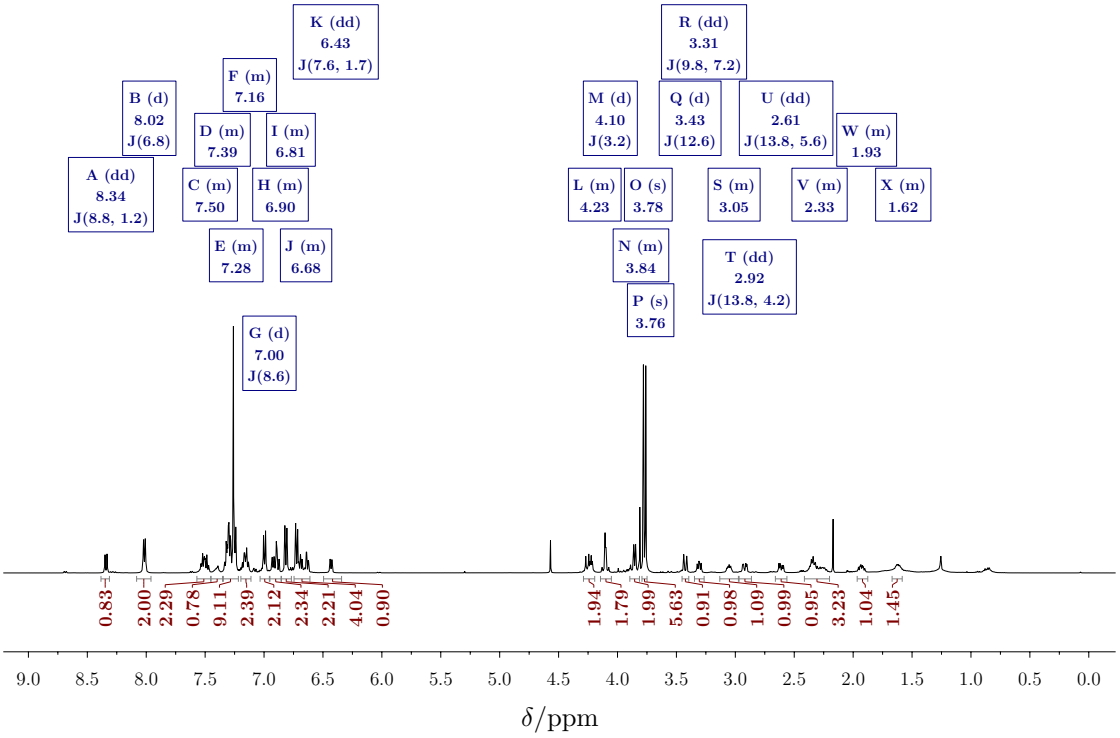

Figure C.13. ^{1}H NMR spectrum of compound **4-7a**.

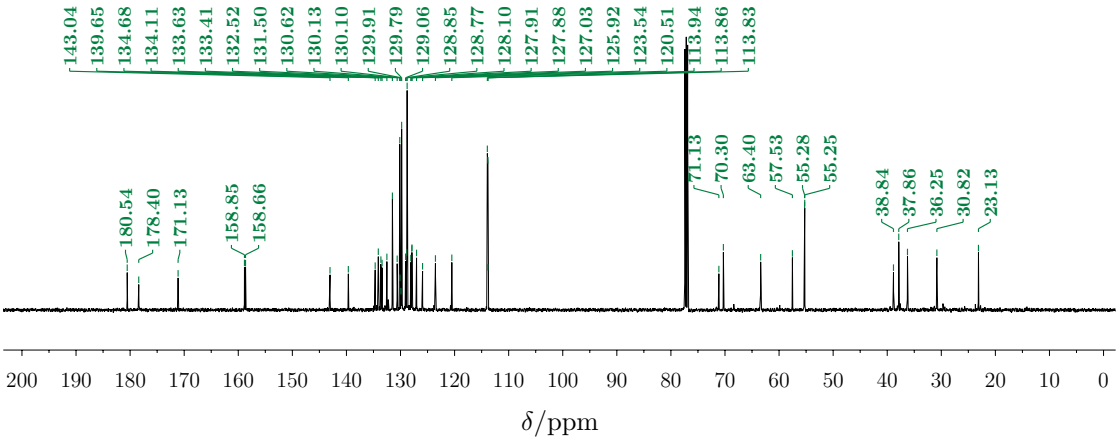

Figure C.14. ^{13}C NMR spectrum of compound **4-7a**.

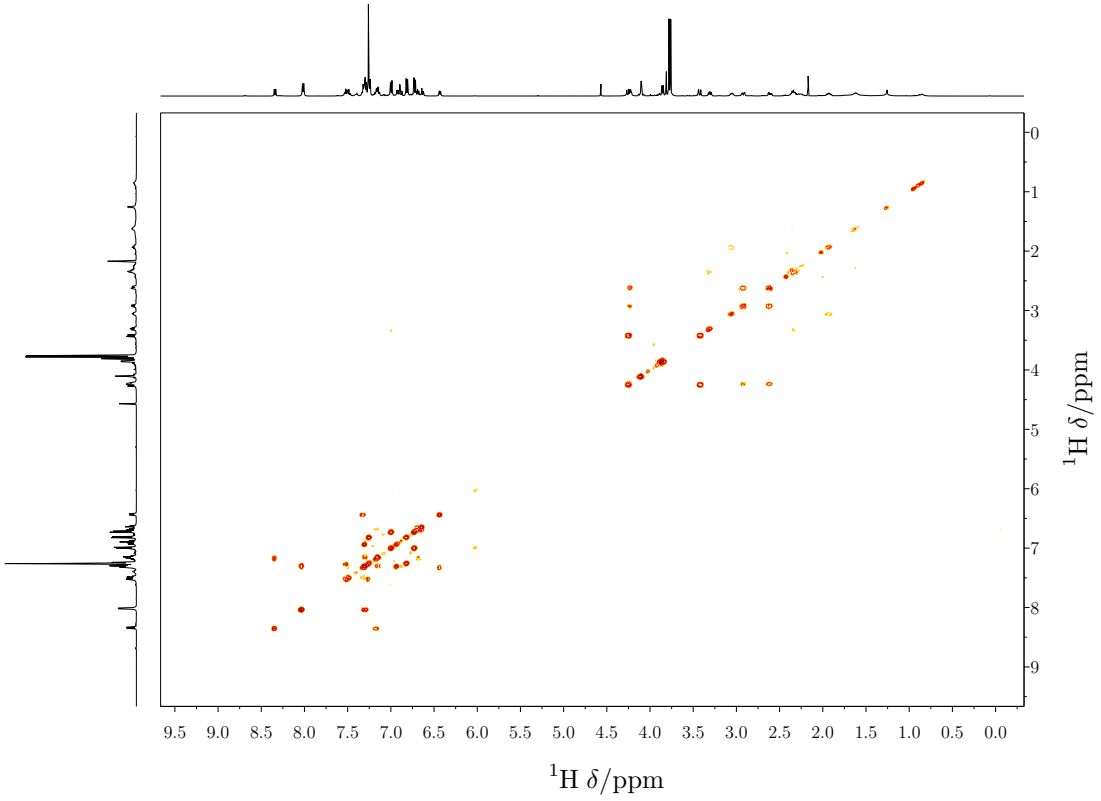

Figure C.15. COSY spectrum of compound **4-7a**.

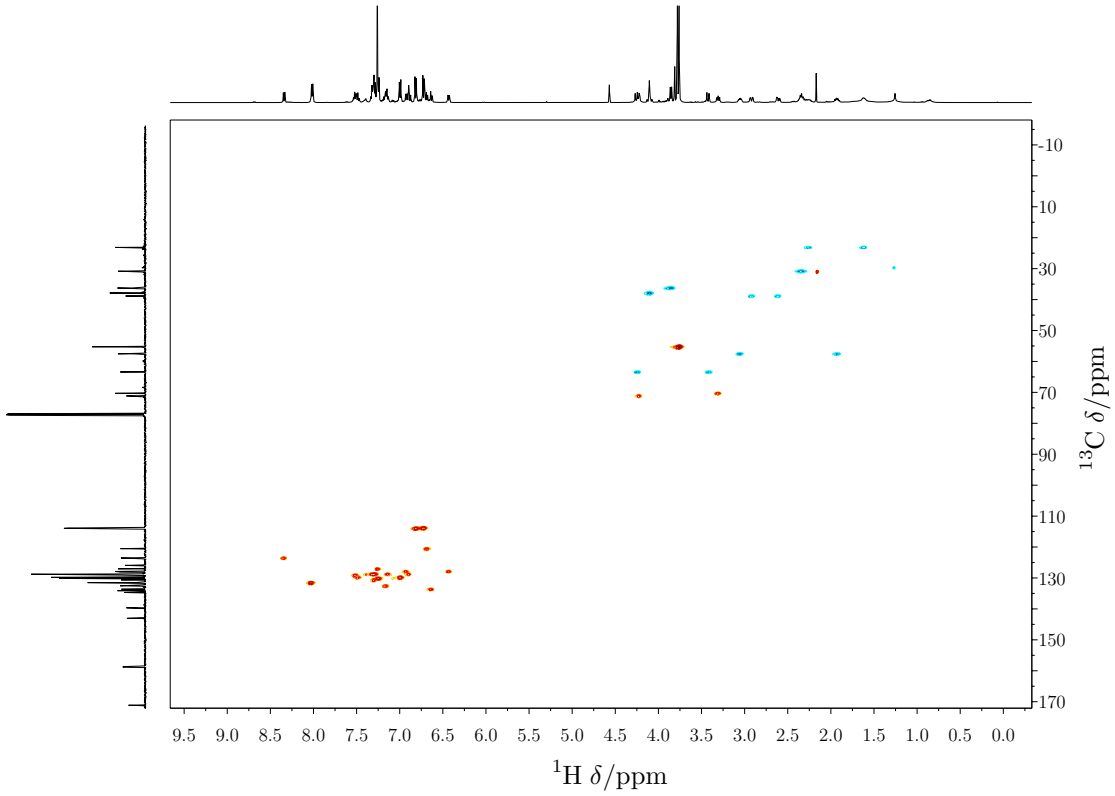

Figure C.16. ^{1}H-^{13}C HSQC spectrum of compound **4-7a**.

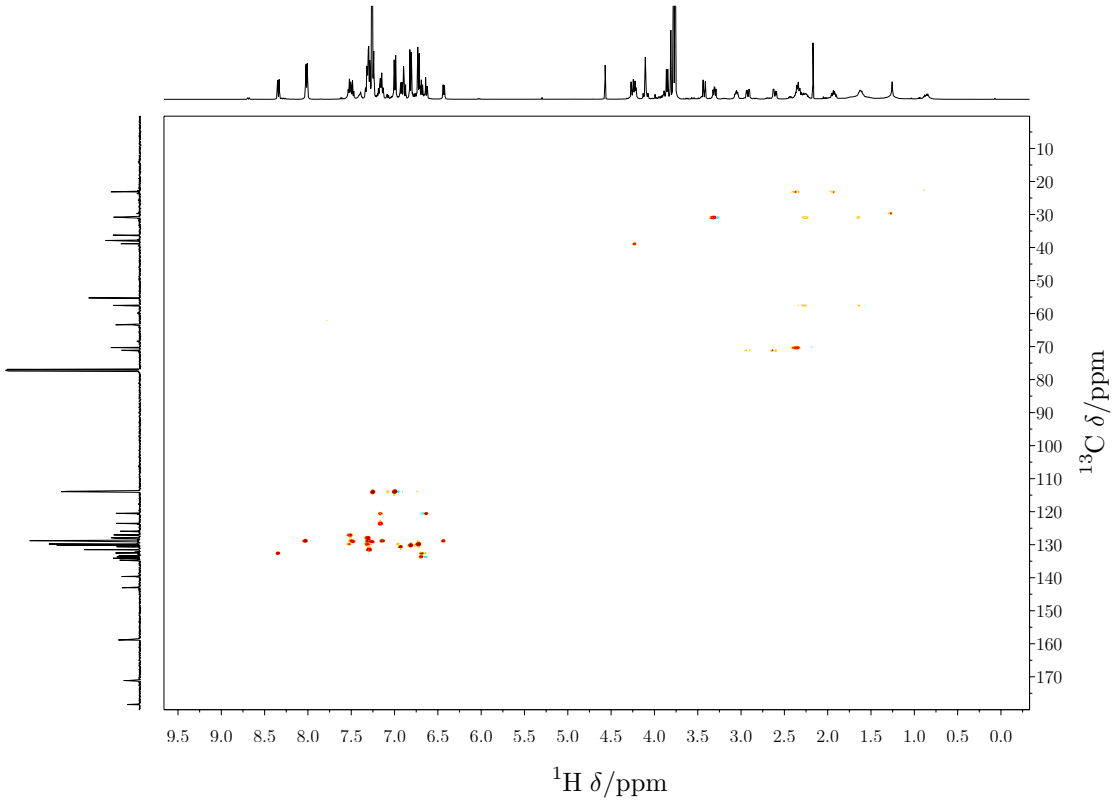

Figure C.17. ^{1}H-^{13}C H2BC spectrum of compound **4-7a**.

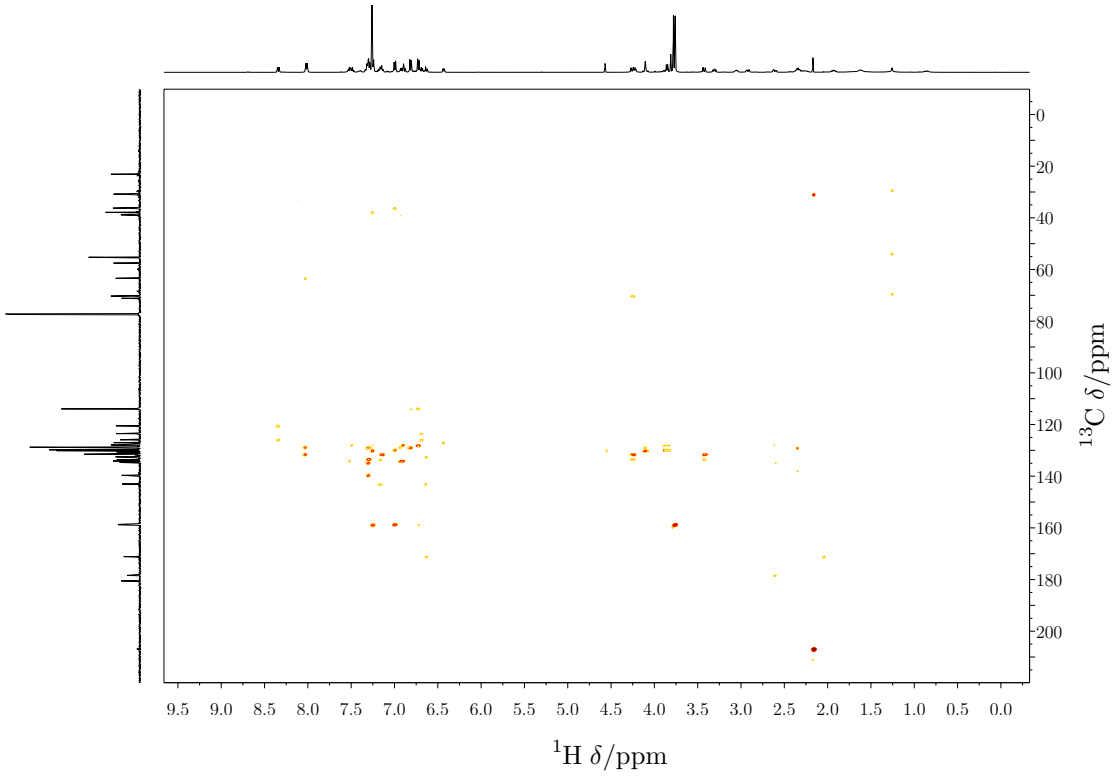

Figure C.18. ^{1}H-^{13}C HMBC spectrum of compound **4-7a**.

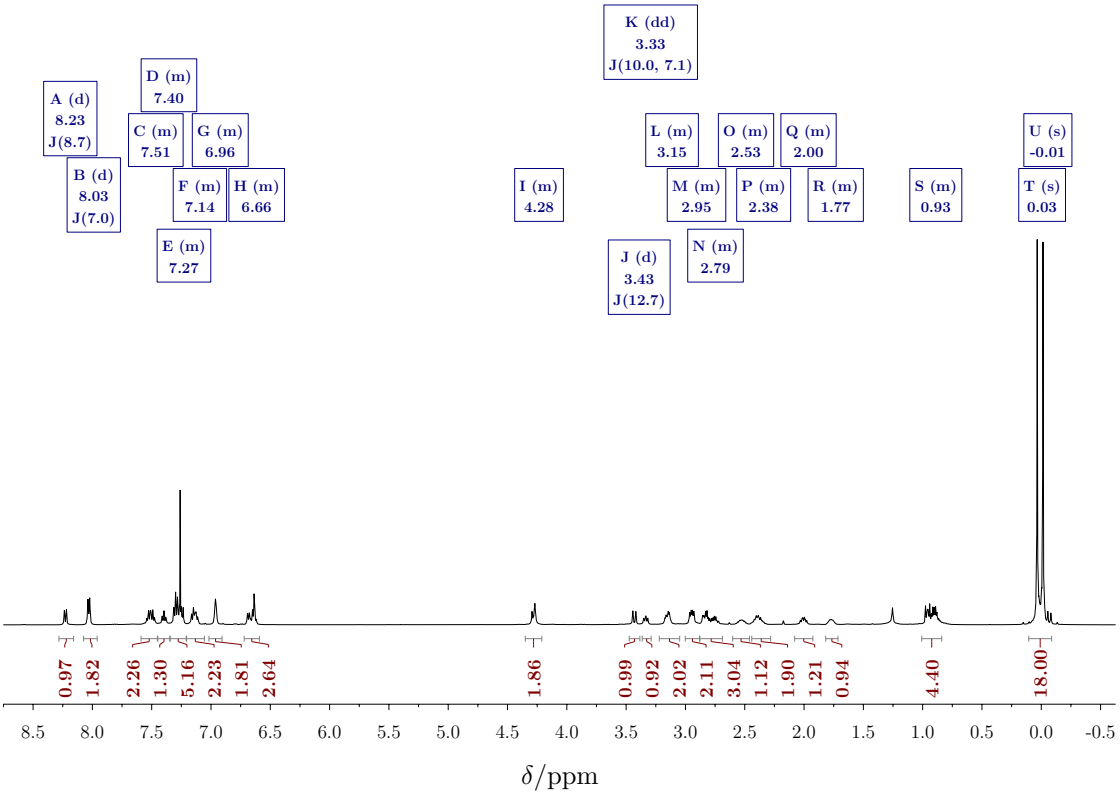

Figure C.19. ^{1}H NMR spectrum of compound **4-7b**.

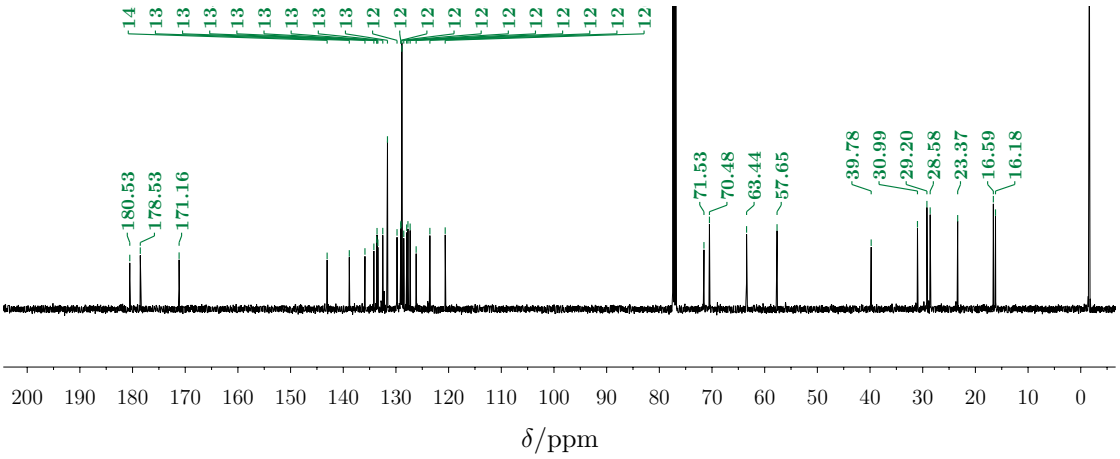

Figure C.20. ^{13}C NMR spectrum of compound **4-7b**.

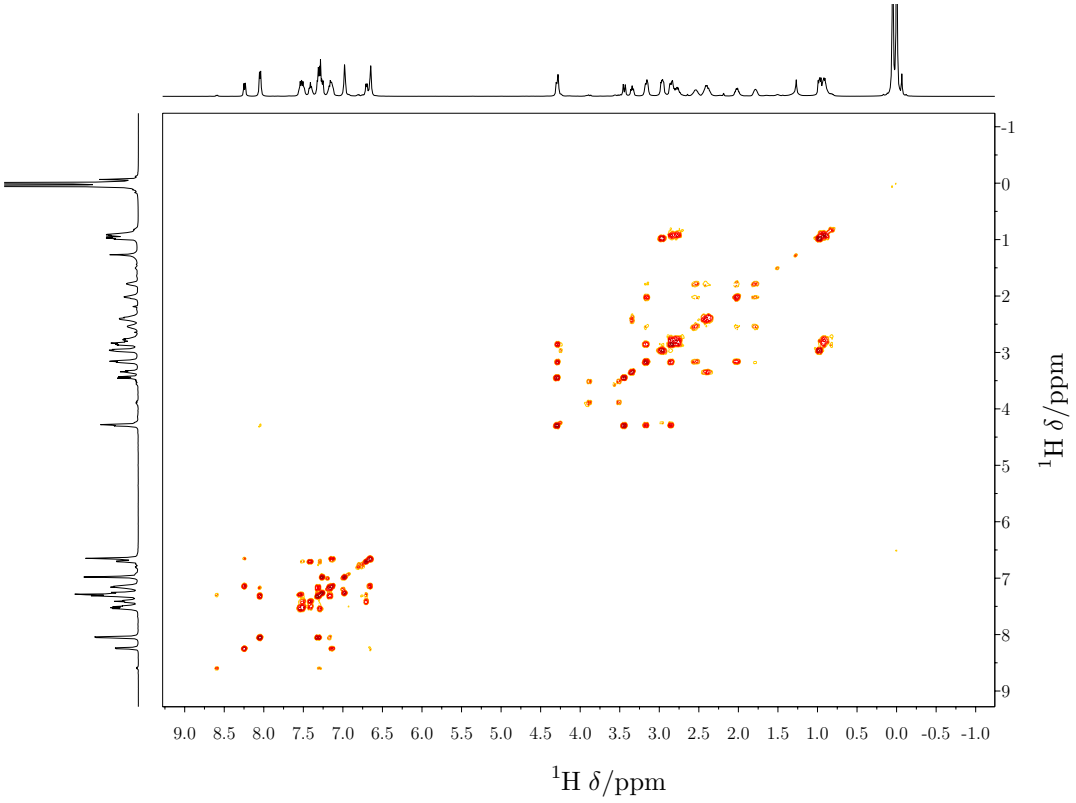

Figure C.21. COSY spectrum of compound **4-7b**.

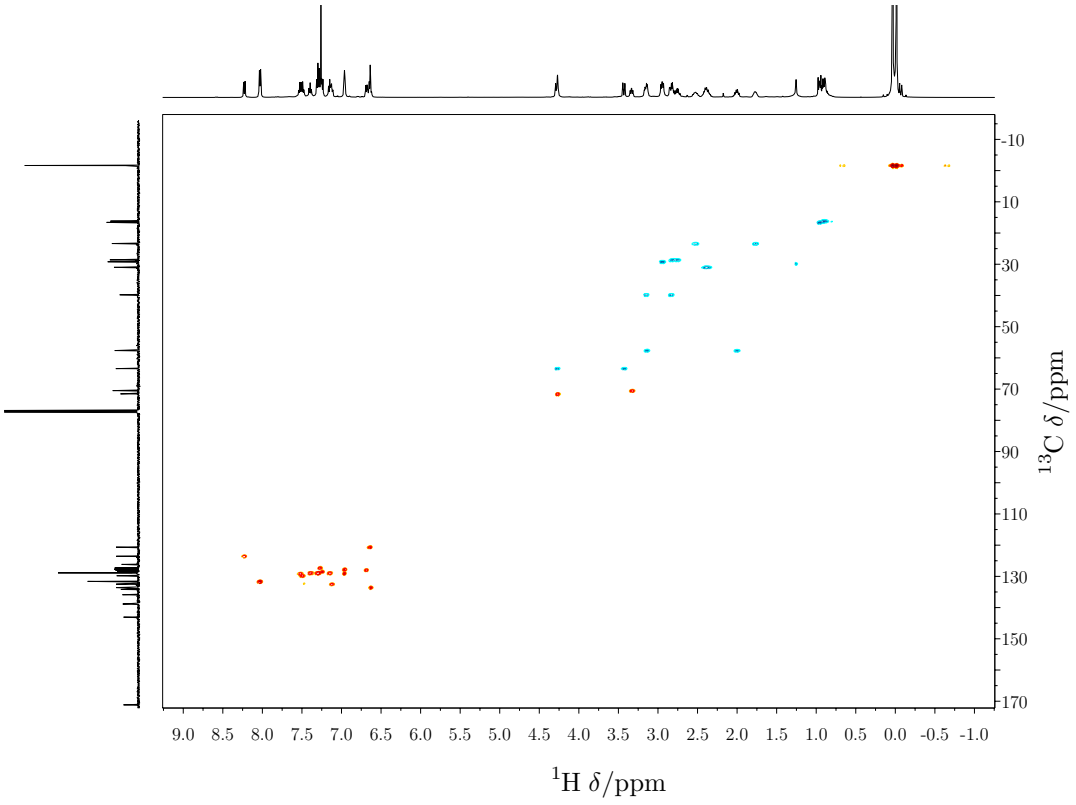

Figure C.22. ^{1}H-^{13}C HSQC spectrum of compound **4-7b**.

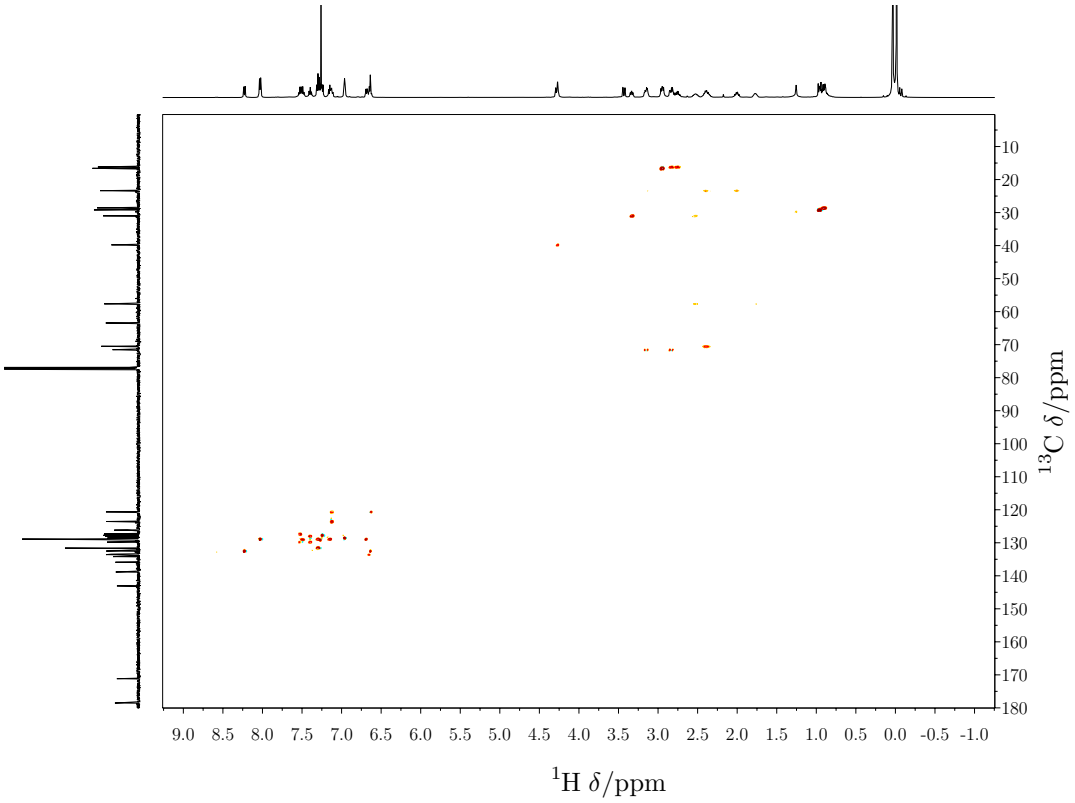

Figure C.23. ^{1}H-^{13}C H2BC spectrum of compound **4-7b**.

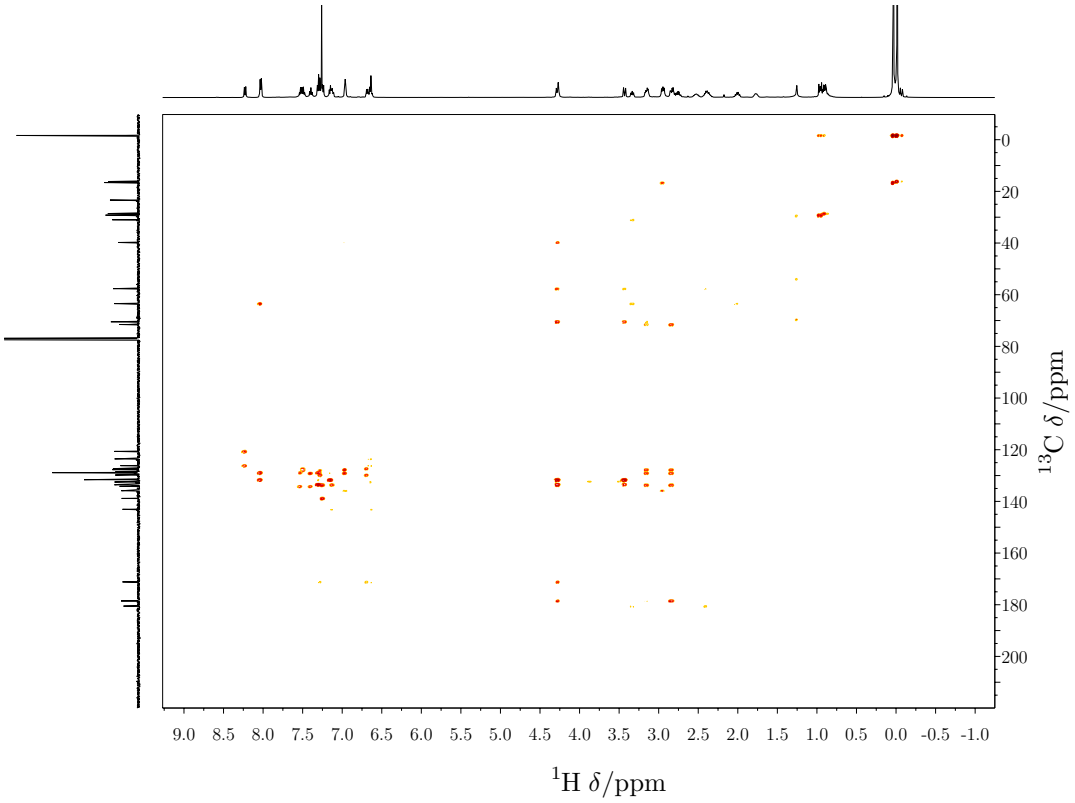

Figure C.24. ^{1}H-^{13}C HMBC spectrum of compound **4-7b**.

APPENDIX D

ATTEMPTED ALTERNATIVE SYNTHETIC ROUTES FOR CHAPTER 4

Chapter 4 has discussed the synthetic approach followed for the synthesis of an unnatural amino acid that contains a 1,2-benzenedithiol side chain (**4-1**). This Appendix presents an overview of the synthetic strategies that were also attempted with aims at preparing **4-1**, but that were unsuccessful or not further pursued. The work presented herein utilized different methodologies to control the stereochemistry of the amino acid moiety, introduce the sulfur groups into the aromatic ring, and/or make use of different protecting groups on the thiol groups in order to be able to facilitate their deprotection.

First, some of the planned reactions involved the use of the same synthetic scheme presented in Scheme 4.2 but with different thiols (Table D.1), namely methanethiol (**4-3c**), 2-methylpropane-2-thiol (**4-3d**), phenylmethanethiol **4-3e**, (2,4-dimethoxyphenyl)methanethiol (**4-3f**),[1] (2,4,6-trimethoxybenzyl)methanethiol (**4-3g**),[1] and triphenylmethanethiol (**4-3h**). In the case of **4-3c** the reaction with **4-2** seemed to go with high yields as expected from the small nucleophile, which is consistent with the observations discussed in Section 4.3. However, upon reduction with DIBAL to the corresponding aldehyde, the ^{1}H NMR spectrum showed two singlets in the low field region corresponding to the −CHO proton, indicating that an inseparable mixture of compounds had been obtained; thus, this synthesis was abandoned. When **4-3d**,**h** were used no reaction was observed, likely due to steric crowding of the nucleophile. Similarly, reactions with **4-3i**,**j** resulted in complex mixtures that ended up in very low yields after difficult purifications. Finally, **4-3e** behaved similarly to PMB, which was discussed in the main text, albeit with slightly lower yields. As with the case of PMB, attempts for the deprotection of the group in the same conditions as were not successful.

One of the attempted strategies aimed at preparing the benzyl alcohol synthon **4-6**, albeit introducing the sulfur groups through a Newman-Kwart rearrange-

Table D.1. Structure of the screened thiols for the preparation of compound **4-4**.

Thiol (**4-3**)	Structure
a	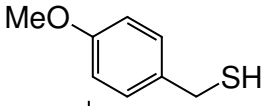
b	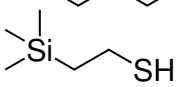
c	CH_3SH
d	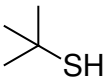
e	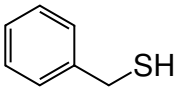
f	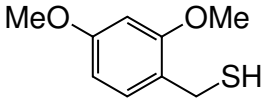
g	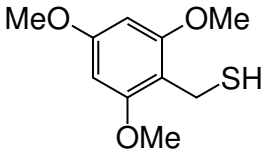
h	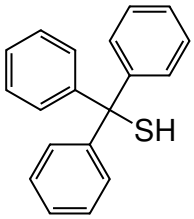

ment (Scheme D.1).[2,3] Briefly, 3,4-dihydroxybenzoic acid is transformed into its methyl ester and the phenol groups modified with *N*,*N*-dimethylthiocarbonyl chloride to yield the corresponding bis(*O*-thiocarbamate). These functional groups undergo a rearrangement reaction at high temperature (240 °C) and, in this particular molecule, form a cyclic *S*,*S*′-dithiocarbonate dithioester. Basic hydrolysis of the latter yields 3,4-disulfanylbenzoic acid. This Newman-Kwart rearrangement, although previously reported in the literature, failed to give yields above 20 % and

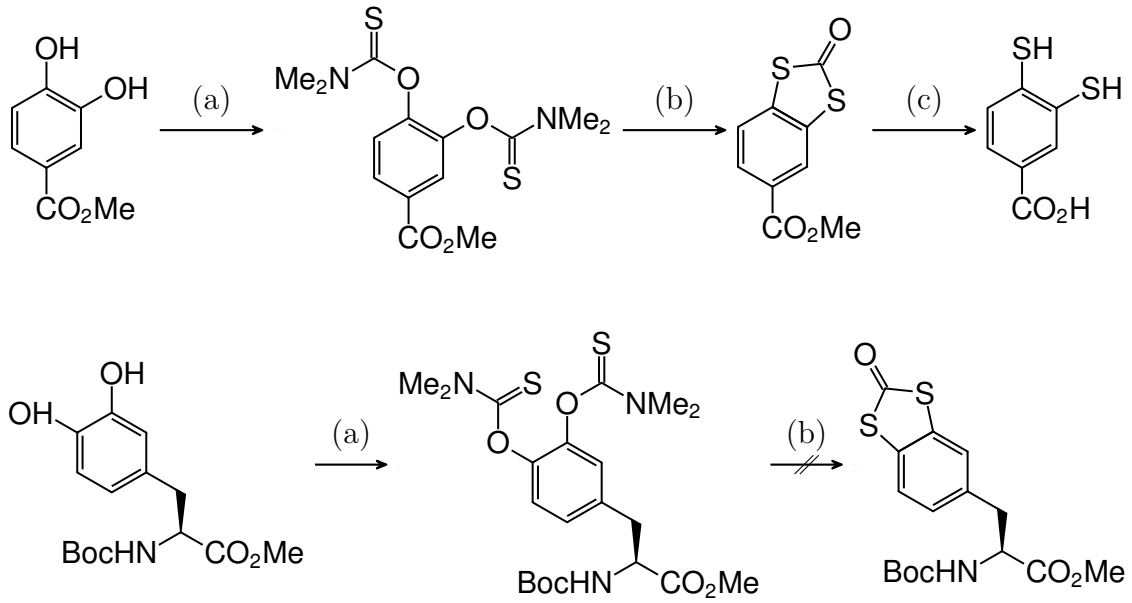

Scheme D.1. Alternative synthetic route for **4-1** involving a Newman-Kwart rearrangement from 3,4-dihydroxybenzoic acid (top sequence) or L-DOPA (bottom sequence). (a) $Me_2NC(S)Cl$, DABCO, DMF; (b) Ph_2O, 240 °C; (c) NaOH.

resulted in a very difficult mixture to purify, thus the approach was abandoned as it was still necessary to protect the thiols with a group stable to reducing conditions that would convert the carboxylic acid into the desired benzyl alcohol. Nonetheless, this approach was also attempted with 3,4-dihydroxyphenylalanine, a naturally occurring amino acid known as L-DOPA. It is likely that the absence of an electron withdrawing group on the ring was the reason the rearrangement did not occur in this case.

Other alternatives for the preparation of synthon **4-6** relied in the use of thiosulfate sodium salts, which can be introduced into an aromatic ring via a copper(I) catalyzed reaction between an aryl halide and sodium thiosulfate (Scheme D.2).[4] The strategy was first tried on **4-2** but no reaction was observed. To rule out the effect of the halide group, 3,4-diiodobenzonitrile was prepared from 3-amino-4-iodobenzonitrile via diazotization and substitution by KI. The aryl

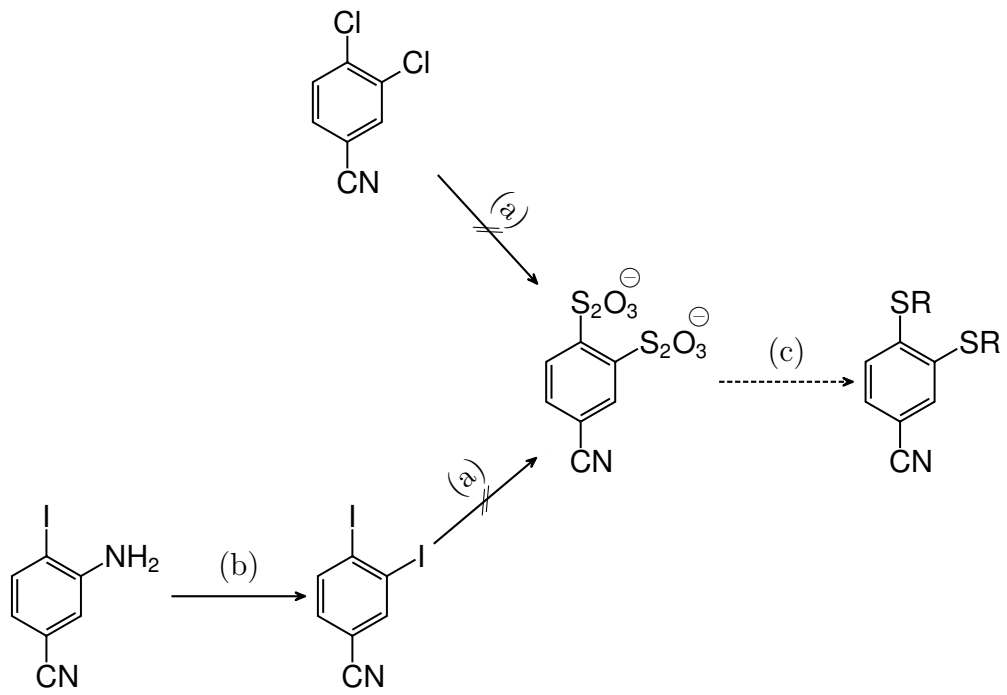

Scheme D.2. Alternative synthetic route for **4-1** involving the preparation of thiosulfate salts. (a) CuI, DMEDA, $Na_2S_2O_3$, DMSO; (b) *i*) $NaNO_2$, TsOH, *ii*) KI; (c) RMgCl.

diiodide did not react under the reaction conditions, suggesting that steric crowding was the cause of the lack of reactivity.

The last strategy that aimed at using NiCA to control the stereochemistry is based on the use of the benzyl bromide instead of the benzyl alcohol. This was tried using the acetamidomethyl (Acm) protecting group, introduced by treating 4-methylbenzene-1,2-dithiol with *N*-hydroxymethylacetamide in acidic conditions. The bis(Acm) derivative was then brominated at the benzylic carbon with *N*-bromosuccinimide (NBS) in moderately low yields. Upon treatment of NiCA with this benzyl bromide in basic conditions, the desired product was not obtained, presumably due to side reactions involving the hydrolysis of the acetamide functionality.

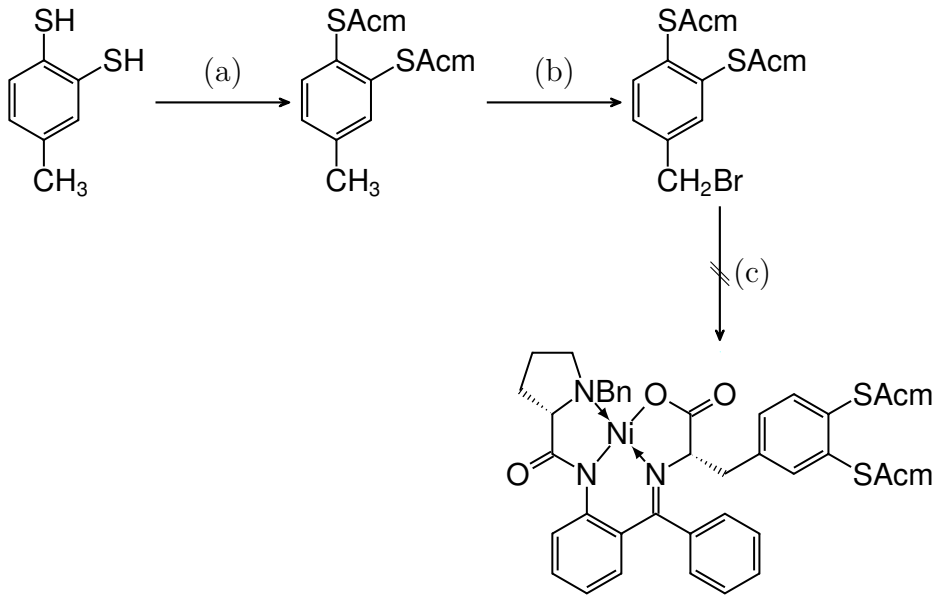

Scheme D.3. Alternative synthetic route for **4-1** using Acm as a thiol protecting groups for the coupling of NiCA to the corresponding benzyl bromide. (a) AcNH-CH_2OH, HCl, DMF; (b) *i*) NBS, AIBN, DCE; (c) NiCA, NaOH, MeCN.

Two of the proposed synthetic routes diverge from compound **4-5** in the scheme shown presented in Chapter 4. The first of these is based on the formation of the corresponding hydantoin and subsequent hydrolysis to form the aryl pyruvate, which can be enzymatically converted to the corresponding amino acid by aminotransferases (Scheme D.4).[5,6] Unfortunately, the hydantoin coupling did not work under the evaluated acetate/acetic acid system. The other alternative is based on formation of the cinnamic acid, which was accomplished through a Knoevenagel

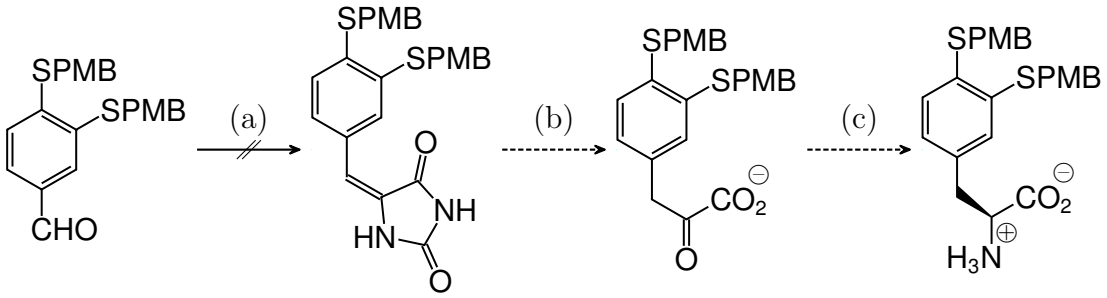

Scheme D.4. Alternative synthetic route for **4-1** through formation of the corresponding hydantoin. (a) NaOAc, HCl, DMF; (b) NaOH; (c) aminotransferase.

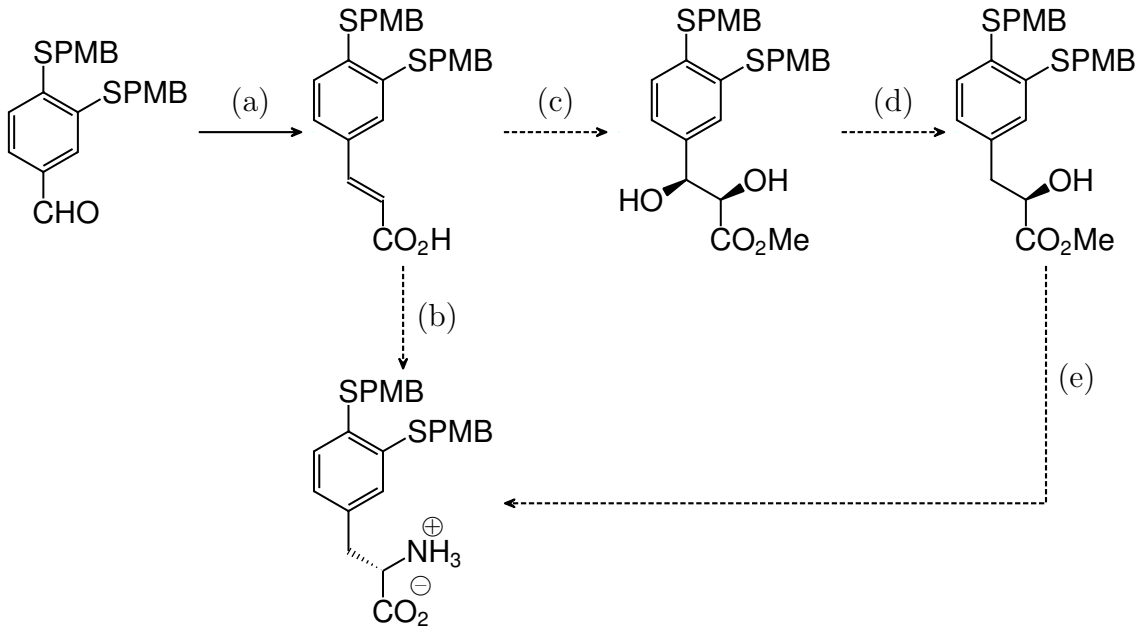

Scheme D.5. Alternative synthetic route for **4-1** via cinnamic acid formation. (a) malonic acid, β-alanine, pyridine; (b) phenylalanine/tyrosine ammonia lyase; (c) AD-mix-α; (d) Et_3SiH, TFA, DCM; (e) *i*) DPPA, DIAD, PPh_3, *ii*) H_2, Pd/C, *iii*) LiOH.

reaction on **4-5a** with good yields.[7] The cinnamic acid can be transformed to the L-amino acid in two ways: 1) by an enzymatic reaction using phenylalanine/tyrosine ammonia lyase;[8,9] or 2) through a proposed synthetic sequence that involves the asymmetric Sharpless dihydroxylation, regioselective reduction of the benzylic alcohol, Mitsunobu substitution of the α-alcohol with azide, and reduction of the latter to yield the amine group (Scheme D.5).[10] These proposed synthetic pathways were not attempted due to the inability to remove the protecting groups, but would still be interesting to pursue once the conditions for the thiol deprotection are optimized.

Another option to using the NiCA involved the catalyzed sp^3 directed arylation of L-alanine.[11] This strategy requires an iodide group on the aromatic ring at the coupling position. Two different pathways were devised for the preparation of the aryl iodide bearing the protected dithiol groups. The first one involved the elec-

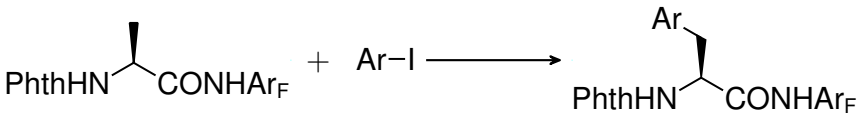

Scheme D.6. General reaction for the directed sp^3 arylation of L-alanine. The conditions for the reaction are: $Pd(TFA)_2$, 2-picoline, TFA, Ag_2CO_3, DCE. Phth = phthaloyl, Ar_F = 2,3,5,6-tetrafluoro-4-(trifluoromethyl)phenyl. Edited from reference 11.

trophilic aromatic substitution on 2-aminobenzenesulfonic acid with ICl,[12] which yielded the desired compound in moderately good yields (Scheme D.7). The potassium 4-iodobenzene-1,2-disulfonate salt was later obtained by a Leuckart thiophenol reaction followed by exhaustive oxidation with $KMnO_4$. Attempts to obtain the disulfonyl chloride for further reduction to the thiols with PCl_5 were unsuccessful.

Another pathway that avoids simultaneous formation of the disulfonyl chloride began with 4-iodobenzenesulfonyl chloride, which was reduced to the thiol with PPh_3 in good yields,[13] and then protected as a methyl thioether in moderately good yields (Scheme D.7). The synthetic sequence aimed at introducing the sul-

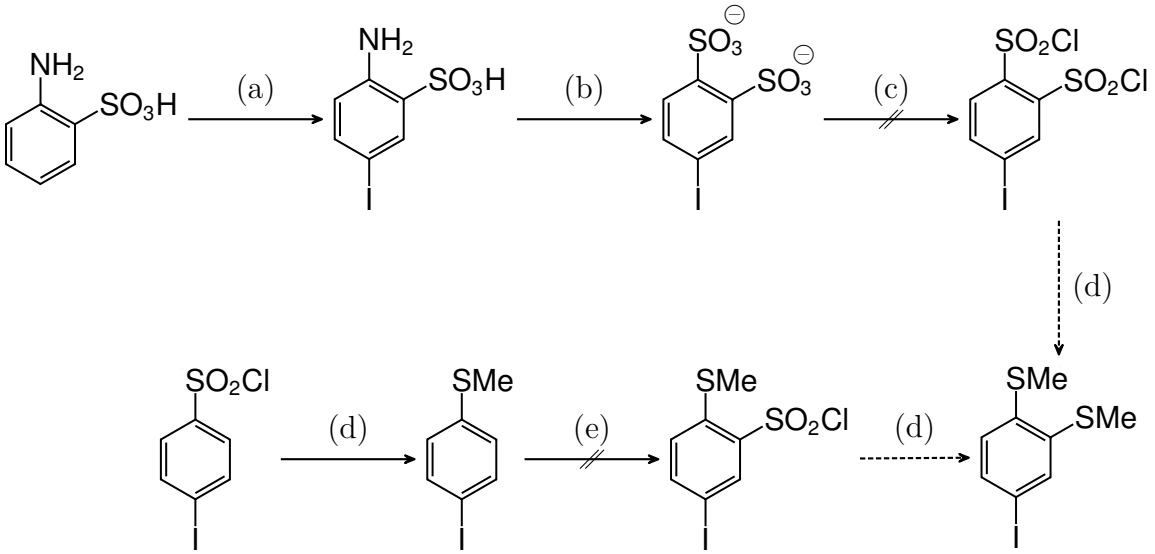

Scheme D.7. Aryl iodide preparation for directed L-alanine arylation. (a) ICl, HCl, H_2O; (b) *i*) KNO_2, *HCl*, *ii*) EtOC(S)SK, H_2O, *iii*) $KMnO_4$, H_2O; (c) PCl_5, 150 °C; (d) *i*) PPh_3, PhMe, *ii*) CH_3I, K_2CO_3; (e) $ClSO_3H$, $CHCl_3$, reflux.

fonyl chloride group with chlorosulfonic acid, followed by another reduction with PPh_3 to yield the free thiol which could be protected with an appropriate protecting group. This sequence would allow the introduction of orthogonal groups to each of the thiols, which could be attractive for some applications. The chlorosulfonation reaction resulted in a variety of products that were difficult to handle, and the product was not able to be isolated.

Finally, the last proposed synthetic route involved the formation of the benzene ring via a catalyzed [2+2+2] cycloaddition reaction involving an appropriate bis(thioalkyne) and L-propargylglycine (L-Prg) (Scheme D.8).[14,15] The procedure to prepare the bis(thioalkyne) involved the use of trimethylsilylacetylene, which was deprotonated with *n*-BuLi and treated with elemental sulfur. Attempts to trap the thioalkyne with di(1*H*-imidazol-1-yl)methanone (Im_2CO) and di(1*H*-imidazol-1-yl)methanethione (Im_2CS) were unsuccessful; but attempts to trap with oxalyl chloride, for example, could be interesting to investigate moving forward.

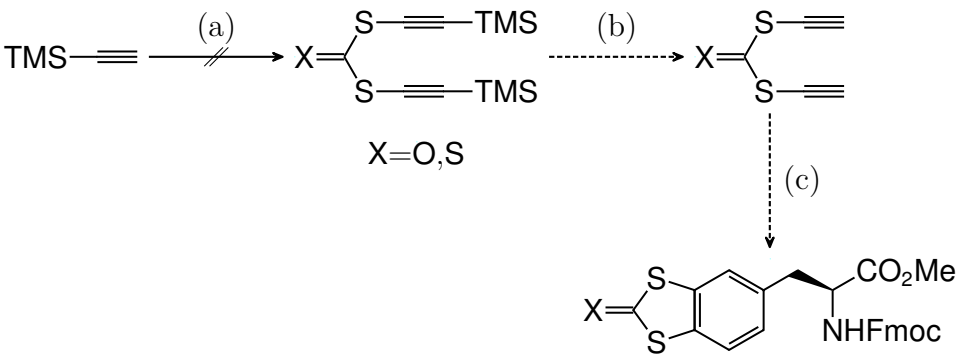

Scheme D.8. Alternative synthetic route toward compound **4-1** involving a [2+2+2] cycloaddition strategy. (a) *i*) *n*-BuLi, THF, −78 °C, *ii*) S_8, *iii*) Im_2CO or Im_2CS; (b) *i*) TBAF, THF; (c) *i*) $RuCl(PPh_3)_3$, EtOH, *ii*) L-Fmoc-Prg-OMe.

D.1 References

1. Vetter, S. Direct Synthesis of Di-and Trimethoxybenzyl Thiols from the Corresponding Alcohol. *Synthetic Communications* **1998**, *28*, 3219–3223 (cit. on p. 126).

2. Liénard, B. M. R.; Selevsek, N.; Oldham, N. J.; Schofield, C. J. Combined Mass Spectrometry and Dynamic Chemistry Approach to Identify Metalloenzyme Inhibitors. *ChemMedChem* **2007**, *2*, 175–179 (cit. on p. 127).

3. Mahendran, A.; Vuong, A.; Aebisher, D.; Gong, Y.; Bittman, R.; Arthur, G.; Kawamura, A.; Greer, A. Synthesis, Characterization, Mechanism of Decomposition, and Antiproliferative Activity of a Class of PEGylated Benzopolysulfanes Structurally Similar to the Natural Product Varacin. *The Journal of Organic Chemistry* **2010**, *75*, 5549–5557 (cit. on p. 127).

4. Reeves, J. T.; Camara, K.; Han, Z. S.; Xu, Y.; Lee, H.; Busacca, C. A.; Senanayake, C. H. The Reaction of Grignard Reagents with Bunte Salts: A Thiol-Free Synthesis of Sulfides. *Organic Letters* **2014**, *16*, 1196–1199 (cit. on p. 128).

5. Raap, J.; Nieuwenhuis, S.; Creemers, A.; Hexspoor, S.; Kragl, U.; Lugtenburg, J. Synthesis of Isotopically Labelled L-Phenylalanine and L-Tyrosine. *European Journal of Organic Chemistry* **1999**, *1999*, 2609–2621 (cit. on p. 130).

6. Jung, J.-E.; Lee, S. Y.; Park, H.; Cha, H.; Ko, W.; Sachin, K.; Kim, D. W.; Chi, D. Y.; Lee, H. S. Genetic incorporation of unnatural amino acids biosynthesized from α-keto acids by an aminotransferase. *Chemical Science* **2014**, *5*, 1881–1885 (cit. on p. 130).

7. Kolb, K. E.; Field, K. W.; Schatz, P. F. A One-Step Synthesis of Cinnamic Acids Using Malonic Acid: The Verley-Doebner Modification of the Knoevenagel Condensation. *Journal of Chemical Education* **1990**, *67*, A304 (cit. on p. 131).

8. Weise, N. J.; Ahmed, S. T.; Parmeggiani, F.; Galman, J. L.; Dunstan, M. S.; Charnock, S. J.; Leys, D.; Turner, N. J. Zymophore identification enables the discovery of novel phenylalanine ammonia lyase enzymes. *Scientific Reports* **2017**, *7*, 13691 (cit. on p. 131).

9. Ahmed, S. T.; Parmeggiani, F.; Weise, N. J.; Flitsch, S. L.; Turner, N. J. Engineered Ammonia Lyases for the Production of Challenging Electron-Rich l-Phenylalanines. *ACS Catalysis* **2018**, *8*, 3129–3132 (cit. on p. 131).

10. Varadaraju, T. G.; Hwu, J. R. Synthesis of anti-HIV lithospermic acid by two diverse strategies. *Organic & Biomolecular Chemistry* **2012**, *10*, 5456–5465 (cit. on p. 131).

11. He, J.; Li, S.; Deng, Y.; Fu, H.; Laforteza, B. N.; Spangler, J. E.; Homs, A.; Yu, J.-Q. Ligand-Controlled C(sp^3)−H Arylation and Olefination in Synthesis of Unnatural Chiral α–Amino Acids. *Science* **2014**, *343*, 1216–1220 (cit. on pp. 131, 132).

12. Boyle, M. CLXXXVI.—The iodobenzenemonosulphonic acids. Part I. *Journal of the Chemical Society, Transactions* **1909**, *95*, 1683–1716 (cit. on p. 132).

13. Bellale, E. V.; Chaudhari, M. K.; Akamanchi, K. G. A Simple, Fast and Chemoselective Method for the Preparation of Arylthiols. *Synthesis* **2009**, *2009*, 3211–3213 (cit. on p. 132).

14. Garcia, L.; Pla-Quintana, A.; Roglans, A. Synthesis of non-proteinogenic phenylalanine derivatives by rhodium-catalyzed [2+2+2] cycloaddition reactions. *Organic & Biomolecular Chemistry* **2009**, *7*, 5020–5027 (cit. on p. 133).

15. Destito, P.; Couceiro, J. R.; Faustino, H.; López, F.; Mascareñas, J. L. Ruthenium-Catalyzed Azide-Thioalkyne Cycloadditions in Aqueous Media: A Mild, Orthogonal, and Biocompatible Chemical Ligation. *Angewandte Chemie International Edition* **2017**, *56*, 10766–10770 (cit. on p. 133).

APPENDIX E

PUBLISHED MATERIAL

Parts of this dissertation have been previously partially or in full. The published materials were included with permission from all co-authors and the publication source.

Chapter 2

Alcala-Torano, R.; Walther, M.; Sommer, D. J.; Park, C. K.; Ghirlanda, G. Rational design of a hexameric protein assembly stabilized by metal chelation. *Biopolymers* **2018**, *109*, e23233.

APPENDIX F

PERMISSION TO REPRODUCE CHAPTER 2 FROM BIOPOLYMERS JOURNAL

Copyright Clearance Center RightsLink®

Home Account Info Help

Title: Rational design of a hexameric protein assembly stabilized by metal chelation

Author: Rafael Alcala-Torano, Mathieu Walther, Dayn J. Sommer, et al

Publication: Biopolymers

Publisher: John Wiley and Sons

Date: Sep 6, 2018

Logged in as:
Rafael Alcala-Torano
LOGOUT

Order Completed

Thank you for your order.

This Agreement between Mr. Rafael Alcala-Torano ("You") and John Wiley and Sons ("John Wiley and Sons") consists of your license details and the terms and conditions provided by John Wiley and Sons and Copyright Clearance Center.

Your confirmation email will contain your order number for future reference.

printable details

License Number	4597820107053
License date	May 28, 2019
Licensed Content Publisher	John Wiley and Sons
Licensed Content Publication	Biopolymers
Licensed Content Title	Rational design of a hexameric protein assembly stabilized by metal chelation
Licensed Content Author	Rafael Alcala-Torano, Mathieu Walther, Dayn J. Sommer, et al
Licensed Content Date	Sep 6, 2018
Licensed Content Volume	109
Licensed Content Issue	10
Licensed Content Pages	8
Type of use	Dissertation/Thesis
Requestor type	Author of this Wiley article
Format	Print and electronic
Portion	Full article
Will you be translating?	No
Title of your thesis / dissertation	Rational Metalloprotein Design for Energy Conversion Applications
Expected completion date	Aug 2019
Expected size (number of pages)	100
Requestor Location	Mr. Rafael Alcala-Torano TEMPE, AZ 85281 United States Attn: Mr. Rafael Alcala-Torano
Publisher Tax ID	EU826007151